

POLY(2-OXAZOLINE)-BASED POLYMERIC MICELLE PLATFORM FOR DRUG DELIVERY

Duhyeong Hwang

A dissertation submitted to the faculty of the University of North Carolina at Chapel Hill in partial fulfilment of the requirement for the degree of Doctor of Philosophy in the Division of Pharmacoengineering and Molecular Pharmaceutics in the Eshelman School of Pharmacy

Chapel Hill
2020

Approved by:

Alexander V. Kabanov

Leaf Huang

Shawn D. Hingtgen

Timothy R. Gershon

Chad V. Pecot

© 2020
Duhyeong Hwang
ALL RIGHTS RESERVED

ABSTRACT

Duhyeong Hwang: Poly(2-oxazoline)-based polymeric micelle platform for drug delivery
(Under the direction of Alexander V. Kabanov)

Polymeric micelles (PMs) have been extensively utilized as drug delivery platform. Particularly, potent hydrophobic small molecules were encapsulated in the PMs to alleviate toxicity issues and improve therapeutic outcomes. We attempt to provide detailed information on PMs for hydrophobic small molecules, such as the design of block copolymers (BCP) and current clinical outcomes from PMs. In particular, we aim to describe advanced analytical approaches for elucidating molecular interactions for effective solubilization.

This dissertation includes a novel computer-aided strategy for rational design of PM-based delivery systems for poorly soluble drugs. We have developed novel descriptors of drug-polymer complexes that were employed to build models to predict both drug loading efficiency (LE) and loading capacity (LC). These models were used for virtual screening of drug libraries and eight drugs for the experimental validation. Three putative true positive as well as three putative negative hits were confirmed (implying 75% prediction accuracy). The success of the computational strategy suggests its broad utility for rational design of drug delivery systems.

This dissertation involves the study of poly(2-oxazoline) micelles (POx) for treatment of medulloblastoma. For patients with SHH-subgroup medulloblastoma, SHH-pathway inhibition may be more effective and less toxic than current non-targeted therapy. We successfully solubilized SHH-pathway inhibitor, vismodegib, in POx micelles (POx-vismo) and showed the PM formulation improved drug efficacy, demonstrated in the treatment of medulloblastoma

animal model. Mechanistic studies revealed that POx-vismo decreased vismodegib binding to serum proteins and improved brain and tumor drug penetration without penetration of the nanoparticle carrier into the CNS.

This dissertation also includes the development of novel poly(2-oxazoline)-based block copolymer with the aromatic heterocyclic side chains and demonstration of its application as a drug delivery platform. The copolymer was synthesized via the condensation of *N,N*-dimethylbiguanide with the methyl ester side chain in poly(2-methoxycarboxyethyl-2-oxazoline) block (PMestOx). Successful encapsulation into these micelles has been demonstrated for several poorly soluble drugs. The capability of this new copolymer to solubilize a uniquely diverse set of active pharmaceutical ingredients suggests potential applications in drug delivery.

In summary, poly(2-oxazoline)-based PM platforms are versatile drug delivery platform and exhibit the broad potential for ideal drug delivery of therapeutic small molecules.

To my parents Hadong Hwang and Soonja Lee and my wife, Hyunji Lee.

ACKNOWLEDGEMENT

First of all, I would like to express my sincere gratitude and appreciation to my supervisor, Dr. Alexander Kabanov, who offered me a tremendous educational opportunity in his group as a graduate student. He always provided me constant support, insightful guidance and feedback throughout my graduate journey. I am truly blessed to have such a remarkable and exceptional mentor. His passion and sense of humor will forever inspire me along my scientific journey.

I would like to especially thank Dr. Marina Sokolsky for her dedicated support and guidance. Marina continuously provided encouragement and was always enthusiastic to assist in any way she could throughout the research project.

I would also like to thank my committee members, Dr. Leaf Huang, Dr. Timothy Gershon, Dr. Shawn Hingtgen and Dr. Chad Pecot for their precious guidance and advices. They advised me through the obstacles in completion of my research and reviewed all my progress and dissertation.

Moreover, I want to express my gratitude to UNC Eshelman School of Pharmacy for allowing me pursuing higher education. I also like to acknowledge my colleagues and friends, Dr. Chaemin Lim, Dr. Youngee Seo, Dr. Junghyun Kim, Dr. Junghyun Seo, Dr. Hyesun Hyun, Dr. Yongsu Kwon, Dr. Olesia Gololobova, Jacob Ramsey, Naoki Makita, Dr. Ryo Kojima, Natasha Vinod, Ali Altitnchi, Dina Yamaleyeva, Jimmy Fay, Dr. Lida Ghazanfari, Matt Haney, Dr. Ayelet David, Jubina Bregu, Bridget Newman, Yuling Zhao, Christian Long, Dr. Elena Batrakova and all

past and present members of the kabanov laboratory for their sincere friendship and kindly help. Especially, I will never forget the happiness, frustration, jokes, and parties we had as well as the inspiring scientific conversations. I would like to acknowledge BRIC imaging core facility and UNC animal facility for their assistance especially Dr. Hong Yuan, Dr. Zibo Li, and Charlene Santos

I would particularly thank my parents, my wife Hyunji, my parents-in-law, brother-in-law and my sister for their unconditional support and love all along the journey. The completion of my dissertation would not have been possible without their support, patience, faith and love.

TABLE OF CONTENTS

LIST OF TABLES.....	xi
LIST OF FIGURES.....	xii
LIST OF ABBREVIATIONS AND SYMBOLS.....	xiv
CHAPTER I: POLYMERIC MICELLE SYSTEMS FOR DELIVERY OF PHYSICALLY ENTRAPPED HYDROPHOBIC SMALL MOLECULES.....	1
1.1 Summary.....	1
1.2 Introduction.....	2
1.3 Functionalities of PM as delivery platform for hydrophobic small molecules.....	5
1.3.1 Anti-fouling polymers in BCP.....	6
1.3.2 Hydrophobic polymers in BCP.....	11
1.4 Drug–polymer molecular interaction within PM: theory, modeling and experimental approaches.....	13
1.4.1 Theoretical approaches	16
1.4.2 Computational modeling approaches.....	21
1.4.3 Experimental approaches	23
1.5 General considerations regarding physicochemical properties of PMs	28
1.6 PMs in clinical trials and regulatory approval for human.....	31
1.6.1 Clinical status of PM formulations	31
1.6.2 Bioequivalence of PM formulations	36
1.6.3 PM formulations for combination therapy.....	37

1.7 Conclusion.....	39
References.....	43
CHAPTER II: CHEMINFORMATICS-DRIVEN DISCOVERY OF POLYMERIC MICELLE FORMULATIONS FOR POORLY SOLUBLE DRUGS	55
2.1 Summary.....	55
2.2 Introduction.....	56
2.3 Materials and Methods.....	60
2.4 Results.....	72
2.5 Discussion.....	81
References.....	96
CHAPTER III: POLY(2-OXAZOLINE) MICELLES WITH VISMODEGIB ENHANCES TARGETING OF SHH PATHWAY IN GENETIC MODEL OFMEDULLOBLASTOMA.....	101
3.1 Summary.....	101
3.2 Introduction.....	102
3.3 Materials and Methods.....	106
3.4 Results.....	116
3.5 Discussion.....	124
References.....	142
CHAPTER IV: NOVEL POLY(2-OXAZOLINE) BLOCK COPOLYMER WITH AROMATIC HETEROCYCLIC SIDE CHAINS AS A DRUG DELIVERY PLATFORM.....	147
4.1 Summary.....	147
4.2 Introduction.....	148
4.3 Materials and Methods.....	150

4.4 Results.....	159
4.5 Discussion.....	166
References.....	188
CHAPTER V: SUMMARY AND FUTURE EXPERIMENTS.....	192

LIST OF TABLES

Table 1.1 Hydrophilic polymers commonly used for constructing PMs.....	41
Table 1.2 Hydrophobic polymers commonly used for constructing PMs	42
Table 2.1 List of nine polymers used in this study with specification of block sizes and end group	83
Table 2.2 List of 25 compounds tested alone at 8 mg with their respective clusters, LE and LC, LogP, MW, and number of performed experiments.....	84
Table 2.3 List of three drugs with highest LE variability tested at 8 mg/mL	85
Table 2.4 Statistical characteristics of LC and LE QSPR models based on 5-fold external cross-validation.....	86
Table 2.5 List of positive and negative hits with experimental values	87
Table 2.6 Top 15 compounds ranked by LE and LC for 8 mg drug vs. 10 mg polymer.....	89
Table 3.1 Actual vismodegib concentration, LE (%), LC (%), and size distribution of POx-vismo micelles prepared at indicated drug:polymer ratios	129
Table 4.1 Loading efficiency (LE%) and capacity (LC%) in P2 or PMeOx-PcBOx for each drug in each feeding ratio.....	173

LIST OF FIGURES

Figure 2.1 Study design	90
Figure 2.2 Coverage of chemical space by previously tested drugs and compounds rationally selected to increase structural diversity	91
Figure 2.3 General scheme of descriptor calculation for polymers	92
Figure 2.4 Descriptor calculation of drug-polymer complexes	93
Figure 2.5 Results of cluster analysis of 25 compounds tested alone at 8 mg.....	94
Figure 2.6 Variable importance for the five models developed.....	95
Figure 3.1 Comparison of normal and G-Smo mice at P15. (A) Head shape and (B) H&E stained sagittal sections of the cerebellar region of normal and G-Smo mice	130
Figure 3.2 (A) Particle size distribution measured by DLS (B) Zeta potential and (C) morphology (D) Stability of the POx-vismo micelles at 4 °C (E) Size of particles after reconstitution of lyophilized POx-vismo (F) Vismodegib release from POx-vismo incubated in fetal bovine serum solution.....	131
Figure 3.3 Pharmacodynamic response to POx-vismo and c-vismo	132
Figure 3.4 Comparison of weight gain between POx-vismo and c-vismo	133
Figure 3.5 Increased efficacy of POx-vismo compared to c-vismo.....	134
Figure 3.6 Widespread vismodegib distribution in the brain, with increased retention after POx-vismo administration, demonstrated by IR-MALDESI.....	135
Figure 3.7 Pharmacokinetic profile of POx-vismo and C-vismo in tumor mice	136
Figure 3.8 POx-vismo show enhanced drug delivery.....	138
Figure 3.9 Differential distribution of vismodegib and POx components of POx-vismo in the vascular and CNS compartments	139
Figure 3.10 Protein binding study of vismodegib.....	141
Figure 4.1 Synthesis of PMeOx-PcBOx via <i>N,N</i> -dimethylbiguanide condensation.....	174
Figure 4.2 ¹ H NMR spectra of PMeOx-PMestOx and reaction mixture	

(PMeOx-PMestOx and <i>N,N</i> -dimethylbiguanide free base in DMF) (lower).....	175
Figure 4.3 ¹ H NMR spectra of PMeOx-PMestOx and PMeOx-PcBOx.....	176
Figure 4.4 Overlay of the ¹ H NMR spectra of PMeOx-PMestOx, cBG and PMeOx-PcBOx (¹ H NMR ((CD ₃) ₂ SO, 298 K)	177
Figure 4.5 Overlay of the ¹³ C NMR spectra of PMeOx-PMestOx, cBG and PMeOx-PcBOx (¹³ C NMR ((CD ₃) ₂ SO, 298 K)	178
Figure 4.6 (A) UV spectra of PMeOx-PcBOx, cBG, PMeOx-PMestOx and <i>N,N</i> -dimethylbiguanide, (B) Acid-base titration curves and derivative plot dOH/dpH as a function of pH of PMeOx-PcBOx, cBG, PMeOx-PMestOx and saline. (C) TEM image of self-assembled PMeOx-PcBOx	179
Figure 4.7 MALDI-TOF MS analysis of PMestOx and PcBOx homopolymers.....	180
Figure 4.8 Volume based size distribution of (A) PMeOx-PcBOx and (B) DachPt-PMeOx-PcBOx (lower) measured by DLS.....	181
Figure 4.9 2D NOESY NMR spectra of (a) PMeOx-PcBOx (1 mg/mL) and (b) PMeOx-PMestOx (1 mg/mL) in D ₂ O.....	182
Figure 4.10 Measurement of the CMC of PMeOx-PcBOx in DI water by light scattering measurement	183
Figure 4.11 Differential solubilization of drugs indicated by their maximum LC	184
Figure 4.12 TEM image, Release profile and stability profile	185
Figure 4.13 (A) Evaluated drug structures and (B) comparison of the maximal LC of each drug in PMeOx-PcBOx and P2 micelles with the molecular characteristics of these drugs	186
Figure 4.14 Cytotoxicity and IC ₅₀ values of PMeOx-PcBOx, DachPt-PMeOx-PcBOx and free oxaliplatin in (A) 344SQ murine NSCLC cells and (B) MDA-MB-231 human breast cancer cells.....	187

LIST OF ABBREVIATIONS AND SYMBOLS

ABC	accelerated blood clearance
ACN	acetonitrile
API	active pharmaceutical ingredient
AUC	area under the curve
BCP	block copolymer
BSA	bovine serum albumin
cBG	<i>N,N</i> ,6-trimethyl-1,3,5-triazine-2,4-diamine
CBMA	poly(carboxybetaine methacrylate)
CCR	correct classification rate
CL	clearance
CLL	chronic lymphocytic leukemia
CMC	critical micelle concentration
COA	certificate of the analysis
CuI	cucurbitacine
DachPt	dichloro(1,2-diaminocyclohexane)platinum(II)
DLS	dynamic light scattering
DMF	<i>N,N</i> -dimethylformamide
DOSY	diffusion-ordered spectroscopy
DOX	doxorubicin
DP	degree of polymerization
EDA	electron deficient aromatic structure

EFS	event-free survival
FH	Flory-Huggins
G-Smo	hGFAP-Cre/SmoM2
Gd	gadolinium
GFA	genetic function approximation
GRAS	generally regarded as safe
HABA	2-(4'-hydroxybenzeneazo)benzoic acid
HBA	hydrogen bonding acceptor
HBD	hydrogen bonding donor
HPMA	poly[<i>N</i> -(2-hydroxypropyl)methacrylamide]
HR	hazard ratio
HTS	high throughput screening
ICP-MS	inductively coupled plasma mass spectrometry
LC	loading capacity
LE	loading efficiency
MALDI-TOF MS	Matrix-assisted laser desorption/ionization time-of-flight mass spectroscopy
MBC	metastatic breast cancer
MD	molecular dynamics
MeOTf	methyl trifluoromethanesulfonate
Mn	manganese
mPEG-b-PDLLA	methoxy-poly(ethylene glycol)-block-poly(D,L-lactide)
MTA	molecularly targeted agent

NCL	National Characterization Lab
NMP	n-methyl pyrrolidone
NMR	nuclear magnetic resonance
NOESY	nuclear overhauser effect spectroscopy
NSCLC	non-small cell lung cancer
OOB	out-of-bag
ORR	overall response rate
P(Asp)	poly(aspartic acid)
P(Glu)	poly(glutamic acid)
P(Sar)	poly(sarcosine)
PAA	poly(amino acid)
PACM	poly(N-acryloyl morpholine)
PBL	poly(butylactone)
PBuOx	poly(2-butyl-2-oxazoline)
PCL	poly(caprolactone)
PCNA	proliferating cell nuclear antigen
PDLLA	poly(D,L-lactide)
PDMA	poly(N,N-dimethyl acrylamide)
PDMS	poly(dimethylsiloxane)
PEG	poly(ethylene glycol)
PEG-b-P(CB-co-LA)	methoxy-poly(ethylene glycol)-b-poly(carbonate-co-lactide)
PEO	poly(ethylene oxide)
PEtOx	poly(2-ethyl-2-oxazoline)

PFS	progress free survival
PK	pharmacokinetic
PLGA	poly(lactide-co-glycolide)
PM	polymeric micelle
PMeOx	poly(2-methyl-2-oxazoline)
PMestOx	poly(2-methoxycarboxyethyl-2-oxazoline)
PMMA	polymethylmethacrylate
POx	poly(2-oxazoline)
POx-PTX	paclitaxel in poly(2-oxazoline)-based polymeric micelle
POx-vismo	vismodegib in POx micelle
PPO	poly(propylene oxide)
pRB	phosphorylated RB
PTX	paclitaxel
PVL	poly(valerolactone)
PVP	polyvinylpyrrolidone
QSPR	quantitative-structure properties relationship
RES	reticuloendothelial
RF	random forest
Ru	ruthenium
SANS	small angle neutron scattering
SBMA	poly(sulfobetaine methacrylate)
SiRMS	simplex representation of molecular structure
SITUA	stable isotope tracer ultrafiltration assay

SLL	small lymphocytic lymphoma
Smo	Smoothened
SOLE	support vector regression-based online learning equipment
SP	solubility parameter
SRM	selected reaction monitoring
ssNMR	solid-state nuclear magnetic resonance
TEM	transmission electron microscopy
TME	tumor microenvironment
USFDA	US Food and Drug Administration
Vd	volume of distribution

CHAPTER I: POLYMERIC MICELLE SYSTEMS FOR DELIVERY OF PHYSICALLY ENTRAPPED HYDROPHOBIC SMALL MOLECULES¹

1.1 SUMMARY

Polymeric micelles (PMs) have been extensively utilized as drug delivery platforms for the optimized delivery of various therapeutic compounds over the last three decades. Particularly, hydrophobic small molecules with high potency and severe toxicity were encapsulated in PMs and PMs have shown the potential to improve pharmacokinetic (PK) profile of encapsulated drugs in preclinical animal models. Though PMs have shown enhanced efficacy with superior safety profile for the therapeutic drugs, clinical outcomes of PMs are still poor and further development is needed for human use. In this review, we attempt to provide detailed information on PMs for potential hydrophobic small molecules such as the design of block copolymers (BCPs), analysis of hydrophobic drug encapsulation in PMs, and current clinical outcomes from PM formulations in clinical trials. In particular, we aim to describe the latest studies on advanced analytical approaches for elucidating detailed molecular interactions within the core of PMs for effective solubilization as well as advanced analytical techniques for characterizing nanomedicine's PK profiles.

¹ This chapter previously appeared as a manuscript soon to be submitted

1.2 Introduction

Biocompatible polymers have been extensively employed in pharmaceutical science as excipients for traditional pharmaceutical research, such as basic drug dosage forms, and in current research, such as nanomedicine for enhancing therapeutic outcome of potent drugs [1, 2]. About three decades ago, amphiphilic block copolymers (BCP) were conceived as solubilizing agents for hydrophobic therapeutic compounds and forms polymeric micelles (PM) in aqueous solution [3, 4]. Since then, the applications of amphiphilic BCPs on the design of PM as therapeutics have been extensively developed [5-8]. A plethora of novel BCPs have been proposed to develop novel PM-based delivery system as potential nanomedicines for humans [9-12]. Many significant advances on PMs have shown the potential for ideal delivery of therapeutic modalities in preclinical animal models, and such advances have driven several PM formulations to enter clinical trials for regulatory approval [12, 13].

The design of BCP are intended to effectively encapsulate therapeutic compounds into PM via various molecular interactions, resulting in the improvement of the pharmacokinetic (PK) profile of the therapeutic compounds alongside the protection of the cargo from the external environment [14]. Ideal PM formulations are expected to improve therapeutic outcome based on the functionalities of the PM. The PK profile of the therapeutic compounds in PM may differ from native compounds as PM are capable of releasing the cargo in a controlled manner from the core during systemic circulation. Also, structural factors of PM, such as the hydrophilic shell effectively avoids both unexpected drug loss from serum component (albumin) and opsonization by complement system which typically results in rapid clearance from systemic circulation [15, 16]. Based on those functionalities derived from PM, overall PK profile of the therapeutic compounds such as maximum systemic concentration (C_{max}), area under the curve (AUC), clearance (CL),

volume of distribution (Vd), and biodistribution of the therapeutic compounds could be improved [13]. By virtue of the functionalities of the PM, ideal PMs are expected to reduce the toxicity of the therapeutic compounds. The safety profile of the therapeutic compounds within PM could improve therapeutic outcomes since the therapeutic window of the therapeutic compounds could be expanded. For examples, side effects of the anticancer drugs such as paclitaxel (PTX) and doxorubicin, such as neurotoxicity and cardiotoxicity, are some of the most important factors that governs the dosage regimen for effective treatment of cancers. These also greatly affect the quality of life of the patients [9, 17]. Those side effects could be alleviated in both preclinical and clinical studies by using PM formulations.

PM systems primarily exploit block copolymer (BCP) for delivery of potentially active therapeutic compounds such as small molecule drugs, proteins, and nucleic acids [2]. The desired physicochemical properties of BCPs will vary based on the physicochemical properties of each therapeutic compound. For examples, generally hydrophobic small molecules could be encapsulated in BCPs with hydrophobic blocks [18, 19], while nucleic acids require polycationic segments in the BCP to be encapsulated in PM via electrostatic interactions [20, 21]. Among those applications, exploitation of BCP as the carrier of hydrophobic small molecules in order to solubilize the drugs and form nano-sized micelle formulation has shown the potential to improve the therapeutic outcome of the small molecule drugs. For example, paclitaxel (PTX) has been physically encapsulated in PM formulation using BCPs to improve therapeutic outcome of PTX and alleviate drug-induced side effect such as neurotoxicity in both preclinical studies and clinical trials [6, 8, 10, 22]. Since then, several PTX-loaded polymeric micelles entered clinical trials, resulting in one PM formulation, Genexol[®] PM, having received regulatory approval in South Korea and other countries as a cancer therapeutic.

In this review, we attempt to describe BCP systems for the effective delivery of hydrophobic small molecules. BCP segments which play an essential role in solubilization of hydrophobic small molecules as well as hydrophilic BCP segments for effective anti-fouling properties will be described. Also, multi-disciplinary approaches for investigating detailed molecular interaction between hydrophobic drug and BCPs will be introduced to improve the understanding of the solubilization of hydrophobic drugs by BCPs and to aid in the informed development of ideal PMs for effective delivery.

1.3 Functionalities of PMs as a delivery platform for hydrophobic small molecules

Amphiphilic BCPs self-assemble in aqueous media to form PMs that have hydrophilic shell for protection of the cargo and hydrophobic core for solubilizing poorly soluble small molecules. In general, diblock copolymer (A–B) or triblock copolymer (A–B–A) of hydrophilic (A)/hydrophobic (B) segments are employed for the preparation of PM formulation. Structural factors such as molecular weight of the block copolymer, molar ratio of hydrophilic and hydrophobic segments, and encapsulating hydrophobic drugs may affect the formation of PM, thereby varying the size and morphologies in aqueous solution [23-25].

The hydrophilic shell has anti-fouling properties that prohibit the binding of serum components which ultimately protects the encapsulated drug in the core, thus avoiding unexpected loss of the cargo from the PM during systemic circulation. For this purpose, minimizing the interaction between PMs and external plasma components, such as serum proteins or the complement system, is necessary (Table 1.1). Otherwise, hydrophobic drugs within the core of the PM could be easily cleared from the body by plasma protein adsorption or the activation of complements system and subsequent recognition by the reticuloendothelial system (RES) during systemic circulation [26, 27]. Thus, several hydrophilic blocks were introduced in the structure of BCPs to endow anti-fouling properties on the PM so as to improve the systemic circulation and in vivo stability of PM [28, 29]. The functionalities of hydrophilic shell of PMs were extensively studied and according to those studies physicochemical properties of hydrophilic polymers such as molecular weight and surface density were closely related to the anti-fouling properties of PM in in vivo studies [16, 30].

The hydrophobic block is another component of BCPs which is intended to solubilize poorly soluble drugs in the core and control the release of the drug from the PM (Table 1.2) [31-

33]. Hydrophobic interactions are the main molecular interaction for solubilizing hydrophobic drugs in amphiphilic BCPs, and such interaction between the drug and hydrophobic block of BCPs may retard the overall release rate of the drug. Additional molecular interactions existing in the core, such as hydrogen bonding and pi-pi interactions, may strengthen the molecular interactions in the core and thereby decreasing the release rate of the hydrophobic drugs [34]. Many hydrophobic polymers have been synthesized which show capacity to solubilize hydrophobic drugs. Moreover, the solubilization process, in terms of molecular interactions within the core, was investigated using several scientific approaches [35-38].

In this section, frequently employed polymers of BCPs will be identified and their functionalities as delivery platforms will be discussed.

1.3.1 Anti-fouling polymers in BCP

Polyethylene glycol (PEG)

PEG has been the most frequently employed as hydrophilic shell-forming segment for BCPs due to its safety profile in human and classification as Generally Regarded as Safe (GRAS) by US Food and Drug Administration (USFDA). When PEG forms the hydrophilic shell of the PM, its hydrophilicity and flexibility enable the PM to avoid the adsorption of plasma protein and opsonization processes that may cause the unexpected rapid clearance of the cargo and PM during systemic circulation by the RES system [30]. PEG with molecular weights ranging from 10 kDa to 60 kDa are an ideal molecular weight for endowing nanoparticles with effective anti-fouling properties and are commonly being employed to prepare BCPs for drug delivery [28, 39, 40]. The mechanism of anti-fouling process of PEG has been comprehensively investigated in many studies revealing that steric repulsions by PEG mainly minimize the adsorption of plasma components on

PM and the physical properties of PEG such as sufficient flexibility and aqueous solubility play a significant role on the anti-fouling properties of PEG [32]. Based on the surface density and the MW of PEG when forming the shell of PMs, the conformation of PEG on the surface of PM, such as brush or mushroom, may affect the anti-fouling properties of the hydrophilic shell [30, 41]. Also, it was reported that PEG conformation on the PMs ultimately affect the circulation time and clearance of PM in in vivo [30].

Synthesis of PEG is usually done by ring-opening anionic polymerization of ethylene oxide and this synthetic process generates well-defined PEG with narrow molecular weight distribution [42, 43]. The modification on the end group of PEG by appropriate chemical reagents (end-capping moiety) could expand the structural versatility of PEG [44]. The chemical versatility of the end group of PEG includes additional reactive moieties for ligand labeling and enables further conjugation with other species of polymers to prepare specific BCPs.

The accelerated blood clearance (ABC) phenomenon of PEG has gained a lot of attention due to its detrimental effects on nanoparticle therapeutics with PEG shielding [45]. It is well studied that systemic exposure of PEG may cause accelerated blood clearance (ABC) phenomenon in humans [46]. This phenomenon mainly arises from initial exposure of PEG in PEG-coated nanoparticle therapeutics and subsequent development of anti-PEG antibodies in the body. ABC phenomenon mainly occurred in human patients treated with PEGylated proteins as well as liposomal formulation coated with PEG [47]. In the case of human patients treated with PEG-uricase, about one third of the treatment group had developed anti-PEG antibodies in the body, resulting in poor efficacy [48]. The clinically approved doxorubicin liposome formulation, Doxil[®], has shown to induced the ABC phenomenon in human patients mainly due to the development of anti-PEG antibodies in the body after the initial treatment of Doxil[®] [49]. The effect of hydrophilic

chains of liposomal formulation on the genesis of ABC phenomenon was extensively studied by Dr. Szoka's group [50]. They found that both PEG hydrophilic shells and Poly(2-methyl-2-oxazoline) hydrophilic shells on liposomes induced the ABC phenomenon in rats after the initial dose of the same liposomes. Other hydrophilic polymers such as HPMA, PVP (poly(vinylpyrrolidone)), PDMA (poly(N,N-dimethyl acrylamide)), and PAcM (poly(N-acryloyl morpholine)) did not cause the ABC phenomenon, indicating they are potentially safe hydrophilic polymers with anti-fouling properties.

Interestingly, in contrast to ABC phenomenon from liposome with PEG shielding and PEGylated proteins, previous studies revealed that polymeric micelle formulations with PEG shielding did not induce significant ABC phenomenon in preclinical animal models as determined by the reduced anti-PEG antibody production. According to Shiraishi et al., anti-PEG antibodies did not affect the PK of PEG-b-poly(b-benzyl L-aspartate) PMs, while the PK profile of PEG-liposomes was marked by significantly decreased circulation times [51]. Another study revealed that hydrophobic block of PEG-conjugate was closely related to the binding of anti-PEG antibodies on PEG-conjugate. That is, proximal hydrophobic block is another key factor for the binding of PEG-specific anti-PEG antibodies on PEG moieties to induce ABC phenomenon [52]. In the case of PEG-coated liposomes, hydrophobic segments were more exposed for anti-PEG antibodies, while the structured polymeric micelle formulation was effective in restricting anti-PEG antibodies from approaching the hydrophobic blocks of BCPs. Thus, PM formulations may be less of a concern in promoting the ABC phenomenon due to repeated injection of the PM formulation.

Poly(2-oxazoline)s

Poly(2-oxazoline)-based block copolymers (POx) recently gained a lot of interest as novel biomaterials due to their biocompatibility and chemical versatility [53]. Hydrophilic poly(2-oxazolines)s such as poly(2-methyl-2-oxazoline) (PMeOx) and poly(2-ethyl-2-oxazoline) (PEtOx) have shown the anti-fouling properties to repel the adsorption of plasma components on PM in both in vitro and in vivo. These studies demonstrated the potential of POx as a stealth PMs [54]. POx can be readily synthesized via living cationic ring-opening polymerization and recently BCPs composed of POx have demonstrated scalable synthesis and chemical versatility [54].

As for anti-fouling properties of POx, Zhang et al reported that both PMeOx and PEtOx had extremely low protein adsorption and cell adhesion that is comparable to that of PEG-coating [55]. Interestingly, the modification on the end group of those polymers had minimal effect on the protein adsorption, but the length of the polymer was significantly related to the anti-fouling properties. Another study done by Pidhatika et al clarified long-term anti-fouling properties of PMeOx coatings [56]. They found that PMeOx had excellent anti-fouling properties comparable to PEG for a short term of protein exposure. However, for a long term exposure of media exposure, it was found that only PMeOx could maintain the anti-fouling properties due to the lack of degradation of PMeOx in biological fluids. In case of PEG, though it had anti-fouling properties at the early time points, it gradually degraded in biological fluids, resulting in the loss of anti-fouling properties. Currently, only PEtOx is approved as food additives by USFDA [57] and the safety profile of POx in human such as biodegradation of POx needs to be investigated for clinical development of POx-based PM formulations.

Other reported anti-fouling polymers

Several other hydrophilic polymers have been identified and have shown anti-fouling properties in preclinical models, suggesting their potential to be applied as shielding agents in PMs.

Hydrophilic poly(amino acid)s (PAAs) were employed in amphiphilic BCPs as the anti-fouling agents in outer surface of PMs. Biodegradability of PAAs by endogenous proteases in vivo potentially guarantees the safety of these materials in the body [58]. Synthesis of hydrophilic PAAs could be done via ring-opening polymerization by using N-carboxyanhydride of amino acids to generate poly(aspartic acid) (P(Asp)), poly(glutamic acid) (P(Glu)), and poly(sarcosine) (P(Sar)) [59]. Among hydrophilic PAAs, P(Sar) has shown effective anti-fouling properties for PMs in recent studies [60, 61].

Polysaccharides such as dextran, heparin, chitosan, hyaluronic acid, and chondroitin sulfate have shown anti-fouling properties and inhibited protein adsorption on the particle surface in biological fluids. Interestingly, some studies revealed that dextran as a shielding agent for nanoparticles showed anti-fouling effects and prolonged circulation in animal models in several studies. A comprehensive and concise review on polysaccharides as anti-fouling agents was reported by Doh et al and this review may provide useful information for researchers in selecting suitable polysaccharides with anti-fouling properties [62].

Poly(vinylpyrrolidone) (PVP) has been employed in several studies to investigate anti-fouling properties of PVP. PVP can be synthesized via radical polymerization and it has been traditionally been used as an excipient in formulation design [63]. Allegedly, both the pyrrolidone moiety and amide groups in side chain are closely related to the anti-fouling properties of PVP, but comprehensive mechanisms of the anti-fouling properties are still unknown [64].

Several other hydrophilic polymers such as poly(*N,N*-dimethyl acrylamide) (PDMA), poly[N-(2-hydroxypropyl)methacrylamide] (HPMA), poly(dimethylsiloxane) and zwitterionic polymers have been reported as anti-fouling macromolecules [65-67]. Those polymers are expected to be developed as BCPs for efficient delivery of hydrophobic small molecules as PM formulations.

1.3.2 Hydrophobic polymers in BCP

Hydrophobic segments of BCPs play an essential role in solubilizing and encapsulating hydrophobic drugs in the core of PMs. The segregated core of the PMs features a hydrophobic environment where encapsulated drug can stably reside in the core during the systemic circulation and gradually release the cargo into the external environment. Hydrophobic segments of the BCPs can vary widely in their structure in order to effectively encapsulate hydrophobic drugs [68]. Commonly employed hydrophobic polymers are polyethers, polyesters, and recently POx based polymers such as poly(2-n-butyl-2-oxazoline) have gained much attention due to their high loading capacity for physically encapsulating hydrophobic drugs.

Polyethers have been used as the core-forming segment for encapsulating hydrophobic drugs. Generally, polyethers are synthesized via ring-opening anionic polymerization of alkenes to produce well-defined polymers with low PDI MW distributions [69]. Poly(propylene oxide), poly(butylene oxide), poly(styrene oxide) have shown hydrophobic properties which have the capacity to solubilize hydrophobic drugs [70, 71]. Poly(ethylene oxide)-poly(propylene oxide)-poly(ethylene oxide) copolymers, which are called Poloxamer or Pluronic[®] under the trademark of BASF, are often exploited as BCPs for solubilizing hydrophobic drugs and preparing PM formulations [72]. Particularly, Pluronic[®] polymers were employed to manufacture the SP1049C

formulation which is composed of the mixture of Pluronic[®] F127 and Pluronic[®] L61. Doxorubicin loading was 8.2 % and SP1049C had a particle size of 30 nm and well-defined spherical morphology in aqueous solution [72].

Polyesters are other exemplary polymer candidates which are frequently used in the formulation design of PMs. Synthesis of polyesters is commonly done by ring-opening polymerization (ROP) of cyclic esters and this synthetic strategy is known to produce high molecular weight polyesters with narrow polydispersity [73]. Examples of polyesters for solubilizing hydrophobic drugs are poly(caprolactone) (PCL), Poly(butylactone) (PBL), poly(valerolactone) (PVL), and poly(lactide-co-glycolide) (PLGA) [74, 75]. The BPCs composed of the hydrophobic polyesters and hydrophilic polymers such as PEG were often utilized to formulate PM systems. Micelle formulation prepared using PCL-b-PEG-b-PCL showed high loading capacity up to 28 % [76]. Genexol[®] PM formulation exploits methoxy-poly(ethylene glycol)-block-poly(D,L-lactide) (mPEG-b-PDLLA) (mPEG = 2,000 g/mol and PDLLA = 1750 g/mol, PDI = 1.0–1.2) to solubilize PTX and form PM formulation in aqueous media [77]. Polyesters pose significant advantages due to their biodegradability. The degradation process of the polyester backbone in vivo prevents the undesired accumulation of the polymer in the body, thus reducing the risk of chronic toxicity.

POx BCPs were recently introduced for drug delivery applications and have shown its potential as a drug carrier [53]. Triblock copolymer of POx consists of hydrophobic poly(2-n-butyl-oxazoline) (PBuOx) in the core with two flanking hydrophilic PMeOx blocks have shown unprecedentedly high loading capacity for many hydrophobic drugs [22, 78]. Our group previously reported several polymeric micelle systems composed of POx-BCPs. The triblock copolymer composed of poly(2-methyl-2-oxazoline) (PMeOx) and poly(n-butyl-2-oxazoline) (PBuOx)

(PMeOx-block-PBuOx-block-PMeOx), such as PMeOx-b-PBuOx-b-PMeOx, was mainly exploited to prepare PM formulations. We have screened potential hydrophobic drug candidates and found that many hydrophobic drugs can be efficiently solubilized in this POx system with extremely high loading capacity. For example, PTX was extremely well-solubilized in POx up to PTX concentration of 40 mg/mL in aqueous solution to form well-defined spherical micelles with a size of less than 50 nm [22]. The maximum loading capacity of PTX in POx was up to 50 % which potentially minimizes the amount of excipients in formulation design. Stability studies confirmed that the POx-PTX (POxol) was stable in aqueous media for a month without any loss of PTX from the formulation and in sink conditions PTX was released from the formulation with approximately 100% released at 24 hours. A number of other hydrophobic drugs such as etoposide, 3rd generation of taxanes, and vismodegib were able to solubilize in the POx micelle system with high loading capacity [79-81]. Due to its high loading capacity and safety profile, the POx system has drawn a lot of interest for use as a polymer carrier for drug delivery.

The synthesis of POx can be achieved via living cationic ring opening polymerization process which provides a versatile library of polymer structure with various degrees of polymerization (DP) and limited side reactions [54]. The safety profile analysis of POx polymers in humans have not been conducted yet, which might be a mandatory step for proceeding to the clinical trials using POx-based therapeutics in the future.

1.4 Drug-polymer molecular interaction within PM: theory, modeling and experimental approaches

The self-assembly of amphiphilic BCPs composed of immiscible blocks elicits the formation of micelle architecture in aqueous media when above the critical micelle concentration (CMC) [82]. Several factors such as molecular weight, molar fraction of blocks, chemical structure

of each block of the BCP, and the condition of aqueous solution (polymer concentration, temperature, ionic strength, and pH) may affect the size and morphology of micelle in solution [82]. The assembled micelles feature highly ordered macromolecular structure and segregated hydrophobic compartment in the core with hydrophilic shell on outer surface of the micelle which confines the overall micelle structure. From a thermodynamics perspective, the self-assembly process is driven by the which minimization of interfacial free energy [14]; 1) the aggregated hydrophobic segment which is decreasing the interfacial area with the aqueous environment which reduces interfacial free energy and 2) minimized interfacial free energy by stretched hydrophilic segments which reduces the interaction between hydrophobic segment and water. Kinetic stability of the assembled micelles reveals the dynamic status of the micelles in aqueous media and its stability in solution over time [82]. Upon dilution or external environmental changes, the dynamics among individual micelles such as exchange of individual polymers and the merging/disruption of the micelle structure indicates the stability of the micelle structure over time [82].

Mainly driven by hydrophobic interaction between hydrophobic small molecules and amphiphilic BCPs which have segregated hydrophobic compartments, the hydrophobic small molecules can be physically encapsulated in the core of the micelle during self-assembly process which brings about the formation of polymeric micelle in aqueous solution. The hydrophobic interactions among encapsulated drug and hydrophobic block not only assist the formation of the micelle, but also further stabilize micelle structure in solution. Additional hydrophobic interaction (cohesive forces) such as van der Waals forces driven by the proximity of hydrophobic drug and hydrophobic segment of the polymer in the core could lower CMC of the micelle, resulting in further stabilization of the micelle structure upon dilution [83, 84]. Other molecular interactions

such as hydrogen bonding or pi-pi interaction are known to affect CMC values of drug-loaded PMs, which facilitate enhanced stability of the micelle [85].

Theoretical understanding of solubilization process of poorly soluble drugs by hydrophobic segment of block copolymer can be helpful to design novel chemical structure of delivery carrier so that efficient delivery system can be constructed, while sparing loss of time and cost for experiments based on trial-and-error learning for the formulation design. Various computational approaches have been proposed to predict the compatibility between drug and polymer during the encapsulation process, such as solubility parameters (SP) [86], Flory-Huggins (FH) parameters [87], molecular dynamics (MD) [88], and quantitative-structure properties relationship (QSPR) [89]. Validating the prediction data from aforementioned approaches has been performed by experimental approaches and the interpretation from those investigations gave us comprehensive insight into the plausible molecular interactions during micelle formation and a guidance to the development of molecular interaction-based delivery system.

In depth physicochemical analysis of drug-loaded PM by experimental approaches have revealed detailed molecular interaction between the drug and the polymer both during self-assembly process and in dynamics of PM in solution. In-depth investigation of the molecular interactions provides explanations for the role of structural factors of both components in PMs. Recent studies on the experimental analysis of PM have shown that the drug-polymer compatibility was achieved via more complex molecular interactions than simple hydrophobic interaction [79, 90, 91]. In this section, we will describe computational and experimental approaches to explain the solubilization process by PM and showcase the recent progress on the characterization of PM for efficient design of polymer-based delivery system.

1.4.1 Theoretical approaches

Hildebrand and Hansen solubility parameters

Solubility parameters (SP) originally attempted to describe the miscibility of two components, where similar SP values are predicted to be miscible [92, 93]. Hildebrand and Hansen approaches have been largely employed to calculate SP; Hildebrand proposed SP calculation based on the square root of the cohesive energy density to describe molecular self-interaction energies, which provides a numerical value indicating the miscibility of two components and given in MPa (Equation 1).

$$\delta_{HIL} = \sqrt{\frac{E_{coh}}{V}} = \sqrt{CED} \quad (\text{Equation 1})$$

Where:

δ_{HIL} = Hildebrand solubility parameter,

E_{coh} = cohesive energy,

V = total volume,

CED = cohesive energy density

According to the Hildebrand SP, two components are predicted to be miscible when the difference in SPs is less than 3.7 MPa. In order to take a wider range of molecular interaction such as dissimilar patterns of polar and hydrogen-bonding interactions into consideration, Hansen SP is expressed as partial energies of cohesion, which described as the square root of a sum of dispersion, dipolar, and hydrogen-bonding component (Equation 2) [92].

$$\delta_{HAN} = \sqrt{(\delta_d^2 + \delta_p^2 + \delta_h^2)} \quad (\text{Equation 2})$$

Where:

δ_{HAN} = Hansen solubility parameter,

δ_d = partial dispersion component,

δ_p = partial dipole- dipole component,

δ_h = partial hydrogen- bonding component

In case of Hansen SP, two components are predicted to be miscible when the difference in SPs is less than (or equal) to the Hansen SP sphere radius (Equation 3) [93].

$$4(\delta_{d1} - \delta_{d2})^2 + (\delta_{p1} - \delta_{p2})^2 + (\delta_{h1} - \delta_{h2})^2 \leq R_o^2 \quad (\text{Equation 3})$$

Where:

δ_d = partial dispersion component,

δ_p = partial dipole- dipole component,

δ_h = partial hydrogen- bonding component,

R_o^2 = radius of interaction spehre in Hansen space

Interestingly, several studies on the compatibility prediction by the calculation of Hansen SP values of drug and macromolecules revealed that enthalpies of mixing derived from the calculation of SP could indicate the compatibility of drug and polymer for the solubilization. From this point of view, several studies tried to elucidate the correlation of SP on the solubilization of hydrophobic drugs by amphiphilic polymers.

An exemplary study from Dr. Allen group showcased the application of solubility parameter as the indicator of polymer-drug compatibility in order to formulate anticancer drug, ellipticine [94]. The physicochemical analysis of polymer–drug pairs was performed and the difference in total and partial solubility parameters were compared in order to predict polymer–drug compatibility. The partial and total solubility parameters of polymer candidates and ellipticine were calculated using the group contribution method. Interestingly, the drug loading efficiency for micelle formulation by each polymer candidates were in a good correlation by the prediction of polymer–drug compatibility using solubility parameter. Also, along with the compatibility prediction, the release profile of ellipticine from each formulation was closely released; compatible polymer such as polycaprolactone (PCL) had sustained release of ellipticine up to 6 days, while incompatible polymer such as poly(D,L-lactide) (PDLLA) showed faster release of ellipticine within 3 days. These results indicate that solubility parameters could be applied for the prediction of polymer–drug compatibility including solubilization process and in vitro drug release profile.

Flory-Huggins solution theory

Flory-Huggins (FH) theory was introduced in 1940s and has been utilized to describe the thermodynamic behavior of polymer solution by the estimation of the Gibbs free energy change for mixing of a polymer and a solvent [95, 96]. FH parameter, χ_{FH} , is a scalar quantity that indicate the thermodynamic interaction contributing the enthalpy of mixing of polymer and a solvent (Equation 4) [95, 96].

$$\chi_{FH} = \frac{\Delta H_{mix}}{kTN_1\phi_2} \quad (\text{Equation 4})$$

Where:

χ_{FH} = Flory– Huggins interaction parameter

ΔH_{mix} = enthalpy change upon creation of a binary mixture,

k = Boltzmann constant,

T = Absolute temperature

N_1 = number of molecules of solvent

ϕ_2 = volume fraction of polymer

According to FH theory, two components are predicted to be miscible if χ_{FH} is less than 0.5, whereas phase separated if $\chi_{FH} > 0.5$. Values can be obtained by either SP values calculated for each component or MD approach. Compared to the values calculated from SP values, the combination of and MD produces more reliable predictions on drug-polymer compatibility due to MD approaches being able to include the conformational factors such as hydrogen bonding or spatial distribution of hydrophobic drug in the core [97]. The FH theory has been further developed in order to predict the compatibility of polymer and drug in drug formulation development. Recently, several studies have reported the utility of FH theory for the efficient design of polymer for drug delivery.

Michael et al reported the application of FH interaction parameter for the prediction of the solubilization of model drug, bicalutamide in methoxy-poly(ethylene glycol)-b-poly(carbonate-co-lactide) (PEG-b-P(CB-co-LA)) block copolymer. Chemical modification of methoxy-poly(ethylene glycol)-b-poly(L-lactide) (PEG-b-PLLA) with carbonate moieties enhanced the loading of bicalutamide and the prediction made by FH interaction according to the addition of carbonate groups were consistent with the actual drug loading amount in the micelle formulation [98]. In another study, Mahmud et al. reported that the calculation by FH interaction parameters

for cucurbitacine I (CuI) and various block copolymer candidates for the efficient solubilization and controlled release of CuI from micelle system [99]. They found that the prediction by FH parameters were correlated with the compatibility of polymer–drug resulting in higher loading of the drug in the micelle formulation. Interestingly, the release profile of the drug was not closely related to FH parameters, rather related to the viscosity of the core in the micelle which probably hinder the diffusion of the drug from the core of micelle.

More recently, some studies revealed that FH parameter calculations by solubility parameters do not effectively indicates the solubility of hydrophobic drugs in PM formulations. Lubtow et al reported that empirical determinations of the properties of poorly soluble drugs were more important and the prediction by FH to obtain the reliable prediction data [100]. Also, HSP were able to predict the trend regarding good and poor solubilized, but the overall prediction capacity was unsatisfying. Thus, calculation of FH interaction parameters with molecular dynamics (MD) is often employed in order to improve the prediction for polymer–drug compatibility. Erlebach et al. recently reported their work on the evaluation of polymer–drug compatibility in PEG-PLA micelle system [101]. They obtained FH interaction parameter from MD simulation, thereby explicitly includes specific interaction between the drug and polymer chains; MD simulations were able to effectively include molecular interactions such as hydrogen bonding, conformational factors of drug and polymer in micelle. The prediction from those FH parameters was closely related to the encapsulation of hydrophobic molecules in a given polymer system, PEG-PLA. Though FH parameters have been largely exploited for prediction of compatibility of polymer–drug, these two different studies indicate us the necessity of the development of smarter prediction system for drug solubilization process.

1.4.2 Computational modeling approaches

Molecular dynamics (MD)

Computational approaches such as molecular dynamics (MD) has been extensively utilized to investigate the molecular interactions on PM and obtain microscopic insight of molecular interaction in modeling [102]. MD is theoretically based on Newton's second law and traces the successive molecular motions or conformational changes of the components in solution based on the computation of the interactions among molecules in the modeling [103]. In case MD simulation on PM formulations, the interactions among hydrophobic drug and BCPs are computed to generate the next successive conformations in a given modeling, which indicates the process of self-assembly including the drug loading in the core [102]. To elucidate the molecular dynamics of drug delivery system such as polymeric micelle, fully atomistic simulations are often inappropriate due to the time scale of the simulation (usually in the order of microseconds or longer for molecular interaction within PM), thus coarse-grained (CG) simulations are more frequently exploited, which the number of degree of freedom is reduced in order to expedite the molecular simulations [102]. A number of MD modeling on PM formulations have been conducted to investigate the drug loading and molecular interactions within PM formulation.

Patel et al. successfully performed a series of studies on MD modeling for PM formulation to elucidate the essential factors on hydrophobic solubilization using poly(ethylene glycol)-b-poly(caprolactone) (PEG-b-PCL) [104-106]. In their first study, they found that MD modeling could successfully predict the solubility of model drugs (fenofibrate and nimodipine) in PEG-b-PCL with a good agreement of experimental data. In subsequent studies, the MD modeling figured out that another model drug (cucurbitacin) had enhanced solubility in a given polymer with increasing PCL/PEG ratio due to additional polar interactions and hydrogen bonds among

cucurbitacin and PCL block. When PCL block was branched to form PEG-b-3PCL, curcubitacin solubility was further enhanced, which is consistent with the outcome from the MD simulation. This study clearly explained how the molecular interaction might be occurring in the core of the micelle with model drug and why effective solubilization of the model drug could be possible by the model polymer via MD simulation.

QSPR (Quantitative structural properties relationship)

MD approaches are often inappropriate for the prediction in large data sets since the MD simulations of large number of PM formulation will require enormous time and cost for such scale of simulation [102]. Instead, statistical approaches can be exploited for the prediction of polymer–drug compatibility and several promising studies have been published recently that highlight the utility of statistic-based computational approach. Quantitative structure-property relationship (QSPR) modeling is based on the statistical analysis of data set, which previously commonly exploited in the field of medicinal chemistry and chemical toxicology for the prediction of efficacy/toxicity of small molecules [107]. Recently, several researches conducted QSPR modeling for the prediction of solubilization and have reported promising results. According to Wu et al QSPR model of doxorubicin loaded PM on four/six-arm star polymers structures using genetic function approximation (GFA) algorithm [89]. The star polymers consisted of six polymers of four-miktoarm star polymers (PCL)₂(PDEA-b-PPEGMA)₂, four polymers of six-miktoarm star polymers (PCL)₃(PDEA-b-PPEGMA)₃ and three polymers of four homoarm star polymers (PCL-b-PDEA-b-PPEGMA)₄. The relationship between drug loading and polymer structure via QSPR approach revealed the quantitative estimation of the drug loading in specific polymers described above.

For maximize the capacity of prediction by QSPR, a larger data set is required to have a statistical analysis by QSPR, which might potentially improve the predictability by QSPR. Recently, our group has published cheminformatics-driven discovery of PM formulation for water-insoluble drugs in order to showcase the rationale design of PM formulation by QSPR approach [78]. Total 41 hydrophobic drugs were tested in PM formulation by using poly(2-oxazoline)-based block copolymer at different concentration either individually and in combination with another drugs, which produces 408 data points as micelle formulation that provides both loading efficiency (LE) and loading capacity (LC) in PMs. With the statistical analysis by QSPR with given dataset above, QSPR approach could predict the solubility of model hydrophobic drugs in POx polymer in terms of both LE and LC with high accuracy up to 75 %. This study demonstrates the prediction capacity of statistics-based approach for drug solubilization and the potential of computer-aided design of drug delivery system.

1.4.3 Experimental approaches

Experimental approaches have been mainly used to determine the physicochemical properties of micelle formulation. Generally, drug loading/release profile and size distribution of micelle have been regarded as the key properties of the polymeric micelle system that largely affect pharmacokinetic profile in vivo. However, molecular-level understanding of the formation of PM via self-assembly is rarely reported though important and promising to understand the internal structure of PM. Detailed molecular interaction between drug and polymer can elucidate the conformational factors that governs the formation of the core and the stability of PM in aqueous solution. For this purpose, experimental approaches to investigate the molecular-level interaction is highly warranted to efficiently design novel polymers for drug delivery. Vague assumption on

the core of PM, namely simple hydrophobic region for dissolving hydrophobic drugs derived from simple core-shell structure of PM, may not be valid and it is necessary to explore the microstructures within PM that potentially govern the solubilization capacity of PMs as well as potentially PK profiles of PM in vivo. In this section, advanced experimental approaches to reveal molecular interaction within the core of PM will be introduced and the application of these approaches in previous literature will be discussed. Particularly, Dr. Luxenhofer group have reported several pioneering as well as pragmatic studies on experimental approaches for elucidating detailed molecular-level interactions within POx micelle architecture. Thus, this section will be rather focused on POx-based micelle systems that could be possibly applicable other PM systems for hydrophobic small molecule delivery.

Nuclear magnetic resonance (NMR)

Advanced NMR techniques have been employed for characterization of PMs to reveal the molecule interaction between drug and polymer in PMs. Solid-state NMR (ssNMR) can be a valid experimental approach to realize non-covalent molecular interaction within the core of PM since the changes in the chemical shifts and the respective line widths may provide clear evidences for drug loading and corresponding molecular interactions and local environment with hydrophobic segment of BCPs. The applications of ssNMR on PM have been recently published and revealed interesting results that provides us detailed insight into the internal core of PM. The work by Callari et al. showcased the utility of 1D and 2D solid-state NMR spectroscopy (ssNMR) to investigate a correlation between drug loading and physicochemical properties of micelle formulation, which ultimately affects in vitro cytotoxicity [108]. The micelle formulation was prepared using glycopolymers composed of a fructose hydrophilic block and a PMAA block and by the conjugation

of platinum drug (Phen-Pt) with carboxylic groups of the PMMA block. From ssNMR analysis of their micelle formulation, they found that, based on the loading of platinum drug via conjugation, swelling and mobility of core and shell of the micelle was largely affected, resulting in the higher cellular uptake and subsequent higher toxicity in low loading micelle. The low loading micelle had softer hydrophilic shell and enhanced interaction of sugar moieties with cells, resulting in higher uptake and higher toxicity.

Another study done by Poppler et al reported the investigation of structural model of PMs with various drug loading via physical entrapment by using ssNMR [91]. They used poly(2-oxazoline)-based block copolymers and curcumin as model hydrophobic drug to prepare PM formulation in the study. Interestingly, ssNMR analysis revealed that the degree of curcumin loading in PM affected the localization of the drug in the core, where primarily curcumin accumulated in the core at low loading via hydrogen bonding between phenolic OH group of curcumin and amide group of polymer backbone, whereas, as the drug saturated towards high loading in the micelle, the drug located at the hydrophilic-hydrophobic interface via molecular interaction between carbonyl-carbon of hydrophilic polymer and and interpolymer structure among hydrophilic chains.

2D NMR techniques were applied to examine the molecular interaction within PMs. Recently, Haider and coworkers reported their finding on the role of hydrophilic block on the solubilization of hydrophobic drugs in block copolymer system and rebutted the oversimplified structure of PMs in previous literature [109]. According to their results, it was highlighted that the interaction between hydrophilic segment of block copolymer and hydrophobic drug affects the physicochemical properties of PMs; unprecedentedly high loading capacity of poly(2-oxazoline)-based block copolymer was possible in part due to the function of hydrophilic segment of block

copolymer, poly(2-methyl-2-oxazoline)s (PMeOx). On the contrary, poly(2-ethyl-2-oxazoline)s (PEtOx) as hydrophilic shell were not able to achieve such high loading capacity due to the interaction with hydrophobic drug loaded in the core as the loading capacity increases, resulting in the collapse of the PMs in aqueous solution. The interaction between hydrophilic shell and the drug in the core was extensively analyzed via NMR techniques. ¹H diffusion-ordered spectroscopy (DOSY) study revealed the averaged diffusion coefficient of each PMs which indicates hydrodynamic volumes of each PMs, which indicate the molecular interactions between hydrophilic shell and loaded hydrophobic drug. The DOSY analysis could precisely measure the characteristics of PMs (hydrodynamic volumes), while the difference of hydrodynamic size by dynamic light scattering (DLS) was marginal in each PMs. Moreover, nuclear overhauser effect spectroscopy (NOESY) analysis could analyze micelle structures in aqueous media and reveal that PEtOx units are in close proximity of hydrophobic core, while PMeOx units are remaining separated from the core. This novel study indicates significant but less known factors, the role of hydrophilic segment in block copolymers, for designing novel polymers for efficient PM delivery system.

Small angle neutron scattering (SANS)

SANS is an experimental method to investigate macromolecular structure ranging from nanometer to micrometer by using elastic neutron scattering at small angle of scattering. Earlier studies reported the analysis of PM by SANS to reveal the microstructure of PMs such as CMC and morphologies of micelle core and corona [110]. More recently, further applications of SANS on the analysis of the architecture of PM have been published that disclosed microstructures in the core of PMs that derived from the interactions between model drug and BCPs.

Schultz et al. reported interesting study on the morphological change of PM formulation upon the incorporation of paclitaxel in POx-based PM (POx-PTX) [79]. Dynamic light scattering (DLS) analysis of POx-PTX revealed that the hydrodynamic size distribution of POx in the absence of PTX was about 200 nm, while POx-PTX PM had well-defined spherical micelles by the incorporation of PTX in POx. Further physicochemical analysis of POx-PTX by SANS revealed that wormlike micelle of POx in the absence of PTX was changed to spherical morphology above a certain level of PTX encapsulation (>8% PTX loading), where the encapsulation of paclitaxel in the core formed raspberry-like micellar core and drove the overall micelle structure into spherical in aqueous media. Each raspberry microstructures had several nm size and were aggregated each other to form the core of POx-PTX. This study firstly showed the microstructures in PMs that potentially assists extraordinary high-loading capacity of POx-based PMs.

Dr. Luxenhofer group recently reported an interesting study about the structural changes of PM depending on drug loading that enables ultra high loading capacity via SANS techniques [109]. By constructing PMs using model drug, curcumin, and model polymers synthesized from poly(2-oxazoline) and poly(2-oxazine), they figured out the residence of curcumin in the core and partitioning of the drug along with the loading capacity. At low loading capacity, curcumin mainly resides in the core of the micelle. As the loading of curcumin increases, an inner shell is formed which favorably interacts with curcumin and assists further solubilization up to ultra-high loading capacity. This is the first study that revealing the unexpected role of hydrophilic chain in drug solubilization process by BCP that further assists drug solubilization by the formation of inner-shell. The author concluded that core-inner shell-outer shell enabled such ultra-high loading capacity of curcumin in given PMs beyond our current knowledge as well as expectation.

1.5 General considerations regarding physicochemical properties of PMs

Physicochemical properties of PM products are closely related to the success of novel PM in clinical trials. The physicochemical properties must be well analyzed to validate the characteristics of the PM products as the form of certificate of the analysis (COA) to avoid unexpected inconsistency of the physicochemical properties from the manufacturing process of the PM [111, 112].

First of all, loading capacity of drug within PM and ratio of drug to excipient can be one of the significant factors for successful PM products as therapeutics. Higher loading capacity of PM is highly warranted as it potentially reduces the amount of excipient being used in the formulation, thus minimizing unexpected toxicity derived from the excipients. The toxicity derived from excipients have often occurred in patients and it was the main reason for limiting dosage of drug formulation for treatment. For examples, Taxol[®] formulation consists of Cremophor ER and anhydrous ethanol [113]. Though Taxol[®] have shown anti-cancer efficacy on human patients and still approved for humans, these toxic excipients caused severe toxicity issue in human patients and forced minimizing the dosage of Taxol[®], resulting in reducing dose of PTX [113]. Due to biocompatibility profile of BCPs, PM formulation that encapsulates PTX have shown reduced excipient-derived toxicity. For instance, it was proven that General PM formulation was much safer than Taxol[®] in cancer patients (390 and 200 mg/m², respectively) and no hypersensitivity reactions which often observed in Taxol[®] treatment [9]. NK105 formulation also have shown improved safety profile in clinical trial. In phase III trial in 2016, it was reported that NK105 could reduce PTX-related toxicity with higher dose compared to Taxol[®] [114]. Another study done previously by our group showed that high loading capacity of PTX in POx micelle formulation had superior safety in preclinical animal model [22]. POx formulation could encapsulate paclitaxel

up to 1:1 ratio of drug and excipient, resulting in loading capacity of 50%. Maximum tolerated dose of paclitaxel in mouse was about 7.5 fold higher in POx micelle (150 mg/kg) compared to that of Taxol (20 mg/kg) [22]. This study indicates that both biocompatibility of excipient and high loading capacity are required to minimize excipient-derived toxicity. High loading capacity is also important for combinational PM formulation that may contain two or more drugs in a single micelle as combination therapy. For effective and safe delivery of drug combination, the combination drugs should be well-solubilized in PM so that the amount of the excipient and injection volume could be minimized for parenteral injection [115, 116].

Secondly, hydrodynamic size of PM would be another important factor to consider for clinical application of potential PMs. It is well-established that the size distribution of nanomedicine may affect biodistribution of nano-sized particles when administered, resulting in either extended systemic circulation or faster clearance from the body. Particles with size ranging over 200 nm may be caught by the liver, while too smaller size of nanoparticles less than 10 nm would be easily cleared by the kidney [117]. In previous studies, it was proven that size from 50 nm–100 nm is effective in terms of systemic circulation in preclinical model, suggesting ideal particle size distribution is necessary for efficacy of PMs [118, 119]. In terms of the size of PMs in clinical trials, one can see the size of those PM formulations are less than 100 nm [6, 8]. Thus, one may speculate that size range from 20 nm to 100 nm can be conceived as good properties as PMs. Of course, other factors that affect the hydrodynamic size of PMs must be clarified to confirm the effect of the size of PM in systemic circulation. Such factors are 1) effect of dilution of PMs by plasma that might alter the hydrodynamic size of PMs during administration, 2) surface charge and morphology/shape of PMs that affects biodistribution of PMs in systemic circulation, and 3)

release profile of drug from PMs which subsequently affect the hydrodynamic size of PMs in systemic circulation.

Stability of PM and drug release profile from PM in systemic circulation are important factors in that these dynamic status of PMs govern drug exposure to systemic circulation. First of all, CMC of PM should be low enough to endure extreme dilution upon infusion, thus the micelle structure would be intact during the systemic circulation to avoid unexpected drug loss and achieve ideal delivery of the drug [2]. Also, it should be noted that PM formulation in which drug loaded via hydrophobic interaction exists as dynamic state, resulting in gradual drug release into external environment [120]. In fact, unlike PM formulations prepared via stable covalent conjugation which may only react upon external stimuli and release the cargo via the cleavage of the covalent bond, PM formulations that physically encapsulate hydrophobic drugs are gradually releasing drug via both diffusion of the drug from the core and drug binding to serum proteins. Thus, PM formulation may exist in systemic circulation as dynamic state, resulting in various forms of hydrophobic drug; encapsulated drug and unencapsulated drug (free (unbound) drug and protein-bound drug)). For careful evaluation of those forms that highly related to therapeutic outcome, the stable isotope tracer ultrafiltration assay (SITUA) was previously reported by Skoczen et al and this approach enabled the analysis of drug forms in systemic circulation in preclinical animal model [121]. The approach uses isotopes of the model drug and separate the aforementioned forms by ultracentrifugation method. For examples, paclitaxel isotopes were employed in preclinical animal model to investigate the dynamics of Genexol[®] PM in mouse model (Summary for US FDA, Inter-Agency Award 224-16-3001S). Meticulous analysis of drug forms in vivo may indicate PK profiles and subsequent therapeutics outcome from given formulation as well as possibility of

bioequivalence to reference formulation that assist further possibility for clinical trials via 505(b)(2) approval process.

Manufacturing process of PM should be well considered in order to produce micelle formulation with consistent physicochemical properties and desired scale of production. The selection of applicable manufacturing process may largely impact on characteristics of the final PM formulation such as drug loading, size distribution and stability of PM in aqueous media. Several manufacturing processes have been introduced to produce PM in a larger scale such as film hydration method [78], co-solvent evaporation [122], direct dissolution [123], dialysis [124], and oil-in-water emulsion [124]. For manufacturing of PM several factors should be considered such as the usage of organic solvent, number of overall steps, yield of the PM from the pure drug and excipient, sterilization process for endotoxin-free formulation, and final formulation design (solution or lyophilized powder for reconstitution with injectable distilled water). Supposedly, minimal step of manufacturing of PM is highly warranted and for this purpose, thin film hydration method could be the best option since 1) less number of step 2) easy to remove organic solvent during film formation 3) no needs to dialysis and avoid potential contamination from water. As the final formulation, lyophilized powder form is a better option since it may be helpful to avoid potential contamination or drug release/degradation of micelle formulation in aqueous media.

1.6 PMs in clinical trials and regulatory approval for human

1.6.1 Clinical status of PM formulations

A large number of PM formulations for physical entrapment of hydrophobic small molecules have been reported in literature since the earliest reports on PM formulations and such

contribution by researchers has generated PM formulations that have reached clinical trials in USA [4].

Genexol[®] PM

Genexol[®] PM (Cynviloq[®]) is a PM formulation incorporating PTX as active pharmaceutical ingredient (API) originally developed by Samyang Biopharm and the first PM formulation approved for human use in South Korea and other countries for the patient with metastatic breast cancer (MBC), non-small cell lung cancer (NSCLC), and ovarian cancer. Block copolymer composed of methoxy-poly(ethylene glycol)-block-poly(D,L-lactide) (mPEG-b-PDLLA) (mPEG = 2,000 g/mol and PDLLA = 1750 g/mol, PDI = 1.0–1.2) was employed to manufacturing the product by solid dispersion method and the micelle featured nano-sized PM with well-defined spherical structure in aqueous media (20–50 nm in diameter and 16.7% loading capacity of PTX in PM) [6]. In sink condition, paclitaxel was slowly released out with 65% released at 24 hours and 95% released at 48 hours.

In phase I trial revealed that General PM had shown improved safety in healthy human candidates and less hypersensitivity reaction after treatment [9]. The dose was determined as to 390 mg/m² for Genexol[®] PM and 200 and 300 mg/m² for Taxol[®] and Abraxane[®], respectively [9]. Based on safety profile of Genexol[®] PM, in multi-centered phase II study was performed on cancer patients with advanced breast cancer non-small cell lung cancer (NSCLC) with the dose ranged from 230 to 435 mg/m², which is higher than the common dose for Taxol[®] (approx. 170 mg/m²) [10]. Phase II study on MBC patients reported anticancer efficacy of Genexol[®] PM with the overall response rate (ORR) of 58.5%, which is superior than that of Abraxane (47.6%) and Taxol (21–54%). With effective therapeutic outcome in clinical trials conducted in South Korea, Genexol[®]

PM received regulatory approval in South Korean and other countries (Philippines, India, and Vietnam) for the treatment of human cancers such as MBC, NSCLC, and ovarian.

Clinical development of Genexol[®] PM in USA (under the trade name of Cynviloq[®]) was initiated by Sorrento Therapeutics after the exclusion distribution rights to Genexol[®] PM was acquired by Sorrento Therapeutics in 2013. In 2014, bioequivalence studies of Cynviloq[®] versus Abraxane[®] were conducted in patients with metastatic or locally recurrent breast cancer and patients with NSCLC (NCT02064829). Preliminary positive data in eight patients was reported in 2014 which possibly support bioequivalence and the bioequivalence of Cynviloq[®] to Abraxane[®] could grant 505(b)(2) pathways by the FDA, which potentially expedite the regulatory process as the pathway could eliminate the extensive clinical trials to validate efficacy versus the standard of care. Unfortunately, no updates are available on the bioequivalence on this potential PTX-loaded nanomedicine since Cynviloq[®] was acquired in 2015 by NantWorks which was founded by Dr. Patrick Soon-Shiong, who developed Abraxane[®].

NK105

NK105 is PTX-loaded PM formulation that was originally developed by Dr. Kataoka in early 1990s and advanced to clinical trials (phase III completed, NCT01644890). Block copolymer composed of poly(ethylene glycol)-block-poly(aspartate) (PEG-b-P(Asp)) (PEG = 12,000 g/mol and P(Asp) = 8,000 g/mol) was chemically modified, where P(Asp) was conjugated with 4-phenyl-1-butanol via esterification reaction to enhance drug-polymer compatibility and drug loading in the micelle [8]. About half of carboxylic acid groups in P(Asp) was converted to 4-phenyl-1-butanolate and loading capacity of PTX in NK105 was 23% and hydrodynamic size of NK105 in aqueous media was 85 nm.

In a phase I trial, NK105 at the dose of 150mg/m² showed significantly enhanced PTX exposure to tumor and increased drug concentration in blood compared to that of Taxol[®] at the dose of 210 mg/m² [114]. Also, side effect of PTX such as neurotoxicity was less seen in the group of NK105 than in the group of Taxol[®]. Subsequent phase II trial of NK105 on the patients with advanced stomach cancer revealed that the clinical efficacy of NK105 was modest with ORR of 25%, the median progress free survival (PFS) of 3.0 months, and the median overall survival (OS) of 14.4 months [125]. In July 2016, phase III study completed and the results from the study revealed that NK105 could not reach primary end point of the study in patient with metastatic or recurrent breast cancer [126]. In clinical trials, NK105 could only demonstrate the safety profile of PTX over conventional products.

SP1049C

SP1049C is doxorubicin (DOX)-loaded Pluronic[®]-based PM formulation developed by Dr. Kabanov group and entered Phase II clinical trials that have shown positive results [11]. The formulation was prepared using a blending of two Pluronic[®] block copolymers (L61 and F127) that consist of poly(ethylene oxide) (PEO) and poly(propylene oxide) (PPO) at 1:8 weight ratio of L61:F127 [72]. Physicochemical analysis of SP1049C revealed that the micelle had well-defined spherical morphology with a size of less than 30 nm and DOX loading capacity in SP1049C was 8.2 %. According to Batrakova et al, Pluronic[®] L61 exhibited sensitization of resistant cancer cell, thereby enhancing the cytotoxicity of DOX and F127 showed stabilization of DOX-loaded micelle formulation in aqueous solution [72].

In phase I clinical trial for SP1049C in 1999, SP1049C exhibited similar PK profile of DOX to conventional DOX formulation with similar MTD dose of 70 mg/m² in the patients with

metastatic or recurrent solid tumors [127]. Interestingly, DOX-related toxicity such as hand–food syndrome was less seen in the group of SP1049C compared the group of conventional DOX.

Later, Phase II trial of SP1049C demonstrated improved efficacy of DOX in the patients with advanced carcinoma of the esophagus and gastroesophageal junction with response rate of 47% and clinical benefit (response rate accompanying stable disease) of 89% [11]. The phase II study confirmed that the efficacy of SP1049C was comparable to that of conventional DOX treatment (the median OS of 10 months and PFS of 6.6 months). In 2008, FDA granted an orphan drug designation for SP1049C, however, since then no clinical data has reported.

Nanoxel-M

Nanoxel-M is PM formulation for docetaxel (DTX) that developed by Samyang Biopharm and currently under clinical evaluation. Block copolymer composed of methoxy-poly(ethylene glycol)-block-poly(D,L-lactide) (mPEG-b-PDLLA) was exploited to manufacture Nanoxel-M via thin-film hydration method, thereby producing nano-sized micelle solution that has mono disperse and narrow size distribution with hydrodynamic size of 25.4 nm with a short term of stability up to 6 h in saline [128].

Phase I clinical trial was conducted in South Korean and the study reported that Nanoxel-M had superior safety profile than conventional docetaxel formulation in patients with advanced solid tumor [128]. Due to its comparable efficacy and superior safety, Nanoxel-M received regulatory approval in South Korea in 2013. Currently phase II (NCT02639858) and phase III trials (NCT-2982395) are recruiting cancer patients in South Korea to evaluate Nanoxel-M antitumor efficacy.

1.6.2 Bioequivalence of PM formulations

Complicated process of PM dynamics in systemic circulation requires advanced analytic technique to investigate release process of the drug from PM and several forms of PMs which are closely related to therapeutic outcome. Indeed, when PMs administered systemically, PMs may exist in several forms; a) PM-encapsulated, b) unencapsulated, free/unbound, and (c) unencapsulated, protein-bound [121]. The ratio of all three fraction may vary based on the physicochemical properties of the drug such as protein-binding, aqueous solubility, and drug–polymer compatibility. Identification of PM forms in systemic circulation is essential to investigate the therapeutic efficacy of drug based on PK profile of PM as well as to determine bioequivalence of one nanoformulation to reference nanomedicine.

National Characterization Lab (NCL) have investigated comprehensively on a novel bioanalytical technique to fractionate nanomedicine subpopulation in preclinical model. Recently they reported summary for study on nanomedicine bioequivalence which showcase pragmatic methodology as the guidance for the measurement of PM subpopulations in serum [121]. They reported extensive bioequivalence studies on several nanomedicines to compare PK profiles to reference products (Janssen’s Doxil[®] vs. Sun Pharma’s Doxorubicin hydrochloride (DOX•HCl) liposome formulation and Celgene’s Abraxane[®] vs. Samyang’s Genexol[®]-PM) (Summary for US FDA, Inter-Agency Award 224-16-3001S). The stable isotope tracer ultrafiltration assay (SITUA) was employed in the analysis of serum samples of animal model in order to separate the subpopulation of each product. Analysis by the SITUA method demonstrated that both DOX nanoformulations (Doxil[®] and Sun Pharma’s formulation) had comparable PK parameters (unencapsulated DOX and encapsulated DOX). Also, PTX nanoformulations (Abraxane[®] and Samyang’s Genexol[®]-PM) showed very similar PK profiles of PTX subpopulations. However,

bioequivalence analysis by statistical analysis (two one-sided t-test) revealed that both DOX nanoformulations and PTX nanoformulations were not bioequivalent. This novel methodology showcased advanced analysis of subpopulations of nanoformulation which closely related to therapeutic outcome as well as pragmatic analytical approach to determine bioequivalence of one formulation to reference product to grant 505(b)(5) regulatory process.

1.6.3 PM formulations for combination therapy

Combination therapy has been largely exploited for treatment of various type of cancer, based on related pathways on oncogenesis or combination of the agents that affects tumor microenvironment (TME) [129]. Frequently employed type of combinations are 1) combination of chemotherapies for killing cancer cells, 2) combination of chemotherapy with additional agents such as TME modifiers, or more recently 3) combination of immunotherapy with anticancer agents to induce anti-tumor immunotherapy [129]. Ideal combination therapy requires precise drug combination exposure to induce synergistic therapeutic efficacy, thus administration and subsequent disposition of combination to target tissue with desired ratio of the combination is highly warranted [130]. For combination therapy of potent small molecules, therapeutic outcome of the combinations of the small molecules are hindered due to their physicochemical properties that ultimately affect PK profile of the combination therapy. One of main factors that determine PK profile of small molecule drug is aqueous solubility including lipophilicity as these physicochemical properties hinder the administration via parenteral route and increase non-specific serum protein binding. For this reasons, effective solubilization of hydrophobic small molecules which ultimately co-encapsulation of combination in single micelle is of essential importance for successful combination therapy for hydrophobic small molecules. In clinics, one

liposomal formulation, CPX-351 (Vyxeos[®]) received regulatory approval by USFDA in August 2017 for treatment of adult patients with chronic lymphocytic leukemia (CLL) or small lymphocytic lymphoma (SLL) [131]. The clinical trials on CPX-351 revealed a significantly reduced mortality risk with increase in the median overall survival (Hazard ratio (HR) of 0.69; P = 0.005)

Currently no PM formulations for combination therapy is FDA approved for treatment of cancers, but PM formulation design of pharmacologically effective drug combination is highly warranted in order to deliver drug combo to target site at the desired ratio of the combination. For this purpose, PM formulations have been frequently employed to 1) solubilize drug combinations in the micelle formulation, 2) deliver drug combination to target site with desired ratio of combination therapy.

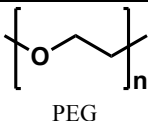

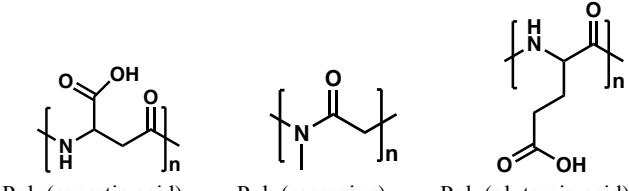
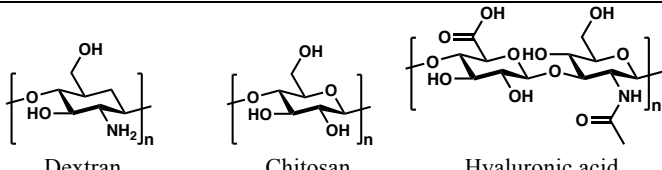
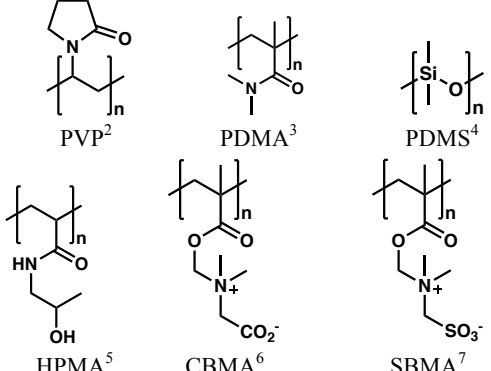
1.7 Conclusion

PM formulation for hydrophobic small molecules have been extensively studied over three decades as an ideal delivery platform for drug delivery. With successful preclinical results, several PM formulations have entered clinical trials, but only a few have received regulatory approval for human use. The main reasons for these failures in clinical trials were limited efficacy of the drug in the PMs and the toxicity profiles of the encapsulated drug.

In this review, we extensively described PM formulations for delivery of hydrophobic small molecules. BCP segments required for forming amphiphilic copolymers were described in order to aid in the proper selection of BCP components for the efficient solubilization of target hydrophobic small molecules. To improve our understanding on drug solubilization, multi-disciplinary approaches for investigating detailed molecular interactions between hydrophobic segments of BCPs and encapsulated drugs were described. Interestingly, hydrophobic interaction, which is occurring in the core of PMs, is much more complex than simple hydrophobic compartment providing hydrophobic environment for the drugs. Indeed, conformational factors were closely related to the solubilization process and even the hydrophilic shell plays a significant role in improving drug solubility in PMs.

Clinical investigations of PM formulations have revealed promising therapeutic outcomes for human use, while we also have witnessed a number of clinical trial failures from other PM formulations. Comprehensive analysis of PK profile of PM formulations in preclinical models and subsequent correlation of PK profile in human patients are highly warranted. For these reasons, advanced PK analysis of PMs to investigate subpopulations of PMs is necessary, and recently SITUA method has revealed dynamic status of PMs in systemic circulation.

PM formulations hold a clinical importance as delivery platform for potential hydrophobic small molecules, and for this purpose current PM formulation systems have to further evolve to serve as efficient drug carriers. We believe that the comprehensive analysis of drug encapsulation and subsequent drug release profile in systemic circulation will provide us insight for the future design of novel PM systems for human use.

Polymer	Chemical structure	Synthesis
PEG ¹	 PEG	Ring-opening anionic polymerization
Poly(2-oxazoline)s	 Poly(2-methyl-2-oxazoline) Poly(2-ethyl-2-oxazoline)	Living cationic ring-opening polymerization
Polyamino acids	 Poly(aspartic acid) Poly(sarcosine) Poly(glutamic acid)	Ring-opening polymerization of amino acid derivatives
polysaccharides	 Dextran Chitosan Hyaluronic acid	Enzymatic synthesis
Miscellaneous	 PVP ² PDMA ³ PDMS ⁴ HPMA ⁵ CBMA ⁶ SBMA ⁷	-

¹ poly(ethyleneglycol), ² polyvinylpyrrolidone, ³ poly(*N,N*-dimethylacrylamide), ⁴ poly(dimethylsiloxane), ⁵ poly[N-(2-hydroxypropyl) methacrylamide], ⁶ poly(carboxybetaine methacrylate), ⁷ poly(sulfobetaine methacrylate)

Table 1.1 Hydrophilic polymers commonly used for constructing PMs

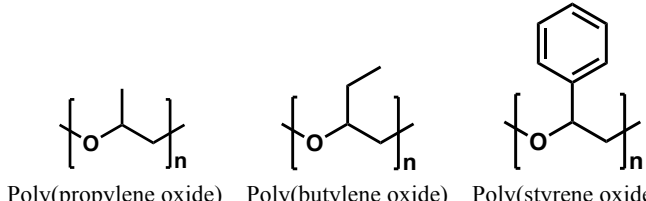
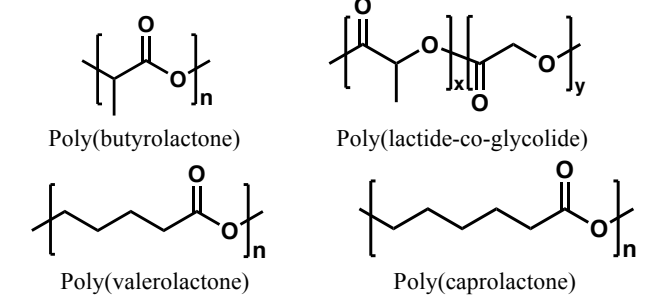
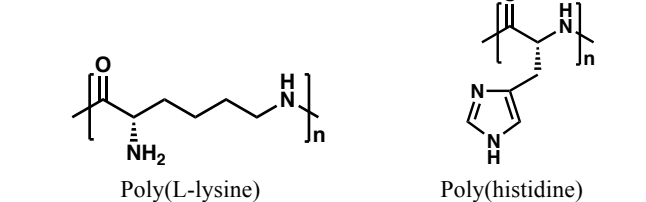
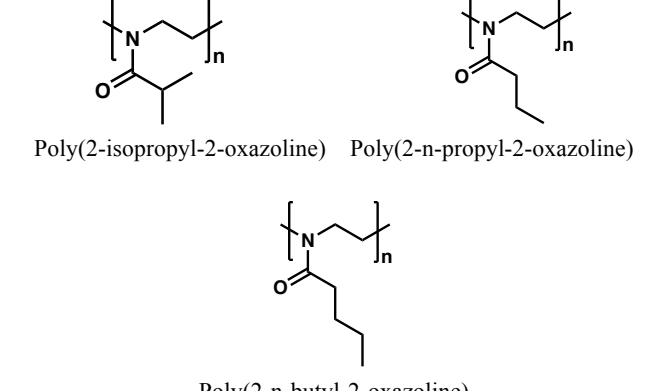
Polymer	Chemical structure	Synthesis
Polyethers	 <p>Poly(propylene oxide) Poly(butylene oxide) Poly(styrene oxide)</p>	Anionic ring-opening polymerization
Polyesters	 <p>Poly(butyrolactone) Poly(lactide-co-glycolide) Poly(valerolactone) Poly(caprolactone)</p>	Polycondensation reaction
Polyamino acids	 <p>Poly(L-lysine) Poly(histidine)</p>	Ring-opening polymerization of amino acid derivatives
Poly(2-oxazoline)s	 <p>Poly(2-isopropyl-2-oxazoline) Poly(2-n-propyl-2-oxazoline) Poly(2-n-butyl-2-oxazoline)</p>	Living cationic ring-opening polymerization

Table 1.2 Hydrophobic polymers commonly used for constructing PMs

REFERENCES

1. Bharate, S.S., Bharate, S.B. and Bajaj, A.N., 2016. Interactions and incompatibilities of pharmaceutical excipients with active pharmaceutical ingredients: a comprehensive review. *Journal of Excipients and Food Chemicals*, 1(3), p.1131.
2. Cabral, H., Miyata, K., Osada, K. and Kataoka, K., 2018. Block copolymer micelles in nanomedicine applications. *Chemical reviews*, 118(14), pp.6844-6892.
3. Bader, H., Ringsdorf, H. and Schmidt, B., 1984. Watersoluble polymers in medicine. *Die Angewandte Makromolekulare Chemie: Applied Macromolecular Chemistry and Physics*, 123(1), pp.457-485.
4. Kabanov, A.V., Chekhonin, V.P., Alakhov, V.Y., Batrakova, E.V., Lebedev, A.S., Melik-Nubarov, N.S., Arzhakov, S.A., Levashov, A.V., Morozov, G.V., Severin, E.S. and Kabanov, V.A., 1989. The neuroleptic activity of haloperidol increases after its solubilization in surfactant micelles: micelles as microcontainers for drug targeting. *FEBS letters*, 258(2), pp.343-345.
5. Kwon, G.S. and Kataoka, K., 1995. Block copolymer micelles as long-circulating drug vehicles. *Advanced drug delivery reviews*, 16(2-3), pp.295-309.
6. Kim, S.C., Kim, D.W., Shim, Y.H., Bang, J.S., Oh, H.S., Kim, S.W. and Seo, M.H., 2001. In vivo evaluation of polymeric micellar paclitaxel formulation: toxicity and efficacy. *Journal of Controlled Release*, 72(1-3), pp.191-202.
7. Matsumura, Y., 2008. Poly (amino acid) micelle nanocarriers in preclinical and clinical studies. *Advanced drug delivery reviews*, 60(8), pp.899-914.
8. Hamaguchi, T., Matsumura, Y., Suzuki, M., Shimizu, K., Goda, R., Nakamura, I., Nakatomi, I., Yokoyama, M., Kataoka, K. and Kakizoe, T., 2005. NK105, a paclitaxel-incorporating micellar nanoparticle formulation, can extend in vivo antitumour activity and reduce the neurotoxicity of paclitaxel. *British journal of cancer*, 92(7), pp.1240-1246.
9. Kim, T.Y., Kim, D.W., Chung, J.Y., Shin, S.G., Kim, S.C., Heo, D.S., Kim, N.K. and Bang, Y.J., 2004. Phase I and pharmacokinetic study of Genexol-PM, a cremophor-free, polymeric micelle-formulated paclitaxel, in patients with advanced malignancies. *Clinical cancer research*, 10(11), pp.3708-3716.
10. Lee, K.S., Chung, H.C., Im, S.A., Park, Y.H., Kim, C.S., Kim, S.B., Rha, S.Y., Lee, M.Y. and Ro, J., 2008. Multicenter phase II trial of Genexol-PM, a Cremophor-free, polymeric micelle formulation of paclitaxel, in patients with metastatic breast cancer. *Breast cancer research and treatment*, 108(2), pp.241-250.
11. Valle, J.W., Armstrong, A., Newman, C., Alakhov, V., Pietrzynski, G., Brewer, J., Campbell, S., Corrie, P., Rowinsky, E.K. and Ranson, M., 2011. A phase 2 study of SP1049C, doxorubicin

in P-glycoprotein-targeting pluronics, in patients with advanced adenocarcinoma of the esophagus and gastroesophageal junction. *Investigational new drugs*, 29(5), pp.1029-1037.

12. Cabral, H. and Kataoka, K., 2014. Progress of drug-loaded polymeric micelles into clinical studies. *Journal of Controlled Release*, 190, pp.465-476.

13. Houdaihed, L., Evans, J.C. and Allen, C., 2017. Overcoming the road blocks: advancement of block copolymer micelles for cancer therapy in the clinic. *Molecular pharmaceutics*, 14(8), pp.2503-2517.

14. Kataoka, K., Harada, A. and Nagasaki, Y., 2012. Block copolymer micelles for drug delivery: design, characterization and biological significance. *Advanced drug delivery reviews*, 64, pp.37-48.

15. Owens III, D.E. and Peppas, N.A., 2006. Opsonization, biodistribution, and pharmacokinetics of polymeric nanoparticles. *International journal of pharmaceutics*, 307(1), pp.93-102.

16. Photos, P.J., Bacakova, L., Discher, B., Bates, F.S. and Discher, D.E., 2003. Polymer vesicles in vivo: correlations with PEG molecular weight. *Journal of Controlled Release*, 90(3), pp.323-334.

17. Danson, S., Ferry, D., Alakhov, V., Margison, J., Kerr, D., Jowle, D., Brampton, M., Halbert, G. and Ranson, M., 2004. Phase I dose escalation and pharmacokinetic study of pluronic polymer-bound doxorubicin (SP1049C) in patients with advanced cancer. *British journal of cancer*, 90(11), pp.2085-2091.

18. Lee, H., Zeng, F., Dunne, M. and Allen, C., 2005. Methoxy poly (ethylene glycol)-block-poly (δ -valerolactone) copolymer micelles for formulation of hydrophobic drugs. *Biomacromolecules*, 6(6), pp.3119-3128.

19. Savić, R., Eisenberg, A. and Maysinger, D., 2006. Block copolymer micelles as delivery vehicles of hydrophobic drugs: micelle–cell interactions. *Journal of drug targeting*, 14(6), pp.343-355.

20. Kakizawa, Y. and Kataoka, K., 2002. Block copolymer micelles for delivery of gene and related compounds. *Advanced drug delivery reviews*, 54(2), pp.203-222.

21. Kim, H.J., Miyata, K., Nomoto, T., Zheng, M., Kim, A., Liu, X., Cabral, H., Christie, R.J., Nishiyama, N. and Kataoka, K., 2014. siRNA delivery from triblock copolymer micelles with spatially-ordered compartments of PEG shell, siRNA-loaded intermediate layer, and hydrophobic core. *Biomaterials*, 35(15), pp.4548-4556.

22. He, Z., Wan, X., Schulz, A., Bludau, H., Dobrovolskaia, M.A., Stern, S.T., Montgomery, S.A., Yuan, H., Li, Z., Alakhova, D. and Sokolsky, M., 2016. A high capacity polymeric micelle of paclitaxel: Implication of high dose drug therapy to safety and in vivo anti-cancer activity. *Biomaterials*, 101, pp.296-309.

23. Gaucher, G., Dufresne, M.H., Sant, V.P., Kang, N., Maysinger, D. and Leroux, J.C., 2005. Block copolymer micelles: preparation, characterization and application in drug delivery. *Journal of controlled release*, 109(1-3), pp.169-188.
24. Harada, A. and Kataoka, K., 2006. Supramolecular assemblies of block copolymers in aqueous media as nanocontainers relevant to biological applications. *Progress in polymer science*, 31(11), pp.949-982.
25. Zhang, K., Tang, X., Zhang, J., Lu, W., Lin, X., Zhang, Y., Tian, B., Yang, H. and He, H., 2014. PEG-PLGA copolymers: Their structure and structure-influenced drug delivery applications. *Journal of Controlled release*, 183, pp.77-86.
26. Xiao, K., Li, Y., Luo, J., Lee, J.S., Xiao, W., Gonik, A.M., Agarwal, R.G. and Lam, K.S., 2011. The effect of surface charge on in vivo biodistribution of PEG-oligocholic acid based micellar nanoparticles. *Biomaterials*, 32(13), pp.3435-3446.
27. He, G., Ma, L.L., Pan, J. and Venkatraman, S., 2007. ABA and BAB type triblock copolymers of PEG and PLA: a comparative study of drug release properties and "stealth" particle characteristics. *International journal of pharmaceutics*, 334(1-2), pp.48-55.
28. Logie, J., Owen, S.C., McLaughlin, C.K. and Shoichet, M.S., 2014. PEG-graft density controls polymeric nanoparticle micelle stability. *Chemistry of Materials*, 26(9), pp.2847-2855.
29. Shan, X., Yuan, Y., Liu, C., Tao, X., Sheng, Y. and Xu, F., 2009. Influence of PEG chain on the complement activation suppression and longevity in vivo prolongation of the PCL biomedical nanoparticles. *Biomedical microdevices*, 11(6), p.1187.
30. Shiraishi, K., Sanada, Y., Mochizuki, S., Kawano, K., Maitani, Y., Sakurai, K. and Yokoyama, M., 2015. Determination of polymeric micelles' structural characteristics, and effect of the characteristics on pharmacokinetic behaviors. *Journal of controlled release*, 203, pp.77-84.
31. Lin, W.J., Juang, L.W. and Lin, C.C., 2003. Stability and release performance of a series of pegylated copolymeric micelles. *Pharmaceutical research*, 20(4), pp.668-673.
32. Zhang, Y. and Zhuo, R.X., 2005. Synthesis and in vitro drug release behavior of amphiphilic triblock copolymer nanoparticles based on poly (ethylene glycol) and polycaprolactone. *Biomaterials*, 26(33), pp.6736-6742.
33. Velluto, D., Demurtas, D. and Hubbell, J.A., 2008. PEG-b-PPS diblock copolymer aggregates for hydrophobic drug solubilization and release: cyclosporin A as an example. *Molecular pharmaceutics*, 5(4), pp.632-642.
34. Shi, Y., Lammers, T., Storm, G. and Hennink, W.E., 2017. Physico-Chemical Strategies to Enhance Stability and Drug Retention of Polymeric Micelles for Tumor-Targeted Drug Delivery. *Macromolecular bioscience*, 17(1), p.1600160.

35. Letchford, K., Liggins, R. and Burt, H., 2008. Solubilization of hydrophobic drugs by methoxy poly (ethylene glycol)-block-polycaprolactone diblock copolymer micelles: Theoretical and experimental data and correlations. *Journal of pharmaceutical sciences*, 97(3), pp.1179-1190.
36. Huynh, L., Grant, J., Leroux, J.C., Delmas, P. and Allen, C., 2008. Predicting the solubility of the anti-cancer agent docetaxel in small molecule excipients using computational methods. *Pharmaceutical research*, 25(1), pp.147-157.
37. Hurter, P.N., Scheutjens, J.M. and Hatton, T.A., 1993. Molecular modeling of micelle formation and solubilization in block copolymer micelles. 1. A self-consistent mean-field lattice theory. *Macromolecules*, 26(21), pp.5592-5601.
38. Hurter, P.N., Scheutjens, J.M. and Hatton, T.A., 1993. Molecular modeling of micelle formation and solubilization in block copolymer micelles. 1. A self-consistent mean-field lattice theory. *Macromolecules*, 26(21), pp.5592-5601.
39. Emami, J., Rezazadeh, M., Hasanzadeh, F., Sadeghi, H., Mostafavi, A., Minaiyan, M., Rostami, M. and Davies, N., 2015. Development and in vitro/in vivo evaluation of a novel targeted polymeric micelle for delivery of paclitaxel. *International journal of biological macromolecules*, 80, pp.29-40.
40. Miller, T., Rachel, R., Besheer, A., Uezguen, S., Weigandt, M. and Goepferich, A., 2012. Comparative investigations on in vitro serum stability of polymeric micelle formulations. *Pharmaceutical research*, 29(2), pp.448-459.
41. Song, X., Zhao, S., Fang, S., Ma, Y. and Duan, M., 2016. Mesoscopic simulations of adsorption and association of PEO-PPO-PEO triblock copolymers on a hydrophobic surface: From mushroom hemisphere to rectangle brush. *Langmuir*, 32(44), pp.11375-11385.
42. Gong, C., Shi, S., Dong, P., Kan, B., Gou, M., Wang, X., Li, X., Luo, F., Zhao, X., Wei, Y. and Qian, Z., 2009. Synthesis and characterization of PEG-PCL-PEG thermosensitive hydrogel. *International journal of pharmaceutics*, 365(1-2), pp.89-99.
43. Xiong, M.H., Wu, J., Wang, Y.C., Li, L.S., Liu, X.B., Zhang, G.Z., Yan, L.F. and Wang, J., 2009. Synthesis of PEG-armed and polyphosphoester core-cross-linked nanogel by one-step ring-opening polymerization. *Macromolecules*, 42(4), pp.893-896.
44. Akiyama, Y., Harada, A., Nagasaki, Y. and Kataoka, K., 2000. Synthesis of poly (ethylene glycol)-block-poly (ethylenimine) possessing an acetal group at the PEG end. *Macromolecules*, 33(16), pp.5841-5845.
45. Lila, A.S.A., Kiwada, H. and Ishida, T., 2013. The accelerated blood clearance (ABC) phenomenon: clinical challenge and approaches to manage. *Journal of Controlled Release*, 172(1), pp.38-47.

46. Yang, Q. and Lai, S.K., 2015. Anti-PEG immunity: emergence, characteristics, and unaddressed questions. *Wiley Interdisciplinary Reviews: Nanomedicine and Nanobiotechnology*, 7(5), pp.655-677.
47. Armstrong, J.K., Hempel, G., Koling, S., Chan, L.S., Fisher, T., Meiselman, H.J. and Garratty, G., 2007. Antibody against poly (ethylene glycol) adversely affects PEG-asparaginase therapy in acute lymphoblastic leukemia patients. *Cancer*, 110(1), pp.103-111.
48. Ganson, N.J., Kelly, S.J., Scarlett, E., Sundy, J.S. and Hershfield, M.S., 2005. Control of hyperuricemia in subjects with refractory gout, and induction of antibody against poly (ethylene glycol)(PEG), in a phase I trial of subcutaneous PEGylated urate oxidase. *Arthritis research & therapy*, 8(1), p.R12.
49. Chanan-Khan, A., Szebeni, J., Savay, S., Liebes, L., Rafique, N.M., Alving, C.R. and Muggia, F.M., 2003. Complement activation following first exposure to pegylated liposomal doxorubicin (Doxil[®]): possible role in hypersensitivity reactions. *Annals of Oncology*, 14(9), pp.1430-1437.
50. Kierstead, P.H., Okochi, H., Venditto, V.J., Chuong, T.C., Kivimae, S., Fréchet, J.M. and Szoka, F.C., 2015. The effect of polymer backbone chemistry on the induction of the accelerated blood clearance in polymer modified liposomes. *Journal of Controlled Release*, 213, pp.1-9.
51. Shiraishi, K., Kawano, K., Maitani, Y., Aoshi, T., Ishii, K.J., Sanada, Y., Mochizuki, S., Sakurai, K. and Yokoyama, M., 2016. Exploring the relationship between anti-PEG IgM behaviors and PEGylated nanoparticles and its significance for accelerated blood clearance. *Journal of Controlled Release*, 234, pp.59-67.
52. Shiraishi, K., Hamano, M., Ma, H., Kawano, K., Maitani, Y., Aoshi, T., Ishii, K.J. and Yokoyama, M., 2013. Hydrophobic blocks of PEG-conjugates play a significant role in the accelerated blood clearance (ABC) phenomenon. *Journal of controlled release*, 165(3), pp.183-190.
53. Lorson, T., Lübtow, M.M., Wegener, E., Haider, M.S., Borova, S., Nahm, D., Jordan, R., Sokolski-Papkov, M., Kabanov, A.V. and Luxenhofer, R., 2018. Poly (2-oxazoline) s based biomaterials: A comprehensive and critical update. *Biomaterials*, 178, pp.204-280.
54. Gaertner, F.C., Luxenhofer, R., Blechert, B., Jordan, R. and Essler, M., 2007. Synthesis, biodistribution and excretion of radiolabeled poly (2-alkyl-2-oxazoline) s. *Journal of Controlled Release*, 119(3), pp.291-300.
55. Zhang, N., Pompe, T., Amin, I., Luxenhofer, R., Werner, C. and Jordan, R., 2012. Tailored Poly (2-oxazoline) Polymer Brushes to Control Protein Adsorption and Cell Adhesion. *Macromolecular bioscience*, 12(7), pp.926-936.
56. Pidhatika, B., Rodenstein, M., Chen, Y., Rakhmatullina, E., Mühlebach, A., Acikgöz, C., Textor, M. and Konradi, R., 2012. Comparative stability studies of poly (2-methyl-2-oxazoline) and poly (ethylene glycol) brush coatings. *Biointerphases*, 7(1), p.1.

57. Wang, X., Li, X., Li, Y., Zhou, Y., Fan, C., Li, W., Ma, S., Fan, Y., Huang, Y., Li, N. and Liu, Y., 2011. Synthesis, characterization and biocompatibility of poly (2-ethyl-2-oxazoline)–poly (d, l-lactide)–poly (2-ethyl-2-oxazoline) hydrogels. *Acta Biomaterialia*, 7(12), pp.4149-4159.
58. Itaka, K., Ishii, T., Hasegawa, Y. and Kataoka, K., 2010. Biodegradable polyamino acid-based polycations as safe and effective gene carrier minimizing cumulative toxicity. *Biomaterials*, 31(13), pp.3707-3714.
59. Roweton, S., Huang, S.J. and Swift, G., 1997. Poly (aspartic acid): synthesis, biodegradation, and current applications. *Journal of environmental polymer degradation*, 5(3), pp.175-181.
60. Huesmann, D., Sevenich, A., Weber, B. and Barz, M., 2015. A head-to-head comparison of poly (sarcosine) and poly (ethylene glycol) in peptidic, amphiphilic block copolymers. *Polymer*, 67, pp.240-248.
61. Romberg, B., Oussoren, C., Snel, C.J., Carstens, M.G., Hennink, W.E. and Storm, G., 2007. Pharmacokinetics of poly (hydroxyethyl-l-asparagine)-coated liposomes is superior over that of PEG-coated liposomes at low lipid dose and upon repeated administration. *Biochimica et Biophysica Acta (BBA)-Biomembranes*, 1768(3), pp.737-743.
62. Doh, K.O. and Yeo, Y., 2012. Application of polysaccharides for surface modification of nanomedicines. *Therapeutic delivery*, 3(12), pp.1447-1456.
63. Torchilin, V.P., Levchenko, T.S., Whiteman, K.R., Yaroslavov, A.A., Tsatsakis, A.M., Rizos, A.K., Michailova, E.V. and Shtilman, M.I., 2001. Amphiphilic poly-N-vinylpyrrolidones:: synthesis, properties and liposome surface modification. *Biomaterials*, 22(22), pp.3035-3044.
64. Jiang, J., Zhu, L., Zhu, L., Zhang, H., Zhu, B. and Xu, Y., 2013. Antifouling and antimicrobial polymer membranes based on bioinspired polydopamine and strong hydrogen-bonded poly (N-vinyl pyrrolidone). *ACS applied materials & interfaces*, 5(24), pp.12895-12904.
65. Muppalla, R., Rana, H.H., Devi, S. and Jewrajka, S.K., 2013. Adsorption of pH-responsive amphiphilic copolymer micelles and gel on membrane surface as an approach for antifouling coating. *Applied surface science*, 268, pp.355-367.
66. Zhao, X., Su, Y., Li, Y., Zhang, R., Zhao, J. and Jiang, Z., 2014. Engineering amphiphilic membrane surfaces based on PEO and PDMS segments for improved antifouling performances. *Journal of membrane science*, 450, pp.111-123.
67. Zhao, C., Li, L. and Zheng, J., 2010. Achieving highly effective nonfouling performance for surface-grafted poly (HPMA) via atom-transfer radical polymerization. *Langmuir*, 26(22), pp.17375-17382.
68. Letchford, K. and Burt, H., 2007. A review of the formation and classification of amphiphilic block copolymer nanoparticulate structures: micelles, nanospheres, nanocapsules and polymersomes. *European journal of pharmaceuticals and biopharmaceutics*, 65(3), pp.259-269.

69. Wilms, D., Stiriba, S.E. and Frey, H., 2010. Hyperbranched polyglycerols: from the controlled synthesis of biocompatible polyether polyols to multipurpose applications. *Accounts of chemical research*, 43(1), pp.129-141.
70. Elsbahy, M., Perron, M.È., Bertrand, N., Yu, G.E. and Leroux, J.C., 2007. Solubilization of docetaxel in poly (ethylene oxide)-block-poly (butylene/styrene oxide) micelles. *Biomacromolecules*, 8(7), pp.2250-2257.
71. Cambón, A., Rey-Rico, A., Mistry, D., Brea, J., Loza, M.I., Attwood, D., Barbosa, S., Alvarez-Lorenzo, C., Concheiro, A., Taboada, P. and Mosquera, V., 2013. Doxorubicin-loaded micelles of reverse poly (butylene oxide)-poly (ethylene oxide)-poly (butylene oxide) block copolymers as efficient “active” chemotherapeutic agents. *International journal of pharmaceutics*, 445(1-2), pp.47-57.
72. Kabanov, A.V., Batrakova, E.V. and Alakhov, V.Y., 2002. Pluronic® block copolymers as novel polymer therapeutics for drug and gene delivery. *Journal of controlled release*, 82(2-3), pp.189-212.
73. Cameron, D.J. and Shaver, M.P., 2011. Aliphatic polyester polymer stars: synthesis, properties and applications in biomedicine and nanotechnology. *Chemical Society Reviews*, 40(3), pp.1761-1776.
74. Allen, C., Yu, Y., Maysinger, D. and Eisenberg, A., 1998. Polycaprolactone-b-poly (ethylene oxide) block copolymer micelles as a novel drug delivery vehicle for neurotrophic agents FK506 and L-685,818. *Bioconjugate chemistry*, 9(5), pp.564-572.
75. Makadia, H.K. and Siegel, S.J., 2011. Poly lactic-co-glycolic acid (PLGA) as biodegradable controlled drug delivery carrier. *Polymers*, 3(3), pp.1377-1397.
76. Zhang, L., He, Y., Yu, M. and Song, C., 2011. Paclitaxel-loaded polymeric nanoparticles based on PCL-PEG-PCL: Preparation, in vitro and in vivo evaluation. *Journal of Controlled Release*, 152.
77. Werner, M.E., Cummings, N.D., Sethi, M., Wang, E.C., Sukumar, R., Moore, D.T. and Wang, A.Z., 2013. Preclinical evaluation of Genexol-PM, a nanoparticle formulation of paclitaxel, as a novel radiosensitizer for the treatment of non-small cell lung cancer. *International Journal of Radiation Oncology* Biology* Physics*, 86(3), pp.463-468.
78. Alves, V.M., Hwang, D., Muratov, E., Sokolsky-Papkov, M., Varlamova, E., Vinod, N., Lim, C., Andrade, C.H., Tropsha, A. and Kabanov, A., 2019. Cheminformatics-driven discovery of polymeric micelle formulations for poorly soluble drugs. *Science advances*, 5(6), p.eaav9784.
79. Schulz, A., Jaksch, S., Schubel, R., Wegener, E., Di, Z., Han, Y., Meister, A., Kressler, J., Kabanov, A.V., Luxenhofer, R. and Papadakis, C.M., 2014. Drug-induced morphology switch in drug delivery systems based on poly (2-oxazoline) s. *ACS nano*, 8(3), pp.2686-2696.

80. He, Z., Schulz, A., Wan, X., Seitz, J., Bludau, H., Alakhova, D.Y., Darr, D.B., Perou, C.M., Jordan, R., Ojima, I. and Kabanov, A.V., 2015. Poly (2-oxazoline) based micelles with high capacity for 3rd generation taxoids: Preparation, in vitro and in vivo evaluation. *Journal of controlled release*, 208, pp.67-75.
81. Hwang, D., Zhao, Y., Liu, H., Kabanov, A., Gershon, T. and Sokolsky, M., 2018. MBRS-53 enhanced efficacy of Nano-formulated Vismodegib shows the potential for polyoxazoline micelles to improve drug delivery to brain tumors. *Neuro-Oncology*, 20(Suppl 2), p.i139.
82. Owen, S.C., Chan, D.P. and Shoichet, M.S., 2012. Polymeric micelle stability. *Nano today*, 7(1), pp.53-65.
83. Lee, J., Cho, E.C. and Cho, K., 2004. Incorporation and release behavior of hydrophobic drug in functionalized poly (D, L-lactide)-block-poly (ethylene oxide) micelles. *Journal of Controlled Release*, 94(2-3), pp.323-335.
84. Kwon, G., Naito, M., Yokoyama, M., Okano, T., Sakurai, Y. and Kataoka, K., 1993. Micelles based on AB block copolymers of poly (ethylene oxide) and poly (beta-benzyl-L-aspartate). *Langmuir*, 9(4), pp.945-949.
85. Shi, Y., van Steenberg, M.J., Teunissen, E.A., Novo, L., Gradmann, S., Baldus, M., van Nostrum, C.F. and Hennink, W.E., 2013. Π - Π stacking increases the stability and loading capacity of thermosensitive polymeric micelles for chemotherapeutic drugs. *Biomacromolecules*, 14(6), pp.1826-1837.
86. Thakral, S. and Thakral, N.K., 2013. Prediction of drug-polymer miscibility through the use of solubility parameter based Flory-Huggins interaction parameter and the experimental validation: PEG as model polymer. *Journal of pharmaceutical sciences*, 102(7), pp.2254-2263.
87. Chun, B.J., Lu, J., Weck, M. and Jang, S.S., 2015. Characterization of molecular association of poly (2-oxazoline) s-based micelles with various epoxides and diols via the Flory-Huggins theory: a molecular dynamics simulation approach. *Physical Chemistry Chemical Physics*, 17(43), pp.29161-29170.
88. Loverde, S.M., Klein, M.L. and Discher, D.E., 2012. Nanoparticle shape improves delivery: rational coarse grain molecular dynamics (rCG-MD) of taxol in worm-like PEG-PCL micelles. *Advanced materials*, 24(28), pp.3823-3830.
89. Wu, W., Zhang, R., Peng, S., Li, X. and Zhang, L., 2016. QSPR between molecular structures of polymers and micellar properties based on block unit autocorrelation (BUA) descriptors. *Chemometrics and Intelligent Laboratory Systems*, 157, pp.7-15.
90. Lübtow, M.M., Hahn, L., Haider, M.S. and Luxenhofer, R., 2017. Drug specificity, synergy and antagonism in ultrahigh capacity poly (2-oxazoline)/poly (2-oxazine) based formulations. *Journal of the American Chemical Society*, 139(32), pp.10980-10983.

91. Pöppler, A.C., Lübtow, M.M., Schlauersbach, J., Wiest, J., Meinel, L. and Luxenhofer, R., 2019. Loading-Dependent Structural Model of Polymeric Micelles Encapsulating Curcumin by Solid-State NMR Spectroscopy. *Angewandte Chemie International Edition*, 58(51), pp.18540-18546.
92. Hansen, C.M., 1969. The universality of the solubility parameter. *Industrial & engineering chemistry product research and development*, 8(1), pp.2-11.
93. Hildebrand, J.H., 1916. SOLUBILITY. *Journal of the American Chemical Society*, 38(8), pp.1452-1473.
94. Liu, J., Xiao, Y. and Allen, C., 2004. Polymer–drug compatibility: a guide to the development of delivery systems for the anticancer agent, ellipticine. *Journal of pharmaceutical sciences*, 93(1), pp.132-143.
95. Huggins, M.L., 1942. Some properties of solutions of long-chain compounds. *The Journal of Physical Chemistry*, 46(1), pp.151-158.
96. Flory, P.J., 1942. Thermodynamics of high polymer solutions. *The Journal of chemical physics*, 10(1), pp.51-61.
97. Case, F.H. and Honeycutt, J.D., 1994. Will My Polymers Mix?" Methods for Studying Polymer Miscibility. *Trends Polym. Sci.*, 2(8), pp.259-266.
98. Danquah, M., Fujiwara, T. and Mahato, R.I., 2010. Self-assembling methoxypoly (ethylene glycol)-b-poly (carbonate-co-L-lactide) block copolymers for drug delivery. *Biomaterials*, 31(8), pp.2358-2370.
99. Mahmud, A., Patel, S., Molavi, O., Choi, P., Samuel, J. and Lavasanifar, A., 2009. Self-Associating Poly (ethylene oxide)-b-poly (α -cholesteryl carboxylate- ϵ -caprolactone) Block Copolymer for the Solubilization of STAT-3 Inhibitor Cucurbitacin I. *Biomacromolecules*, 10(3), pp.471-478.
100. Lübtow, M.M., Haider, M.S., Kirsch, M., Klisch, S. and Luxenhofer, R., 2019. Like Dissolves Like? A Comprehensive Evaluation of Partial Solubility Parameters to Predict Polymer–Drug Compatibility in Ultrahigh Drug-Loaded Polymer Micelles. *Biomacromolecules*, 20(8), pp.3041-3056.
101. Erlebach, A., Ott, T., Otzen, C., Schubert, S., Czaplowska, J., Schubert, U.S. and Sierka, M., 2016. Thermodynamic compatibility of actives encapsulated into PEG-PLA nanoparticles: In Silico predictions and experimental verification. *Journal of computational chemistry*, 37(24), pp.2220-2227.
102. Thota, N. and Jiang, J., 2015. Computational amphiphilic materials for drug delivery. *Frontiers in Materials*, 2, p.64.

103. Frenkel, D. and Smit, B., 2001. *Understanding molecular simulation: from algorithms to applications* (Vol. 1). Elsevier.
104. Patel, S., Lavasanifar, A. and Choi, P., 2008. Application of molecular dynamics simulation to predict the compatibility between water-insoluble drugs and self-associating poly (ethylene oxide)-b-poly (ϵ -caprolactone) block copolymers. *Biomacromolecules*, *9*(11), pp.3014-3023.
105. Patel, S.K., Lavasanifar, A. and Choi, P., 2009. Roles of nonpolar and polar intermolecular interactions in the improvement of the drug loading capacity of PEO-b-PCL with increasing PCL content for two hydrophobic cucurbitacin drugs. *Biomacromolecules*, *10*(9), pp.2584-2591.
106. Patel, S.K., Lavasanifar, A. and Choi, P., 2010. Molecular dynamics study of the encapsulation capability of a PCL-PEO based block copolymer for hydrophobic drugs with different spatial distributions of hydrogen bond donors and acceptors. *Biomaterials*, *31*(7), pp.1780-1786.
107. McKim, J.M., Bradbury, S.P. and Niemi, G.J., 1987. Fish acute toxicity syndromes and their use in the QSAR approach to hazard assessment. *Environmental Health Perspectives*, *71*, pp.171-186.
108. Callari, M., De Souza, P.L., Rawal, A. and Stenzel, M.H., 2017. The Effect of Drug Loading on Micelle Properties: Solid-State NMR as a Tool to Gain Structural Insight. *Angewandte Chemie International Edition*, *56*(29), pp.8441-8445.
109. Haider, M.S., Lübtow, M.M., Endres, S., Aseyev, V., Pöppler, A.C. and Luxenhofer, R., 2019. Think Beyond the Core: The Impact of the Hydrophilic Corona on the Drug Solubilization Using Polymer Micelles.
110. Wu, G., Chu, B. and Schneider, D.K., 1995. SANS study of the micellar structure of PEO/PPO/PEO aqueous solution. *The Journal of Physical Chemistry*, *99*(14), pp.5094-5101.
111. Sakai-Kato, K., Nishiyama, N., Kozaki, M., Nakanishi, T., Matsuda, Y., Hirano, M., Hanada, H., Hisada, S., Onodera, H., Harashima, H. and Matsumura, Y., 2015. General considerations regarding the in vitro and in vivo properties of block copolymer micelle products and their evaluation. *Journal of Controlled Release*, *210*, pp.76-83.
112. Gaspar, R. and Duncan, R., 2009. Polymeric carriers: preclinical safety and the regulatory implications for design and development of polymer therapeutics. *Advanced drug delivery reviews*, *61*(13), pp.1220-1231.
113. Campos, F.C., Victorino, V.J., Martins-Pinge, M.C., Cecchini, A.L., Panis, C. and Cecchini, R., 2014. Systemic toxicity induced by paclitaxel in vivo is associated with the solvent cremophor EL through oxidative stress-driven mechanisms. *Food and chemical toxicology*, *68*, pp.78-86.
114. Hamaguchi, T., Kato, K., Yasui, H., Morizane, C., Ikeda, M., Ueno, H., Muro, K., Yamada, Y., Okusaka, T., Shirao, K. and Shimada, Y., 2007. A phase I and pharmacokinetic study of

NK105, a paclitaxel-incorporating micellar nanoparticle formulation. *British journal of cancer*, 97(2), pp.170-176.

115. Shin, H.C., Alani, A.W., Cho, H., Bae, Y., Kolesar, J.M. and Kwon, G.S., 2011. A 3-in-1 polymeric micelle nanocontainer for poorly water-soluble drugs. *Molecular pharmaceutics*, 8(4), pp.1257-1265.

116. Wan, X., Min, Y., Bludau, H., Keith, A., Sheiko, S.S., Jordan, R., Wang, A.Z., Sokolsky-Papkov, M. and Kabanov, A.V., 2018. Drug Combination synergy in worm-like polymeric micelles improves treatment outcome for small cell and non-small cell lung cancer. *ACS nano*, 12(3), pp.2426-2439.

117. Kim, S., Shi, Y., Kim, J.Y., Park, K. and Cheng, J.X., 2010. Overcoming the barriers in micellar drug delivery: loading efficiency, in vivo stability, and micelle–cell interaction. *Expert opinion on drug delivery*, 7(1), pp.49-62.

118. Caster, J.M., Stephanie, K.Y., Patel, A.N., Newman, N.J., Lee, Z.J., Warner, S.B., Wagner, K.T., Roche, K.C., Tian, X., Min, Y. and Wang, A.Z., 2017. Effect of particle size on the biodistribution, toxicity, and efficacy of drug-loaded polymeric nanoparticles in chemoradiotherapy. *Nanomedicine: Nanotechnology, Biology and Medicine*, 13(5), pp.1673-1683.

119. Lee, H., Fonge, H., Hoang, B., Reilly, R.M. and Allen, C., 2010. The effects of particle size and molecular targeting on the intratumoral and subcellular distribution of polymeric nanoparticles. *Molecular pharmaceutics*, 7(4), pp.1195-1208.

120. Skoczen, S., McNeil, S.E. and Stern, S.T., 2015. Stable isotope method to measure drug release from nanomedicines. *Journal of Controlled Release*, 220, pp.169-174.

121. Skoczen, S.L. and Stern, S.T., 2018. Improved ultrafiltration method to measure drug release from nanomedicines utilizing a stable isotope tracer. In *Characterization of Nanoparticles Intended for Drug Delivery* (pp. 223-239). Humana Press, New York, NY.

122. Aliabadi, H.M., Elhasi, S., Mahmud, A., Gulamhusein, R., Mahdipoor, P. and Lavasanifar, A., 2007. Encapsulation of hydrophobic drugs in polymeric micelles through co-solvent evaporation: the effect of solvent composition on micellar properties and drug loading. *International journal of pharmaceutics*, 329(1-2), pp.158-165.

123. Yang, L., Wu, X., Liu, F., Duan, Y. and Li, S., 2009. Novel biodegradable polylactide/poly(ethylene glycol) micelles prepared by direct dissolution method for controlled delivery of anticancer drugs. *Pharmaceutical research*, 26(10), pp.2332-2342.

124. Yokoyama, M., Opanasopit, P., Okano, T., Kawano, K. and Maitani, Y., 2004. Polymer design and incorporation methods for polymeric micelle carrier system containing water-insoluble anti-cancer agent camptothecin. *Journal of drug targeting*, 12(6), pp.373-384.

125. Kato, K., Chin, K., Yoshikawa, T., Yamaguchi, K., Tsuji, Y., Esaki, T., Sakai, K., Kimura, M., Hamaguchi, T., Shimada, Y. and Matsumura, Y., 2012. Phase II study of NK105, a paclitaxel-incorporating micellar nanoparticle, for previously treated advanced or recurrent gastric cancer. *Investigational new drugs*, 30(4), pp.1621-1627.
126. Fujiwara, Y., Mukai, H., Saeki, T., Ro, J., Lin, Y.C., Nagai, S.E., Lee, K.S., Watanabe, J., Ohtani, S., Kim, S.B. and Kuroi, K., 2019. A multi-national, randomised, open-label, parallel, phase III non-inferiority study comparing NK105 and paclitaxel in metastatic or recurrent breast cancer patients. *British journal of cancer*, 120(5), p.475.
127. Danson, S., Ferry, D., Alakhov, V., Margison, J., Kerr, D., Jowle, D., Brampton, M., Halbert, G. and Ranson, M., 2004. Phase I dose escalation and pharmacokinetic study of pluronic polymer-bound doxorubicin (SP1049C) in patients with advanced cancer. *British journal of cancer*, 90(11), pp.2085-2091.
128. Lee, S.W., Yun, M.H., Jeong, S.W., In, C.H., Kim, J.Y., Seo, M.H., Pai, C.M. and Kim, S.O., 2011. Development of docetaxel-loaded intravenous formulation, Nanoxel-PM™ using polymer-based delivery system. *Journal of controlled release*, 155(2), pp.262-271.
129. Miao, L., Guo, S., Lin, C.M., Liu, Q. and Huang, L., 2017. Nanoformulations for combination or cascade anticancer therapy. *Advanced drug delivery reviews*, 115, pp.3-22.
130. Hu, Q., Sun, W., Wang, C. and Gu, Z., 2016. Recent advances of cocktail chemotherapy by combination drug delivery systems. *Advanced drug delivery reviews*, 98, pp.19-34.
131. Lancet, J.E., Uy, G.L., Cortes, J.E., Newell, L.F., Lin, T.L., Ritchie, E.K., Stuart, R.K., Strickland, S.A., Hogge, D., Solomon, S.R. and Stone, R.M., 2016. Final results of a phase III randomized trial of CPX-351 versus 7+ 3 in older patients with newly diagnosed high risk (secondary) AML.

CHAPTER II: CHEMINFORMATICS-DRIVEN DISCOVERY OF POLYMERIC MICELLE FORMULATIONS FOR POORLY SOLUBLE DRUGS¹

2.1 Summary

Many drug candidates have failed therapeutic development because of their poor aqueous solubility. We have conceived a novel computer-aided strategy for rational design of polymeric micelle-based delivery systems for poorly soluble drugs. As part of this strategy, we have developed novel descriptors of drug-polymer complexes that were employed to build models to predict both drug loading efficiency (LE) and loading capacity (LC). These models were used for virtual screening of drug libraries and eight drugs predicted to have either high LE and high LC (four positive hits) or low LE and low LC (four negative hits) were selected for the experimental validation. Three putative true positive as well as three putative negative hits were confirmed (implying 75% prediction accuracy). Fortuitously, simvastatin, a putative negative hit, was found to have the desired micelle solubility, i.e., high LE and LC. Podophyllotoxin and simvastatin, with LE of 95% and 87%, respectively, and LC of 43% and 41%, respectively, were among the top five compounds ever studied for their solubility in polymeric micelles. The success of the computational strategy described herein suggests its broad utility for rational design of drug delivery systems.

¹ This chapter previously appeared as an article in press. The original citation is as follows: Alves, Vinicius et al., “Cheminformatics-driven discovery of polymeric micelle formulations for poorly soluble drugs”, *Science Advances*, 2019, DOI: 10.1126/sciadv.aav9784

2.2 Introduction

One of the major obstacles for the development of highly potent pharmaceuticals is their poor aqueous solubility, which is characteristic of approximately 40 percent of drug candidates [1]. This undesired property could significantly delay or even halt the progression of drug candidates to the clinic. Various drug delivery systems based on liposomes [2], nanoparticles [3], nanogels [4], and polymeric micelles [5] have been studied intensely to improve the solubilization of drugs and drug candidates [6], but relatively few of them have been advanced to clinical products. Various characteristics of such systems have been considered such as physiological barriers, physicochemical properties of drugs, and carrier-forming materials. However, despite certain progress in developing practically useful delivery systems, this experimental approach has remained time consuming and expensive. The need to employ rational, computer-aided approaches to designing delivery systems for drug molecules has been previously articulated in the literature [7]. Such approaches can enable early decisions to streamline the development process and decrease the attrition of drug candidates by matching them with their preferred delivery systems. However, while computational methods found broad application in the field of drug discovery, they have not yet become equally popular in the area of drug delivery. Most computational studies have relied on molecular docking and molecular dynamics to offer insights concerning molecular interactions between drugs and carriers [8-10]. For instance, molecular dynamics approaches have been applied to better understand the micelle structure of polymers [11] and to simulate drug loading into a delivery system [12], while mathematical modeling have been applied to investigate the hydrogel drug release [13]. Shi. et al. [14] have applied molecular docking to identify small molecules as optimal building blocks for designing an optimal telodendrimer for doxorubicin. The authors synthesized a series of nanocarriers and experimentally validated their findings. One of

the nanocarriers has shown improved delivery properties, lower toxicity, and superior anticancer effects. More recently, another docking-based method to predict the drug affinity for PLA-PEG nanoparticles and their effective drug loading was reported [15]. While targeting mechanistic aspects of drug loading into delivery systems or drug release from these systems, such approaches are computationally expensive, which makes it difficult to expect their routine application in pharmaceuticals; besides, such approaches do not target directly the prediction of drug loading efficiency and/or capacity.

There have been also some studies using statistical approaches as applied to modeling and design of drug delivery systems. Such approaches known as Quantitative Structure-Property Relationships (QSPR) modeling found especially prolific use both in medicinal chemistry and chemical toxicology [16-17] but much less so in drug delivery, perhaps, mostly due to the scarcity of experimental data. A recent study reported the development of a series of QSPR models to assess the loading of doxorubicin in polymeric micelles using the genetic function approximation algorithm [18], but since these models were developed for one drug only, they are not generalizable across multiple drugs. In another recent study, the authors predicted fouling release activity for polymer coating materials [19]. Transgene expression efficacy of polymers obtained from aminoglycoside antibiotics has been modeled using an online web tool named “Support vector regression-based Online Learning Equipment” (SOLE) [20].

Previously, we have successfully developed [21] and applied [22] QSPR models to predict loading of amphiphilic drugs into liposomes. However, liposomes by design are not the best system for incorporation of various poorly water-soluble molecules since loading of such molecules is constrained by the structure of the lipid bilayers. Recently, we have developed a novel polymeric micelle system formed by amphiphilic block copolymers of hydrophilic poly(2-methyl-

2-oxazoline) (PMeOx) and hydrophobic poly(2-butyl-2-oxazoline) (PBuOx). This system exhibited an exceptionally high solubilization for some hydrophobic drugs such as taxanes [23-24]. However, poly(2-oxazoline)s (POx) micelles could not solubilize every poorly water-soluble drug equally well. Mechanisms of encapsulation of poorly water soluble drugs into the polymeric micelle systems have been previously studied [25-26], but they continue to be poorly understood, and so far, there have been no approaches that would assure success of loading experiments for any selected drugs or drug candidates.

Our previous studies have led us to assert that POx micelles with very high solubilization of some drugs and very poor solubilization of others represent both practically important and descriptive example to evaluate a computer-aided approach to rational design of a polymeric micelle-based delivery systems for poorly soluble drugs. Herein, as a proof-of-concept, we have (i) rationally selected a set of about 21 poorly soluble and chemically diverse drugs from the Selleck Chemicals library (<http://www.seleckchem.com/>) and tested them for loading efficiency (LE) and loading capacity (LC) to supplement previously collected data on 20 compounds; (ii) compiled, curated, and integrated all LE and LC data for all drugs tested experimentally in one of our laboratories; (iii) developed novel chemical descriptors for polymers and drug-polymer complexes; (iv) generated and interpreted QSPR models for drug loading into polymeric micelle-based delivery systems; (v) identified, by virtual screening, drugs with poorly aqueous solubility predicted to have either high or low LE and LC; and (vi) experimentally measured LE and LC values of selected virtual screening hits and successfully validated model predictions. To the best of our knowledge, this is the first study on rational design of drug delivery systems that combines, in a single workflow, rationally designed experimental data collection to enable model development, computational modeling of drug loading into polymeric micelles, and effective

experimental validation of predicted formulation properties for the studied drug delivery systems. The success of this investigation suggests that computational approaches could substantially streamline and accelerate the development of novel and effective drug delivery systems.

2.3 Materials and Methods

Study Design

The overall workflow for computer-aided design of novel polymeric micelle-based delivery systems for poorly soluble drugs is shown in Fig. 1. Prior to this study, 20 compounds were tested for solubilization in POx micelles (step 0), which was not enough for building predictive QSPR models. Therefore, we rationally selected an additional set of 21 poorly soluble and chemically diverse drugs from the Selleck Chemicals library and tested them for loading efficiency (LE) and loading capacity (LC) to supplement previously collected data (step 1). The full dataset for all drugs tested experimentally was compiled, curated, integrated, and analyzed (step 2) and chemical descriptors for polymers and drug-polymer complexes that were developed specifically for this study were calculated (step 3). Then, QSPR models for drug loading into polymeric micelle-based delivery systems were generated and validated (step 4). Finally, we applied these models for virtual screening of the available drug library to identify compounds with poor aqueous solubility predicted to have either high or low LE and LC. We selected four putatively positive and four putatively negative hits for the experimental validation. In summary, this workflow combines rational design of the experimental data collection to enable model development, computational modeling of drug loading into polymeric micelles, and experimental validation of predicted formulation properties for selected drug delivery systems.

Polymeric micelle preparation

Poly(2-oxazoline) micelles loaded with single drug or multiple drugs were prepared via the thin-film hydration method [23]. Predetermined amount of polymer and drugs were solubilized in an organic solvent (*e.g.*, acetone, acetonitrile, and ethanol) and mixed together. The organic solvent

was then removed under a stream of nitrogen gas or air (40 °C) to produce a thin film of intrinsically mixed drug-polymer blend. In order to completely remove the residual solvents and obtain dry film, the films were deposited in the vacuum chamber (approx. 0.2 mbar) overnight. Subsequently, the formed thin films were rehydrated with the desired amounts of aqueous saline or bi-distilled water and then solubilized at either room temperature or upon heating at 50–60 °C for 5–20 min to produce drug loaded polymeric micelle solutions. The rehydration time was dependent on either the drug concentration or the composition of the drugs or the multi-drug mixtures. The polymeric micelles loaded with the single drug were prepared accordingly with the final polymer concentration of 10 g/L and each drug feed concentration of 2, 4, 6, 8, 10, and sometimes 15 g/L. The polymeric micelles co-loaded with multiple drugs were prepared using the same final polymer concentration (10g/L) and predetermined concentrations of each drug components of multiple drug mixtures. The polymers used in this work are presented in Table 1.

In every case, the formulations were stable for at least 24 hours when the analysis of the drug incorporation was done. Prepared micelle samples were allowed to cool to room temperature and centrifuged at 10,000 rpm for 3 min (Sorvall Legend Micro 21R Centrifuge, Thermo Scientific) to remove precipitates. The transparent supernatant solutions of micelle samples were used for the quantification of the amounts of drugs solubilized in the polymeric micelle. The amounts of drugs encapsulated in polymeric micelles were analyzed via HPLC system (Agilent Technologies 1200 series). The micelle samples were diluted with mobile phase (specified below) and injected (10 µL) into the HPLC column (Agilent eclipse plus C18 3.5 µm column (4.6mm × 150mm). Predetermined mixtures of acetonitrile (ACN)/water (v/v) were used as the mobile phase. For PTX, AZD8055, olaparib, imiquimod, NVP-BEZ235, ABT-263, ABT-737, sabutoclast, LY2109761, AZD5363, LY364947, and the combination of each of these drugs with PTX, a

mixture of acetonitrile/water (50%/50% v/v, 0.01% trifluoroacetic acid) was used as the mobile phase. For VE-822, vismodegib, and their combination, a mixture of acetonitrile/water (35%/65% v/v, 0.01% trifluoroacetic acid) was used as the mobile phase. For PTX, wortmannin, LY294002, LY294002 HCl, etoposide (ETO), cisplatin prodrug (C6) [37], and the combination of wortmannin/PTX, LY294002/PTX, LY294002 HCl/PTX, ETO/cisplatin prodrug (C6), a mixture of acetonitrile (ACN)/water (50%/50% v/v) was used as the mobile phase. For PTX, brefeldin, cisplatin prodrug (C6), and the combination of brefeldin/PTX, cisplatin prodrug (C6)/PTX, a mixture of acetonitrile/water (40%/60% v/v) was used as the mobile phase. For PTX, KU55933, LDN 57444, and the combination of KU55933/PTX, LDN 57444/PTX, a mixture of acetonitrile/water (70%/30% v/v) was used as the mobile phase. For PTX, ETO, VE-822, and the combination of PTX/ETO/VE-822, a stepwise gradient was used. First, the analyte was eluted for 13 minutes with acetonitrile/water (30%/70% v/v, 0.01% trifluoroacetic acid) followed by a second 2-minute elution change from ACN/water (30%/70% v/v, 0.01% trifluoroacetic acid) to ACN/water (60%/40% v/v, 0.01% trifluoroacetic acid). Then, the analyte was eluted for 15 minutes. These measurements produced each drug concentration for each polymeric micelle composition (mg/mL). The flow rate was 1 mL/min, and column temperature was 40 °C. Detection wavelengths were determined by the drugs solubilized. The full description of platinum complexes with sufficient hydrophobicity for encapsulation in POx micelles are described in the Supplementary Materials (Description of platinum complexes) as well as the compilation of all experimental data on solubilization of drugs in POx micelles (Compiling all experimental data).

The LE (Equation 1) and LC (Equation 2) were calculated as follows:

The LE (Equation 1) and LC (Equation 2) were calculated as follows:

$$LE (\%) = \frac{m_{drug}}{m_{drug\ added}} \times 100 \quad \text{Equation (1)}$$

$$LC (\%) = \frac{m_{drug}}{m_{drug} + m_{polymer}} \times 100 \quad \text{Equation (2)}$$

Datasets

Creation of drug-polymer micellar solubilization dataset

Prior to this study, we have collected LE and LC data on 20 drugs chosen from the DrugBank (<http://www.drugbank.ca/>) that belonged to different structural classes. All these compounds had considerable issues with aqueous solubility. Many of these compounds were not approved by FDA or failed as treatments for solid tumors due to their toxicity. We hypothesized that solubilization of these compounds using our POx micelle system would greatly improve their anticancer efficacy. However, although we have demonstrated a very high solubilization capacity some of the drugs using POx micelles, we have also seen compounds where this technology was less helpful.

Rational design of a chemically diverse library of poorly soluble drugs

The chemical space formed by 20 previously tested compounds combined with the Selleck library of FDA-approved drugs was analyzed by plotting the barycentric coordinates in the space of SiRMS descriptors of all the 788 drugs. Barycentric coordinates correspond to the location of points of a simplex (a triangle, tetrahedron, *etc.*) in the space defined by the vertices [38]. In this case, a simplex is defined by all the SiRMS descriptors of a particular chemical substance. Barycentric coordinates were determined using Methods of Data Analysis module of the HiT QSAR software [39]. Then, we have selected the insoluble or poorly soluble drugs as preliminary candidates for solubilization in POx polymeric micelle delivery systems. The selected compounds

were subject to further chemical diversity sampling following a procedure similar to that described in Kuz'min et al. Ultimately, the collection of 61 molecules covering maximal chemical space for investigation of their loading efficiency was obtained. Twenty-one compounds were selected from this collection based on diversity of both clinical applications and mechanisms of action as well as availability and cost, and these compounds were tested for LC and LE. Thus, the total experimental dataset for model building included 20 compounds tested previously and 21 new compounds selected from the Selleck library as described above.

Selleck database

This dataset containing 853 FDA-approved drugs was retrieved from <http://www.selleckchem.com/>. After curation, 768 compounds remained, and a diverse subset of 61 molecules was selected from this dataset as described above (cf. also Step 1 in Fig. 1).

DrugBank database

This dataset containing 7,133 drug entries, including FDA-approved small-molecule drugs, nutraceuticals, illicit, withdrawn, and experimental drugs, was retrieved from the DrugBank website (<http://www.drugbank.ca/>). After curation, 6,461 drugs were kept for virtual screening.

Data curation

We have compiled all the data on drug loading into polymeric micelles generated over the years in our experimental laboratory. Originally, the dataset consisted of 408 records for 41 compounds tested in different concentrations and combinations for loading into micelles made of seven different polymers. Most of the compounds were tested in different concentrations and under different laboratory conditions. As part of the data curation procedure, each record was manually

inspected. Chemical structures were retrieved from either ChemSpider (<http://www.chemspider.com/>) or SciFinder (<https://scifinder.cas.org>) databases using the Chemical Abstracts Service (CAS) registry numbers and chemical names. The dataset was thoroughly curated according to the workflows developed by our group [40-43]. Briefly, structural normalization of specific chemotypes, such as aromatic and nitro groups, was performed using ChemAxon Standardizer (v. 16.10.24.0, ChemAxon, Budapest, Hungary, <http://www.chemaxon.com>). Organometallic compounds and mixtures were kept. After structure standardization, the structural duplicates were identified using HiT QSAR [39]. During this process, we identified 33 records that appeared more than once (up to twelve times), totaling 108 duplicates. The records describing the mixtures containing three drugs (nine records) and eight cases of real duplicates, where the experiment was performed more than once for the same drug-polymer complex, were removed from the modeling process. The concordance of property values for duplicated records was very high (average deviation was equal to 7.6%), thus, only one record associated with the averaged property value was kept for modeling. The high concordance between values for true duplicative measurements indicated high experimental reproducibility. The following experimental conditions were retained and used as descriptors for model building: polymer and drug solvent, total solvent volume before evaporation, hydration solvent, and hydration temperature. The final curated dataset of 391 records is available in the Supplementary Information (Data File S1).

Molecular descriptors

SiRMS descriptors

2D Simplex Representation of Molecular Structure (SiRMS) descriptors [27] (number of tetratomic fragments with fixed composition and topological structure) were generated by the HiT QSAR software [39]. At the 2D level, the connectivity of atoms in a simplex, atom type, and bond nature (single, double, triple, or aromatic) have been considered. SiRMS descriptors account not only for the atom type, but also for other atomic characteristics that may influence biological activity of molecules, *e.g.*, partial charge, lipophilicity, refraction, and atom ability for being a donor/acceptor in hydrogen-bond formation (H-bond). For atom characteristics with continuous values (charge, lipophilicity, and refraction), the division of the entire value range into definite discrete groups has been carried out. The atoms have been divided into four groups corresponding to their (i) partial charge $A \leq -0.05 < B \leq 0 < C \leq 0.05 < D$; (ii) lipophilicity $A \leq -0.5 < B \leq 0 < C \leq 0.5 < D$; and (iii) refraction $A \leq 1.5 < B \leq 3 < C \leq 8 < D$. For H-bond characteristic, the atoms have been divided into three groups: A (acceptor of hydrogen in H-bond), D (donor of hydrogen in H-bond), and I (indifferent atom). The usage of sundry variants of differentiation of simplex vertexes (atoms) represents the principal feature of the SiRMS approach [44]. Detailed description of HiT QSAR and SiRMS can be found elsewhere [27,39].

Polymer descriptors

Each block of the polymer was described by the number of its repetitions in the polymer. In addition, traditional SiRMS descriptors were calculated for simplified polymer representation as a pseudo small molecule with all repetitive monomers introduced only once. Overall scheme of descriptor calculation for polymers developed for this study for the first time is shown in Fig. 3.

Descriptors for drug-polymer complexes

We have modified the SiRMS approach developed earlier to calculate descriptors for organic compound mixtures [28, 29] to make it suitable for the QSPR analysis of drug-polymer complexes as follows. Each complex was represented as a binary mixture consisting of the drug molecule and a simplified representation of a polymer as a pseudo small molecule as described in the previous section. Then, the simplex descriptors were calculated as usual. Bounded simplexes describe only single components of the mixture (compounds A or B), when unbounded simplexes can describe both the constituent parts and the mixture as a whole. It is necessary to indicate whether the parts of unbounded simplexes belong to the same molecule or to different ones. In the latter case, such unbounded simplexes will not reflect the structure of a single molecule but will characterize a pair of different molecules. Simplexes of this kind are specific for a given drug-polymer complex (Fig. 4). Special mark is used during descriptor generation to distinguish such "mixture" simplexes from ordinary ones. The mixture composition is taken into account, *i.e.*, descriptors of constituent parts (compounds A and B) are weighted according to their molar fraction and mixture descriptors are multiplied by the doubled molar fraction of the minor component. If in the same task both drug-polymer complexes (mixtures) and pure compounds have been considered, pure compounds are considered as a mixture with composition A_1B_0 . In this case, only descriptors of the pure compound A will be generated with the weight equal to 1. Thus, the structure of every mixture is characterized by both descriptors of the mixture as well as of its individual constituents.

A simpler approach was used for complexes consisting of a polymer and a mixture of drugs. Here the polymer was represented in the same way, but descriptors for all the members of such mixture of drugs-polymer complex were calculated separately, weighted according to their concentration

and then summarized in one string corresponding to a given complex. This approach was used for datasets containing both drug-polymer and mixture of drugs-polymer complexes. It allowed the use of the maximal amount of available experimental data for model building. In the end, constant, near constant, and cross-correlated variables ($r \geq 0.9$) were removed to reduce the dimensionality of the chemical space without loss of important information.

Experimental conditions

Certain experimental conditions were used as features, in addition to molecular descriptors, to describe the system under the investigation. Specifically, we have considered solvents used to prepare both polymer and drug samples, total solvent volume before evaporation, hydration solvent, and hydration temperature.

Cluster analysis

Chemical clusters were generated by the Sequential Agglomerative Hierarchical Non-overlapping method implemented in the ISIDA/Cluster software [45]. Briefly, the software generates a dendrogram of the parent-child relationships between clusters and a heat map of the proximity matrix colored according to the pairwise chemical similarity between compounds. This approach is well known; it has been extensively used by our [46-48] and other groups [45-49]. Of course, clusters are data-specific, *e.g.*, if the new data would be introduced to the dataset, clusters might change. However, repeating cluster analysis for the same dataset will result in the same clusters. In this study, we used clustering only to analyze whether LogP and MW are relevant for drug loading of similar compounds. We did not use cluster analysis to predict loading parameters, which was done by QSPR models.

QSPR modeling

Binary QSPR models were developed and rigorously validated according to the best practices of QSPR modeling [50]. Models were developed with random forest (RF) algorithm [51]. One thousand trees were built for each forest and the outputs of all trees were aggregated to obtain one final prediction. In each tree, ca. 1/3 of the set of N compounds were sampled by bootstrap as out-of-bag (OOB) set and the remaining compounds were used as a training set. The best split by the CART algorithm [52] among the m randomly selected descriptors from the entire pool in each node was chosen and each tree was then grown to the largest possible extent; there was no pruning. The predicted classification values are defined by the majority voting for one of the classes. Thus, each tree predicts values for only those compounds that are not included in the training set of that tree (for OOB set only). The final model is chosen by the lowest error for prediction of the OOB set.

Models were built using the QSAR module in the R package (<https://r-forge.r-project.org/projects/qsarr/>) implemented in KNIME (<https://www.knime.com/>). We followed the “Mixtures out” procedure for the validation of QSAR models of mixtures described by Muratov et al. [28] In this method, all data points corresponding to mixtures composed of the same constituents, but in different ratios, are simultaneously removed and placed in the same external fold. Thus, every mixture is present either in the training or external set, but never in both sets. This approach allows one to minimize the influence of known information on the prediction and obtain reliable results for predicting novel drug-polymer complexes created by known polymer and a new drug. Thus, we combined “Mixtures out” strategy with 5-fold external cross-validation procedure [16, 53].

Briefly, the full set of compounds with known experimental activity was divided into five subsets of equal size. Each subset (20% of the compounds) was selected once as a test set, while the other subsets (80% of the compounds) were merged into a training set to develop a model. This procedure was repeated with the other subsets, allowing each one of the five subsets to be used once as a test set. In addition, 30 rounds of Y-randomization test [40] were performed for each dataset to ensure that the accuracy of models was not obtained due to chance correlations.

The QSPR models were built for two endpoints: LE and LC. For LE, the model was generated using the threshold of 80%. Thresholds of 10, 20, 30, and 40% were separately applied to build four models for LC. Such system of binary models would allow us to predict LC within certain ranges (0-10%; 10-20%; 20-30%; 30-40%, 40-50%), which is more informative than standard binary prediction. Compounds predicted above the threshold by all the individual models were selected as positive hits, while those predicted below the threshold were selected as negative hits. The applicability domain of the models was calculated as $D_{\text{cutoff}} = \langle D \rangle + Zs$, where Z is a similarity threshold parameter defined by a user (0.5 in this study), and $\langle D \rangle$ and s are the average and standard deviation, respectively, of all Euclidian distances in the multidimensional descriptor space between each compound and its nearest neighbors for all compounds in the training set [54].

Statistical analysis

The following statistical metrics were used to assess different aspects of performance of classification models (Equations 3-7):

Correct Classification Rate (CCR):

$$CCR = \frac{(\text{sensitivity} + \text{specificity})}{2} \quad \text{Equation (3)}$$

Sensitivity (Se):

$$Se = \frac{N_{TruePositives}}{N_{TruePositives} + N_{FalseNegatives}} \quad \text{Equation (4)}$$

Specificity (Sp):

$$Sp = \frac{N_{TrueNegatives}}{N_{TrueNegatives} + N_{FalsePositives}} \quad \text{Equation (5)}$$

Positive Predictive Value (PPV):

$$PPV = \frac{N_{TruePositives}}{N_{TruePositives} + N_{FalsePositives}} \quad \text{Equation (6)}$$

Negative Predictive Value (NPV):

$$NPV = \frac{N_{TrueNegatives}}{N_{TrueNegatives} + N_{FalseNegatives}} \quad \text{Equation (7)}$$

2.4 Results

Rational design of a diverse set of poorly soluble drugs

In the absence of rational approaches to the experimental design, the discovery of new suitable drug-POx systems is left to serendipity, implying high cost and time-consuming effort. Thus, we endeavored to develop computational QSPR models capable of accurate prediction of drug molecules with high LE and LC values in POx micelles that could be formulated using this drug delivery system and thereby, achieve much greater therapeutic efficacy (see Fig. 1 and Study Design section). Prior to this study, only 20 compounds were tested for solubilization in POx micelles. Among these, we have serendipitously discovered several drugs with good or excellent solubilization in POx micelles whereas at the same time many compounds were found to have poor micelle solubilization properties. These data were not sufficient for building predictive QSPR models. Furthermore, chemical diversity of these compounds was limited as compared to that of a drug library represented by 768 chemicals from the Selleck collection of FDA-approved drugs (Fig. 2). Therefore, using a diversity-sampling approach, we rationally selected a set of chemically diverse drug molecules that were poorly soluble or insoluble. The resulting expanded set of 61 molecules was chemically diverse and structurally representative of the chemical space of FDA-approved drugs (Fig. 2). From these 61 compounds, 21 drugs were selected based on their clinical indications and respective biological pathways, as well as price and availability followed by their testing using our standard experimental protocols to ensure data consistency. Combining the results of testing obtained on these 21 compounds as well as on 20 compounds tested previously, we thus obtained a unique training set of 41 compounds comprising 408 experimental data points. The complete micelle solubilization data for single and binary drug combination are given in the

Data File S1. These data were used for molecular modeling studies (see Cheminformatics analysis section).

Cheminformatics analysis

We have compiled a dataset of 41 compounds investigated in several concentrations and under different experimental conditions. Originally, our collection included 408 data points for these 41 compounds reflecting different drug concentrations, structural diversity of POx polymers, and experimental conditions (see Materials and Methods). In our previous studies, we have employed standard chemical descriptors of molecules and/or certain experimental conditions to establish a correlation with drug loading or bioactivity, respectively. Modeling of drug loading into polymeric micelles proved to be a more challenging exercise as drug chemical descriptors and experimental conditions were found insufficient to enable the development of statistically significant models.

To address this challenge in this study, we have developed novel descriptors of drug-polymer systems reflective of the chemical structures of both small molecules and polymers. These new descriptors were developed on the basis of SiRMS descriptors [27] originally devised for small organic molecules and later adapted for mixtures of organic molecules [28, 29]. These new descriptors were obtained by considering drug-POx systems as stoichiometric mixtures of polymers (represented by unique monomeric blocks used for their synthesis) and drug molecules (see Methods for more detail).

We have also observed (see Chemical Data Curation Section) that drug concentration and other experimental conditions had a strong influence on both LE and LC. For instance, although drug concentration does not influence the encapsulation effectiveness, most of the compounds that could be solubilized had high both LE and LC values for low drug concentration. When the

polymeric micelle is saturated with the drug and if the drug concentration is higher than the saturation point, the polymer may collapse. Therefore, to achieve the best LE and LC, compounds were tested using a variety of concentrations and experimental conditions. All the concentrations and experimental conditions were used as additional descriptors of drug-polymer complexes for both model building and virtual screening to improve model accuracy.

To illustrate the influence of polymer structure, experimental conditions, MW, and LogP on the compound solubilization in POx micelle, we have identified clusters of drugs tested at 8 mg/mL, i.e., at the highest concentration used for testing the largest number of drugs. For this analysis, original SiRMS descriptors were normalized and low variance descriptors (threshold = 0.1) were removed. Hierarchical clustering was performed using SciPy package (<https://www.scipy.org/>) in Python 3.6 (<https://www.python.org/>) based on Euclidean distance and the Ward method [30]. A heatmap of proximity matrix and dendrogram are reported in Fig. 5. The summary of clusters showing the LE and LC (mean, standard deviation, and maximum value) for the drugs tested at 8 mg is shown in Table 2.

As can be seen in Table 2, similar compounds belonging to the same cluster could have considerably different LE values. For instance, the cisplatin prodrug derivatives (Cluster 1) had optimal chain length of six carbons (Cisplatin prodrug, C6), with maximum LE = 85.1%. The analogs with four and ten carbons had similar LE, while the one with eight carbons had the lowest LE. VE-822 and NVP-BEZ235 have similar LogP and MW, which in turn were different from those of the remaining compounds (LY364947 and Imiquimod) in cluster 2. There, only VE-822 showed high LE max (83.34%), but Imiquimod, LY364947, and NVP-BEZ235 were not soluble in POx micelles. Compounds in Cluster 3 contain similar chemical features, but only AZD5363 shows high LE (63.8% respectively). In Cluster 4, LY294002 and EFV also have similar LogP and

MW, but only EFV presents high LE max (86.23). In Cluster 7, ABT-263 and ABT-737 have similar chemical structures and similar MW and LogP, but the LE max for both compounds are drastically different with maximal LE of 100% for ABT-263 and maximal LE of 7.3% for ABT-737.

These results show that the knowledge of chemical structure alone is not sufficient to evaluate whether a compound has a good chance to be highly soluble in polymeric micelles. Moreover, even the same drug combined with different polymers or even with the same polymer but under different experimental conditions may exhibit very different LE. Variable importance estimated from all developed models indicated that some experimental conditions (hydration solvent, hydration temperature, and total solvent volume before evaporation) had very high scores (Fig. 6). For instance, combination of DTX (10 mg/mL) and polymer P6 has been tested twice under the same experimental conditions, varying only the hydration solvent. When DTX was dissolved in deionized water, LE of 81.8% and LC of 44.9% were observed; using mix of deionized water, saline, and phosphate-buffered saline led to the increase of both LE and LC to 90% and 47.4%, respectively.

This analysis illustrates the need to consider the experimental conditions that define the outcome of the loading process as important descriptors of the system. To reflect on this point further, we shall highlight several factors that need to be considered to enable predictive models with much higher accuracy than historical success rate of purely experimental investigations: (i) close interaction between experimental and computational groups; (ii) rational design of the training set; (iii) special descriptors of drug-polymer complexes reflecting the interactions between drugs and micelles; (iv) the use of experimental conditions available for our datasets as descriptors, such as solvents in which both polymer and drug samples were prepared, their volumes before

evaporation, hydration solvent, and hydration temperature; and (v) experimental validation of drug delivery properties for selected both negative and positive hits. Our analysis further highlights the importance of recording and employing all parameters/characteristics related to the experiment. For instance, we have traced the size and morphology data for 15 drug-polymer complexes. Although these data are insufficient to be used for model building, our preliminary observations show that most drug-polymer complexes look like worms or spheres, while the specific polymer used in this study alone only forms worm-like structures. The particle size also changes upon the transition from worms to spheres induced by the drug and the transition point clearly depends on the selected drug. In addition, at a certain point, which is different for each drug, we have observed saturation and sediment formation. The particle size and morphology along with the micelle stability and drug release characteristics are important parameters for the pharmacological performance of these drug delivery systems [31]. We anticipate that as we generate and collect new data on size and morphology and other parameters, we will be able to incorporate this data explicitly into our models.

Our data analysis showed that the optimal combination of the experimental conditions varies from case to case. Overall, this indicates the following: (i) the importance of experimental conditions for drug solubilization; (ii) the necessity of choosing the optimal solvent, temperature, etc., for each specific drug-polymer combination; (iii) a need to use experimental conditions as descriptors during modeling and virtual screening; and (iv) requirement to select not only the computational hits for experimental confirmation, but also optimal experimental conditions (solvent, temperature, etc.) to improve the success rate.

In addition, the type and length of block chains of polymers showed to be important, as we shall discuss below. Table 3 presents summary data for three drugs tested at 8 mg/mL with the

highest experimental variability. As one can see, LE values for DTX vary from 1.56% to 80.06%. Three variables that change their values include polymer batch, mass of the polymer, and hydration temperature. It is possible to see that, when tested in different polymers, DTX is more soluble in polymer P8 (LE = 57.59%) than in polymer P2 (LE = 1.56%) when the mass of the latter polymer is 10 mg. However, when the mass of polymer P2 increased to 20 mg, a LE of 80.06% was achieved. For LDN-57444, the variation in the polymer and drug solvent, the total solvent volume before evaporation, and hydration temperature led to a difference of 26% in the LE. Lastly, the LE of PTX varied from 2.44% to 100%. In this case, the difference is mostly due different polymers. Both the P2 (LE = 2.44%) and the P8 (35.72%) presented low LE, while P1 (LE = 86.1%), P4 (100%), and P6 (LE = 91.18%), presented high LE.

Most of the POx polymers used in our studies (P1, P3, P4, P5, P6) are tri-block copolymers: poly(2-methyl-2-oxazoline)-block-poly(2-butyl-2-oxazoline)-block-poly(2-methyl-2-oxazoline) (P(MeOx-b-BuOx-b-MeOx)), differing in the chain length of each block. These differences, however, all within 10-15% variability typical for batch-to-batch variations, were not expected to result in any substantial difference in solubilization. Polymer P2 is a di-block copolymer P(MeOx-b-BuOx); it had a decreased ability to solubilize PTX and DTX compared to the respective tri-block, which illustrated the effect of the copolymer architecture [32]. The tri-block polymer P8 contains a few aromatic 2-benzyl-2-oxazoline (BzOx) units copolymerized with aliphatic BuOx (P(MeOx-b-co-BuOx/BzOx-b-MeOx)). Another polymer (P7) is a tri-block containing 2-nonyl-2-oxazoline (NOx) units instead of BuOx units in the hydrophobic block (P(MeOx-b-NOx-b-MeOx)). Both modifications obtained by adding aromatic groups or long chain alkyl groups to the core of the POx micelle appear to have adverse effects on the solubilization of PTX [33]. These observations reinforce the importance of building QSPR models incorporating all available

information about both chemical structures of drugs and polymers as well as the experimental conditions to predict new positive hits with high confidence.

The results of the cluster analysis confirmed that LogP and MW alone are not sufficient to predict drug loading. Thus, we developed series of robust and externally predictive (CCR = 0.76-0.85) binary QSPR models for forecasting LC and LE. Corresponding statistical characteristics estimated by 5-fold external cross-validation are summarized in Table 4. All models showed both high sensitivity (>70%) and specificity (>76%), as well as high positive predictive (PPV, >75%) and negative predictive (NPV, >76%) values.

Virtual screening of DrugBank and experimental evaluation

We have employed our QSPR models for virtual screening of the DrugBank database in order to identify drugs predicted to have both high LE and high LC for POx micelles. Aqueous solubility of drugs was used for initial filtering. Only compounds classified as poorly soluble (< 10 mg/ml) including those defined as practically insoluble (< 0.1 mg/ml) [34] were selected. All remaining compounds were paired with the polymer of interest and the LE and LC values for the drug loading into polymeric micelles were predicted by respective models. Rational design of the training set allowed all DrugBank compounds chosen for virtual screening to be inside models' applicability domains. Selected hits were dissimilar from the training set, but they were still found inside the applicability domain of the model, which increased our confidence in predictions.

Then, four compounds (podophyllotoxin, rutin, teniposide, and diosmin) predicted to have high solubilization in POx micelles and four compounds (olanzapine, simvastatin, spironolactone, and tamibarotene) predicted to be insoluble in POx were selected for experimental validation. Low

aqueous solubility of these compounds was confirmed experimentally before the experimental evaluation of the LE and LC in POx.

Experimental results for these eight drug-POx complexes are shown in Table 5. Overall, we have reached 75% experimental hit rate. Thus, three out of four drugs predicted as positive hits displayed moderate to excellent solubilization in POx micelles. Podophyllotoxin, rutin, and teniposide could be solubilized under certain experimental conditions (i.e., feed ratio of polymer 10 mg/mL) at concentrations as high as 8 mg/mL. Podophyllotoxin presented exceptional ability for incorporation into POx micelles as it could be solubilized under the experimental conditions at concentrations as high as 8 mg/mL, with LE = 95.2% and LC = 43.2%. Teniposide showed LE = 85% and LC = 14.5 at 8 mg/mL, while rutin presented LE = 45.1% and LC = 26.5%. Diosmin was a false positive, i.e., insoluble in POx micelles. Conversely, one of the predicted negative hits, olanzapine, showed very low or negligible LC and LE at all studied drug feed concentrations. Specifically, the concentration of olanzapine did not exceed 1 mg/mL. The very low LC and LE of this drug implies that at least about 90% or even 99% of the drug is lost upon formulation. Spironolactone and tamibarotene showed high solubilization, but only at low concentrations. These drugs were solubilized at 2 mg/mL with LE of 89.7% and 82.9%, respectively, and LC of 14.2% and 15.2%, respectively, but both featured very low solubilization when tested at 8 mg/mL (LE = 20.9% and LC = 14.3% for spironolactone and LE = 9.9% and LC = 7.4% for tamibarotene). As an instance of fortuitous mis-prediction, simvastatin was found to be a false negative, i.e., it was soluble in POx micelles at concentrations as high as 7 mg/mL, with LE of 87.2% and LC of 41.1%. Most likely, Simvastatin was mis-predicted because its nearest neighbor, Wortmannin, ($T_c = 0.72$) has poor solubility in POx micelles. Although Wortmannin presents moderate solubility in POx micelles when tested mixed with PTX, this drug alone has low both LE (2.3-5.8%) and LC

(0.9-2.2%). Irrespective of the reasons, mis-prediction of simvastatin represents a fortuitous prediction error as this drug appears to greatly benefit from POx solubilization.

Overall, four compounds showed good solubility, with both LE and LC values among the top 15 compounds ever tested by our group (Table 6). Podophyllotoxin and simvastatin demonstrated exceptional ability for incorporation into POx micelles. Podophyllotoxin and its analogs have shown several important biological activities (e.g., cytotoxic, antiviral, and antifungal) [35], therefore the discovery of new formulations described here may have a significant impact on the development of this drug candidate. The case of simvastatin (negative hit) with high LE and LC is an example of a fortuitous error of prediction, since this drug appears a great candidate for POx solubilization. Simvastatin depends on solubilization enhancements techniques to achieve optimal bioavailability and the improved solubilization with POx could potentially improve its bioavailability and pharmacological response [36]. Overall, three out of four positive and one negative hit showed highly desirable solubilization properties.

As one can see from Table 6, variation of both LE and LC values is small for almost all drugs. At the same time, both PTX and DTX had much higher standard deviation than the other compounds. In the course of preclinical development, these two compounds have been studied very extensively in the variety of experimental conditions. This observation reinforces the high impact of experimental conditions on the studied properties.

2.5 Discussion

We have developed and successfully used a computer-aided strategy for the rational design of novel drug-polymeric micelle combinations. Our approach employed special, novel descriptors of drug-polymer complexes for building predictive models of drug solubility in polymeric micelles, virtual screening of drug library, and experimental validation of selected hits. Another unique aspect of this investigation was that in addition to previously collected data, we have generated new experimental data for compounds selected rationally from the library of approved drugs. This was done solely to enable model development for sufficiently large and chemically diverse dataset. In total, 41 drugs tested in different concentrations both individually and in binary combinations for loading into four different polymeric micelles (408 data points) were used for modeling. This allowed us to develop the set of binary QSPR models for predicting both LE and LC of drugs in polymeric micelles.

The high predictive power of the developed models (external balanced accuracy of 76–85%) was confirmed by the “mixtures out” approach [28, 29] especially designed for estimating true predictivity of the QSPR model obtained for compound mixtures (see Methods for additional detail). The developed models were employed for virtual screening of the DrugBank database and four drugs with high (positive hits) along with four drugs with low (negative hits) predicted LE and LC were prioritized for testing. Predicted LE and LC values for three positive and three negative computational hits were confirmed experimentally. Luckily, the remaining negative hit, simvastatin, with LE = 87% and LC = 41%, had, in fact, desired delivery properties. Moreover, simvastatin and podophyllotoxin (LE = 95% and LC = 43%) were among the top five compounds ever studied in POx loading experiments. This is especially important because simvastatin’s solubilization rate is too low to achieve optimal bioavailability [36] and podophyllotoxin has

several desired biological properties (e.g., cytotoxic, antiviral, and antifungal) [35]; therefore, the discovery of new formulations described here may have a significant impact on the further development of both drugs.

Another significant advantage of the proposed computer-aided strategy for rational design of formulations for poorly soluble drugs is the significant increase in success rate. Thus, our modeling set of 41 compounds tested in advance of model development included 20 compounds with significant solubility in POx micelles (that were used to develop models reported herein), implying ca. 48% experimental hit rate. In contrast, the use of models developed with this modeling set to design new formulations increased the hit rate from 48% to 75%, i.e., nearly two-fold. The success of this study illustrates the power of computer-aided design of novel drug delivery systems and calls for a broader application of computational modeling approaches in drug delivery.

Polymer	Publication	b-methyl	b-butyl	co-benzyl	b-nonyl	b-methyl	End group
P1	n/a	37	21	0	0	36	piperazine
P2	(32)	45	25	0	0	0	piperazine
P3	(56)	40	21	0	0	34	piperazine
P4	n/a	44	26	0	0	38	piperazine
P5	n/a	47	26	0	0	36	piperazine
P6	(24, 32, 33)	33	26	0	0	45	piperazine
P7	(32)	34	0	0	12	37	piperazine
P8	(32)	34	13	5	0	34	amino group

Table 2.1 List of nine polymers used in this study with specification of block sizes and end group.

Drug	Cluster	LE (%)				LC (%)				LogP	MW	No. of experiments
		Min	Max	Mean	Std. Dev	Min	Max	Mean	Std. Dev			
Cisplatin prodrug (C10)	1	53.65	53.65	53.65	0	23.85	23.85	23.85	0	9.11	639.22	1
Cisplatin prodrug (C4)	1	58.5	58.5	58.5	0	31.9	31.9	31.9	0	2.28	471.03	1
Cisplatin prodrug (C6)	1	84.8	84.8	84.8	0	40.4	40.4	40.4	0	4.56	527.09	1
Cisplatin prodrug (C8)	1	24.09	24.09	24.09	0	10.71	10.71	10.71	0	6.84	583.15	1
Imiquimod	2	1.36	3.3	2.42	0.98	1.05	2.6	1.88	0.78	2.71	240.14	3
LY364947	2	0.8	0.8	0.8	0	0.6	0.6	0.6	0	3.45	272.11	1
NVP-BE235	2	1.8	1.8	1.8	0	1.4	1.4	1.4	0	4.92	469.19	1
VE-822	2	77	83.34	80.17	4.48	13.3	40	26.65	18.88	3.77	463.17	2
AZD5363	3	60.1	63.8	62.27	1.93	32.5	33.8	33.27	0.68	2.44	428.17	3
AZD7762	3	38	38	38	0	23.3	23.3	23.3	0	1.5	362.12	2
LDN-57444	3	5.5	31.5	18.5	18.38	4.2	20.1	12.15	11.24	5.01	395.98	2
Olaparib	3	23.9	23.9	23.9	0	16.1	16.1	16.1	0	2.44	434.18	1
Brefeldin	4	0	0	0	0	0	0	0	0	2.36	280.17	1
EFV	4	86.23	86.23	86.23	0	40.82	40.82	40.82	0	4.63	315.03	1
KU55933	4	13.6	13.6	13.6	0	9.8	9.8	9.8	0	5.93	394.07	2
LY294002	4	1	1	1	0	0.8	0.8	0.8	0	4.97	307.12	1
Wortmannin	4	2.55	2.55	2.55	0	2	2	2	0	0.71	428.15	1
AZD8055	5	50.8	50.8	50.8	0	28.9	28.9	28.9	0	3.41	465.24	1
LY2109761	5	9.3	9.3	9.3	0	6.9	6.9	6.9	0	2.84	441.22	1
ETO	6	90.15	95.2	91.83	2.92	41.9	43.2	42.33	0.75	0.78	588.18	3
ABT-263	7	100	100	100	0	44.4	44.4	44.4	0	10.69	973.3	1
ABT-737	7	7.3	7.3	7.3	0	5.5	5.5	5.5	0	9.85	812.26	1
DTX	8	1.56	80.06	46.4	40.43	1.23	31.54	18.99	15.81	2.41	807.35	3
PTX	8	2.44	100	63.088	42.16	1.56	45.4	30.378	18.54	2.96	853.33	5
Sabutoclax	9	11.6	11.6	11.6	0	8.5	8.5	8.5	0	10.37	700.28	1

Table 2.2 List of 25 compounds tested alone at 8 mg with their respective clusters, LE and LC (minimum, maximum, mean, and standard deviation values), LogP, MW, and number of performed experiments.

Drug	Polymer batch	Polymer mass (mg)	Polymer and drug solvent	Total solvent volume before evaporation (μL)	Hydration solvent	Hydration temperature	LE (%)	LC (%)
DTX	P2	20	ethanol	500	DI water	50	80.06	24.2
DTX	P2	10	ethanol	500	DI water	50	1.56	1.23
DTX	P8	10	ethanol	500	DI water	60	57.59	31.54
LDN-57444	P1	10	acetonitrile	130	saline	20	31.5	20.1
LDN-57444	P1	10	ethanol	250	saline	60	5.5	4.2
PTX	P1	10	acetone	400	saline	60	86.1	40.8
PTX	P2	10	ethanol	500	DI water	50	2.44	1.56
PTX	P4	10	ethanol	500	DI water	60	100	45.4
PTX	P6	10	ethanol	500	DI water	60	91.18	42.17
PTX	P8	10	ethanol	500	DI water	60	35.72	21.96

Table 2.3 List of three drugs with highest LE variability tested at 8 mg/mL.

Model	CCR	Sensitivity	PPV	Specificity	NPV
LC 10	0.83 ± 0.03	0.89 ± 0.02	0.85 ± 0.04	0.77 ± 0.06	0.83 ± 0.03
LC 20	0.82 ± 0.07	0.75 ± 0.10	0.81 ± 0.07	0.88 ± 0.05	0.84 ± 0.06
LC 30	0.85 ± 0.06	0.82 ± 0.11	0.77 ± 0.08	0.89 ± 0.05	0.92 ± 0.04
LC 40	0.83 ± 0.11	0.70 ± 0.24	0.83 ± 0.12	0.96 ± 0.03	0.93 ± 0.05
LE 80	0.76 ± 0.05	0.76 ± 0.05	0.75 ± 0.10	0.76 ± 0.13	0.76 ± 0.03

Table 2.4 Statistical characteristics of LC and LE QSPR models based on 5-fold external cross-validation.

Positive hits								
Name	Water solubility	Concentration (mg)	Predicted by QSPR				Experimental	
			LE 80	LC 10	LC 20	LC 30	LE (%)	LC (%)
Podophyllotoxin	Very slightly soluble	15	NA	NA	NA	NA	23.8	26.3
		10	1	1	1	1	58.7	37.0
		8	1	1	1	0	95.2	43.2
		4	1	1	0	0	95.6	27.7
		2	1	1	0	0	100.0	16.7
Rutin	Slightly soluble	15	NA	NA	NA	NA	3.9	5.6
		10	1	1	1	1	6.5	6.1
		8	1	1	1	0	45.1	26.5
		4	1	1	1	0	60.3	19.5
		2	1	1	0	0	74.5	13.0
Teniposide	Insoluble	15	NA	NA	NA	NA	1.5	2.2
		10	1	1	1	1	6.1	5.7
		8	1	1	1	1	85.0	14.5
		4	1	1	1	0	76.1	23.3
		2	1	1	0	0	85.0	14.5
Diosmin	Slightly soluble	15	NA	NA	NA	NA	Insoluble	Insoluble
		10	1	1	1	1	Insoluble	Insoluble
		8	1	1	1	0	Insoluble	Insoluble
		4	1	1	1	0	Insoluble	Insoluble
		2	1	1	0	0	Insoluble	Insoluble

Table 2.5 List of positive and negative hits with experimental values.

Negative hits

Name	Water solubility	Concentration (mg)	LE 80	LC 10	LC 20	LC 30	LE (%)	LC (%)
Olanzapine	Insoluble	15	NA	NA	NA	NA	9.7	12.7
		10	0	0	0	0	6.1	5.8
		8	0	0	0	0	4.1	3.2
		4	0	0	0	0	7.0	2.7
		2	0	0	0	0	42.3	7.8
Simvastatin	Insoluble	15	NA	NA	NA	NA	5.0	7.0
		10	0	0	0	0	19.9	16.6
		8	0	0	0	0	87.2	41.1
		4	0	0	0	0	74.6	23.0
		2	0	0	0	0	87.2	14.8
Spirolactone	Insoluble	15	NA	NA	NA	NA	3.4	4.9
		10	0	0	0	0	31.8	24.1
		8	0	0	0	0	20.9	14.3
		4	0	0	0	0	53.8	17.7
		2	0	0	0	0	82.9	14.2
Tamibarotene	Insoluble	15	NA	NA	NA	NA	0.9	1.3
		10	0	0	0	0	2.0	1.9
		8	0	0	0	0	9.9	7.4
		4	0	0	0	0	87.3	25.9
		2	0	0	0	0	89.7	15.2

Table 2.5 List of positive and negative hits with experimental values.

Compound name	LE % (mean)	LC % (mean)
ABT-263	100	44.4
Podophyllotoxin	95.2	43.2
ETO	91.83 ± 2.92	42.33 ± 0.75
Simvastatin	87.2	41.1
Efavirenz	86.23	40.82
Cisplatin prodrug (C6)	84.8	40.4
VE-822	80.17 ± 4.48	26.65 ± 18.88
PTX	63.09 ± 42.16	30.38 ± 18.54
AZD5363	62.27 ± 1.93	33.27 ± 0.68
Cisplatin prodrug (C4)	58.5	31.9
Teniposide	57.2	31.4
Cisplatin prodrug (C10)	53.65	23.85
AZD8055	50.8	28.9
DTX	46.40 ± 40.43	18.99 ± 15.81
Rutin	45.1	26.5

Table 2.6 Top 15 compounds ranked by LE and LC for 8 mg drug vs. 10 mg polymer.

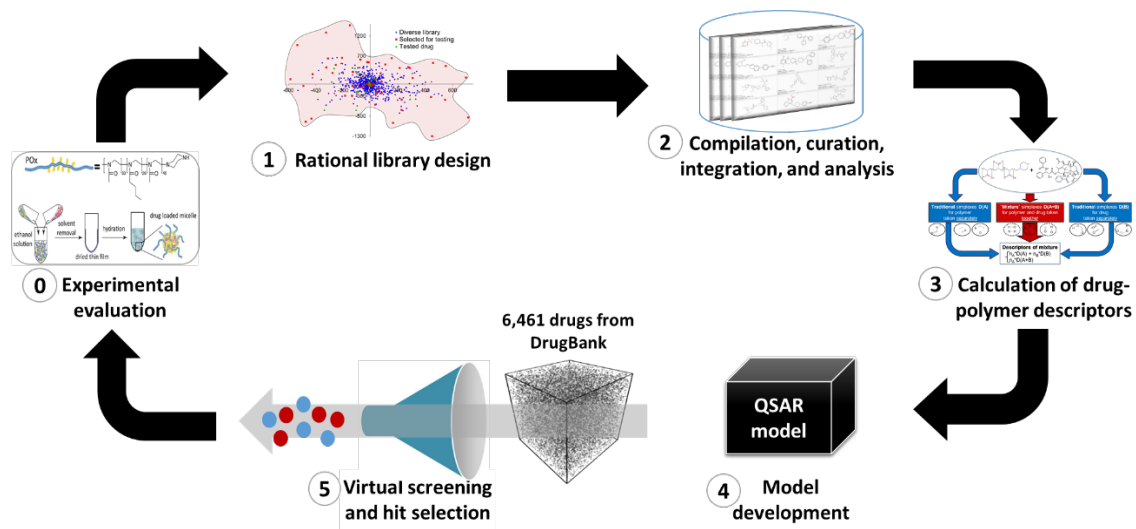


Figure 2.1 Study design

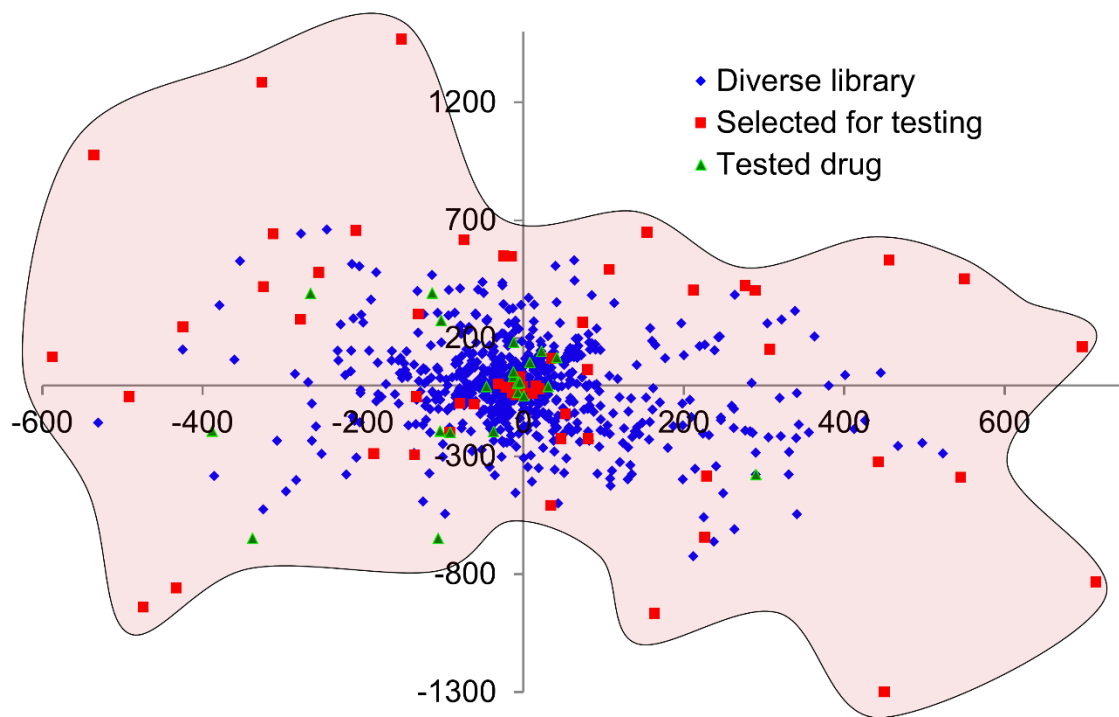


Figure 2.2 Coverage of chemical space by previously tested drugs and compounds rationally selected to increase structural diversity. Barycentric coordinates are calculated using 2D SiRMS (molecular fragments) descriptors differentiated by atom type.

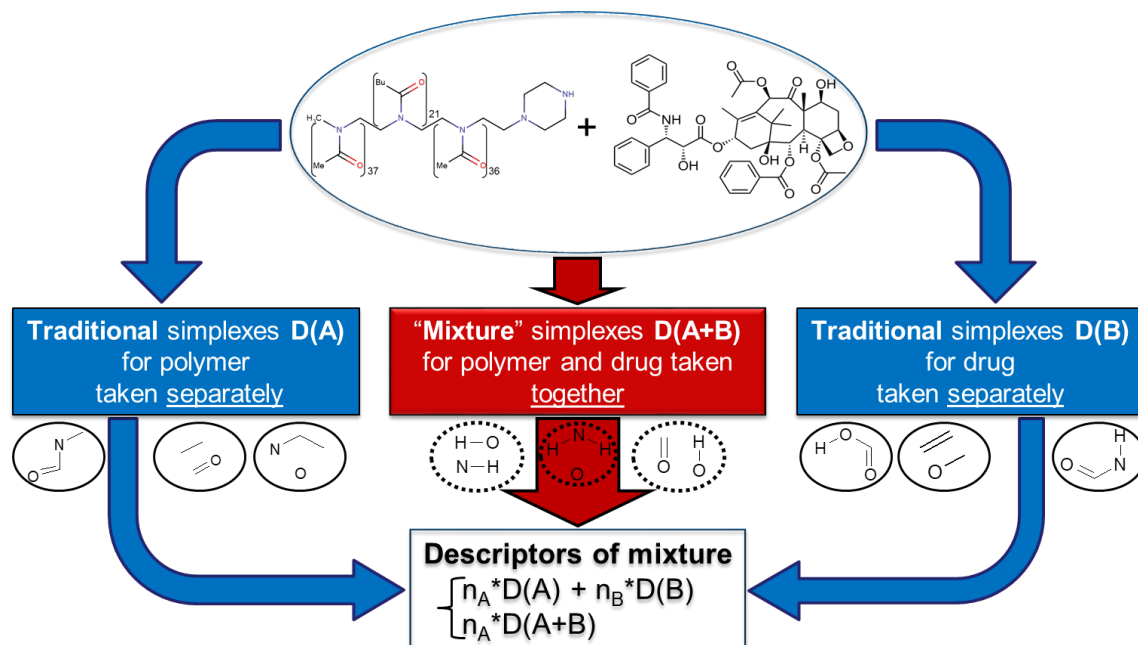


Figure 2.4 Descriptor calculation of drug-polymer complexes. n_A and n_B are molar fractions of components A and B ($n_A < n_B$).

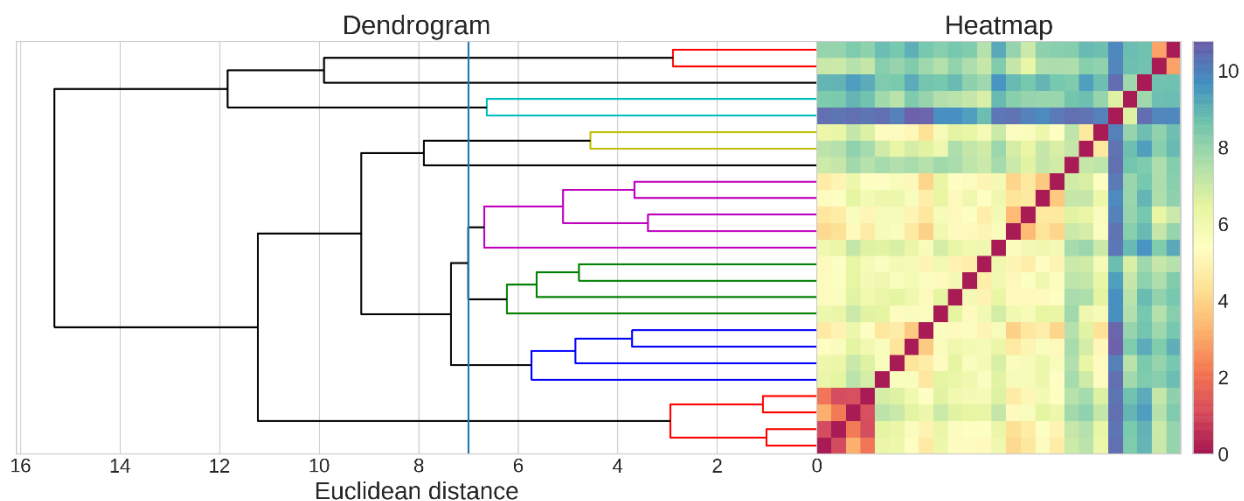


Figure 2.5 Results of cluster analysis of 25 compounds tested alone at 8 mg. Heatmap and dendrogram of the distance matrix are both colored according to structural similarity (red/yellow = similar; blue/violet = dissimilar).

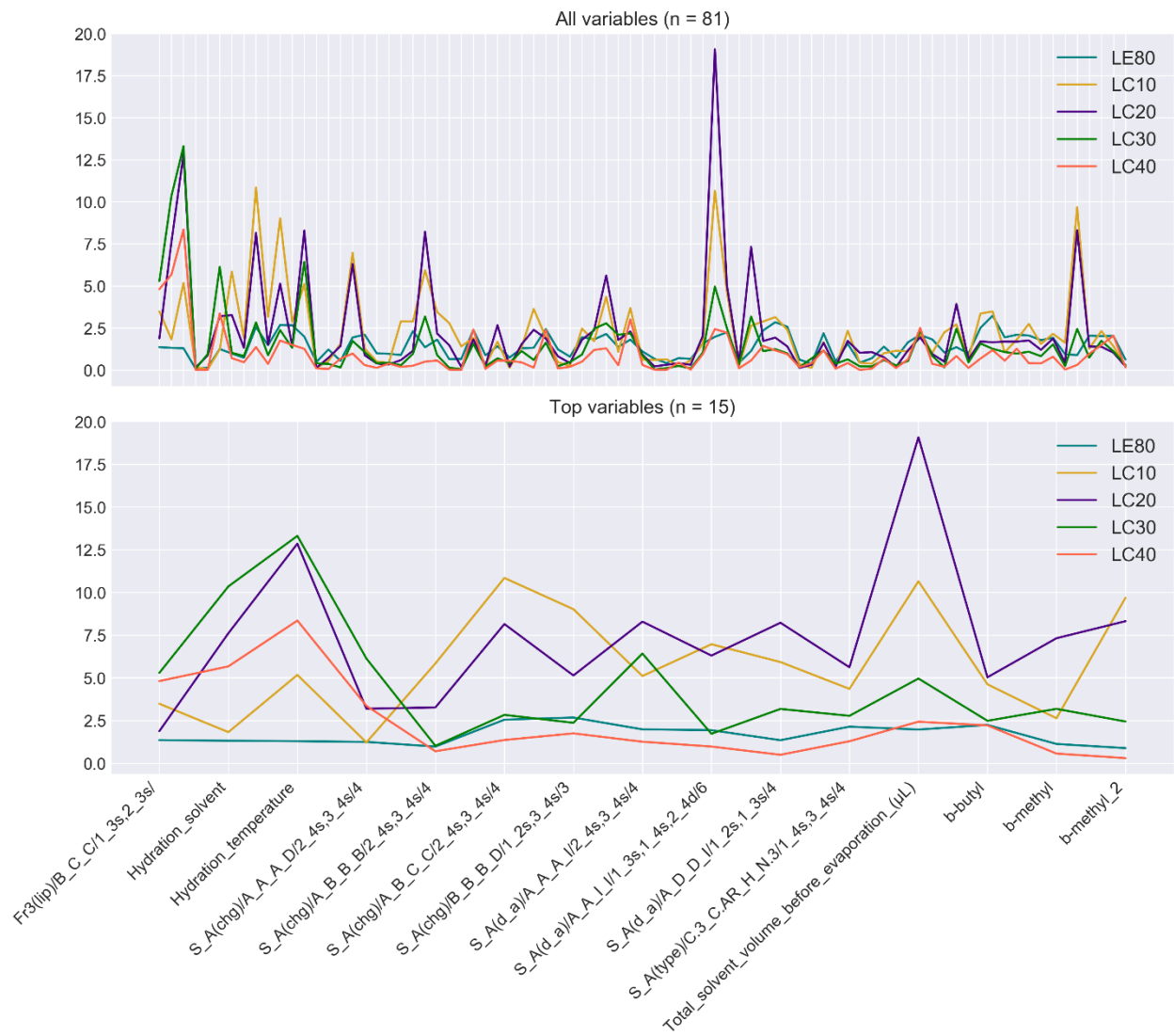


Figure 2.6 Variable importance for the five models developed. (Top) All the 81 variables used to build the models. (Bottom) Top 15 important variables identified.

REFERENCES

1. Lipinski, C.A.L.F., 2002. Poor aqueous solubility—an industry wide problem in drug discovery. *Am Pharm Rev*, 5(3), pp.82-85.
2. Yang, T., Cui, F.D., Choi, M.K., Cho, J.W., Chung, S.J., Shim, C.K. and Kim, D.D., 2007. Enhanced solubility and stability of PEGylated liposomal paclitaxel: in vitro and in vivo evaluation. *International journal of Pharmaceutics*, 338(1-2), pp.317-326.
3. Slowing, I.I., Vivero-Escoto, J.L., Wu, C.W. and Lin, V.S.Y., 2008. Mesoporous silica nanoparticles as controlled release drug delivery and gene transfection carriers. *Advanced drug delivery reviews*, 60(11), pp.1278-1288.
4. Kabanov, A.V. and Vinogradov, S.V., 2009. Nanogels as pharmaceutical carriers: finite networks of infinite capabilities. *Angewandte Chemie International Edition*, 48(30), pp.5418-5429.
5. Kabanov, A.V., Batrakova, E.V. and Alakhov, V.Y., 2002. Pluronic[®] block copolymers as novel polymer therapeutics for drug and gene delivery. *Journal of controlled release*, 82(2-3), pp.189-212.
6. Heimbach, T., Fleisher, D. and Kaddoumi, A., 2007. Prodrugs: Challenges and Rewards Part 1.
7. Nag, A. and Dey, B., 2010. *Computer-aided drug design and delivery systems*. McGraw Hill Professional.
8. Huynh, L., Neale, C., Pomès, R. and Allen, C., 2012. Computational approaches to the rational design of nanoemulsions, polymeric micelles, and dendrimers for drug delivery. *Nanomedicine: nanotechnology, biology and medicine*, 8(1), pp.20-36.
9. Frederix, P.W., Patmanidis, I. and Marrink, S.J., 2018. Molecular simulations of self-assembling bio-inspired supramolecular systems and their connection to experiments. *Chemical Society Reviews*, 47(10), pp.3470-3489.
10. Thota, N. and Jiang, J., 2015. Computational amphiphilic materials for drug delivery. *Frontiers in Materials*, 2, p.64.
11. Kuramochi, H., Andoh, Y., Yoshii, N. and Okazaki, S., 2009. All-Atom molecular dynamics study of a spherical micelle composed of N-acetylated poly (ethylene glycol)– Poly (γ -benzyl l-glutamate) block copolymers: A potential carrier of drug delivery systems for cancer. *The Journal of Physical Chemistry B*, 113(46), pp.15181-15188.
12. Badalkhani-Khamseh, F., Ebrahim-Habibi, A. and Hadipour, N.L., 2017. Atomistic computer simulations on multi-loaded PAMAM dendrimers: A comparison of amine-and hydroxyl-terminated dendrimers. *Journal of computer-aided molecular design*, 31(12), pp.1097-1111.

13. Caccavo, D., Barba, A.A., d'Amore, M., De Piano, R., Lamberti, G., Rossi, A. and Colombo, P., 2017. Modeling the modified drug release from curved shape drug delivery systems–Dome Matrix[®]. *European Journal of Pharmaceutics and Biopharmaceutics*, 121, pp.24-31.
14. Shi, C., Guo, D., Xiao, K., Wang, X., Wang, L. and Luo, J., 2015. A drug-specific nanocarrier design for efficient anticancer therapy. *Nature communications*, 6(1), pp.1-14.
15. Meunier, M., Goupil, A. and Lienard, P., 2017. Predicting drug loading in PLA-PEG nanoparticles. *International journal of pharmaceutics*, 526(1-2), pp.157-166.
16. Cherkasov, A., Muratov, E.N., Fourches, D., Varnek, A., Baskin, I.I., Cronin, M., Dearden, J., Gramatica, P., Martin, Y.C., Todeschini, R. and Consonni, V., 2014. QSAR modeling: where have you been? Where are you going to?. *Journal of medicinal chemistry*, 57(12), pp.4977-5010.
17. Dearden, J.C., 2017. The history and development of quantitative structure-activity relationships (QSARs). In *Oncology: breakthroughs in research and practice* (pp. 67-117). IGI Global.
18. Wu, W., Zhang, C., Lin, W., Chen, Q., Guo, X., Qian, Y. and Zhang, L., 2015. Quantitative structure-property relationship (QSPR) modeling of drug-loaded polymeric micelles via genetic function approximation. *PloS one*, 10(3).
19. Rasulev, B., Jabeen, F., Stafslie, S., Chisholm, B.J., Bahr, J., Ossowski, M. and Boudjouk, P., 2017. Polymer coating materials and their fouling release activity: A cheminformatics approach to predict properties. *ACS applied materials & interfaces*, 9(2), pp.1781-1792.
20. Potta, T., Zhen, Z., Grandhi, T.S.P., Christensen, M.D., Ramos, J., Breneman, C.M. and Rege, K., 2014. Discovery of antibiotics-derived polymers for gene delivery using combinatorial synthesis and cheminformatics modeling. *Biomaterials*, 35(6), pp.1977-1988.
21. Cern, A., Golbraikh, A., Sedykh, A., Tropsha, A., Barenholz, Y. and Goldblum, A., 2012. Quantitative structure-property relationship modeling of remote liposome loading of drugs. *Journal of controlled release*, 160(2), pp.147-157.
22. Cern, A., Marcus, D., Tropsha, A., Barenholz, Y. and Goldblum, A., 2017. New drug candidates for liposomal delivery identified by computer modeling of liposomes' remote loading and leakage. *Journal of Controlled Release*, 252, pp.18-27.
23. Luxenhofer, R., Schulz, A., Roques, C., Li, S., Bronich, T.K., Batrakova, E.V., Jordan, R. and Kabanov, A.V., 2010. Doubly amphiphilic poly (2-oxazoline) s as high-capacity delivery systems for hydrophobic drugs. *Biomaterials*, 31(18), pp.4972-4979.
24. He, Z., Schulz, A., Wan, X., Seitz, J., Bludau, H., Alakhova, D.Y., Darr, D.B., Perou, C.M., Jordan, R., Ojima, I. and Kabanov, A.V., 2015. Poly (2-oxazoline) based micelles with high capacity for 3rd generation taxoids: Preparation, in vitro and in vivo evaluation. *Journal of controlled release*, 208, pp.67-75.

25. Yamamoto, T., Yokoyama, M., Opanasopit, P., Hayama, A., Kawano, K. and Maitani, Y., 2007. What are determining factors for stable drug incorporation into polymeric micelle carriers? Consideration on physical and chemical characters of the micelle inner core. *Journal of controlled release*, 123(1), pp.11-18.
26. Lu, J., Zheng, M., Wang, Y., Shen, Q., Luo, X., Jiang, H. and Chen, K., 2011. Fragment-based prediction of skin sensitization using recursive partitioning. *Journal of computer-aided molecular design*, 25(9), p.885.
27. Muratov, E.N., Artemenko, A.G., Varlamova, E.V., Polishchuk, P.G., Lozitsky, V.P., Fedchuk, A.S., Lozitska, R.L., Gridina, T.Y.L., Koroleva, L.S., Sil'nikov, V.N. and Galabov, A.S., 2010. *Per aspera ad astra*: application of Simplex QSAR approach in antiviral research. *Future medicinal chemistry*, 2(7), pp.1205-1226.
28. Muratov, E.N., Varlamova, E.V., Artemenko, A.G., Polishchuk, P.G. and Kuz'min, V.E., 2012. Existing and developing approaches for QSAR analysis of mixtures. *Molecular informatics*, 31(3-4), pp.202-221.
29. Oprisiu, I., Varlamova, E., Muratov, E., Artemenko, A., Marcou, G., Polishchuk, P., Kuz'min, V. and Varnek, A., 2012. QSPR approach to predict nonadditive properties of mixtures. Application to bubble point temperatures of binary mixtures of liquids. *Molecular informatics*, 31(6-7), pp.491-502.
30. Ward Jr, J.H., 1963. Hierarchical grouping to optimize an objective function. *Journal of the American statistical association*, 58(301), pp.236-244.
31. Wan, X., Min, Y., Bludau, H., Keith, A., Sheiko, S.S., Jordan, R., Wang, A.Z., Sokolsky-Papkov, M. and Kabanov, A.V., 2018. Drug Combination synergy in worm-like polymeric micelles improves treatment outcome for small cell and non-small cell lung cancer. *ACS nano*, 12(3), pp.2426-2439.
32. Seo, Y., Schulz, A., Han, Y., He, Z., Bludau, H., Wan, X., Tong, J., Bronich, T.K., Sokolsky, M., Luxenhofer, R. and Jordan, R., 2015. Poly (2-oxazoline) block copolymer based formulations of taxanes: effect of copolymer and drug structure, concentration, and environmental factors. *Polymers for Advanced Technologies*, 26(7), pp.837-850.
33. Schulz, A., Jaksch, S., Schubel, R., Wegener, E., Di, Z., Han, Y., Meister, A., Kressler, J., Kabanov, A.V., Luxenhofer, R. and Papadakis, C.M., 2014. Drug-induced morphology switch in drug delivery systems based on poly (2-oxazoline) s. *ACS nano*, 8(3), pp.2686-2696.
34. Stegemann, S., Leveiller, F., Franchi, D., De Jong, H. and Lindén, H., 2007. When poor solubility becomes an issue: from early stage to proof of concept. *European journal of pharmaceutical sciences*, 31(5), pp.249-261.

35. Yu, X., Che, Z. and Xu, H., 2017. Recent advances in the chemistry and biology of podophyllotoxins. *Chemistry—A European Journal*, 23(19), pp.4467-4526.
36. Murtaza, G., 2012. Solubility enhancement of simvastatin: a review. *Acta Pol Pharm*, 69(4), pp.581-90.
37. Dhar, S., Kolishetti, N., Lippard, S.J. and Farokhzad, O.C., 2011. Targeted delivery of a cisplatin prodrug for safer and more effective prostate cancer therapy in vivo. *Proceedings of the National Academy of Sciences*, 108(5), pp.1850-1855.
38. Vityuk, N., Voskresenskaja, E. and Kuz'min, V., 1999. The synergism of methods barycentric coordinates and trend-vector for solution—Structure-property tasks. *Pattern Recognit. Image Anal*, 3, pp.521-528.
39. Kuz'min, V.E., Artemenko, A.G. and Muratov, E.N., 2008. Hierarchical QSAR technology based on the Simplex representation of molecular structure. *Journal of computer-aided molecular design*, 22(6-7), pp.403-421.
40. Kuz'min, V.E., Muratov, E.N., Artemenko, A.G., Varlamova, E.V., Gorb, L., Wang, J. and Leszczynski, J., 2009. Consensus QSAR Modeling of Phosphor-Containing Chiral AChE Inhibitors. *QSAR & combinatorial science*, 28(6-7), pp.664-677.
41. Fourches, D., Muratov, E. and Tropsha, A., 2010. Trust, but verify: on the importance of chemical structure curation in cheminformatics and QSAR modeling research. *Journal of chemical information and modeling*, 50(7), pp.1189-1204.
42. Fourches, D., Muratov, E. and Tropsha, A., 2015. Curation of chemogenomics data. *Nature chemical biology*, 11(8), pp.535-535.
43. Fourches, D., Muratov, E. and Tropsha, A., 2016. Trust, but verify II: a practical guide to chemogenomics data curation. *Journal of chemical information and modeling*, 56(7), pp.1243-1252.
44. Kuz'min, V.E., Artemenko, A.G., Muratov, E.N., Volineckaya, I.L., Makarov, V.A., Riabova, O.B., Wutzler, P. and Schmidtke, M., 2007. Quantitative Structure– Activity Relationship Studies of [(Biphenyloxy) propyl] isoxazole Derivatives. Inhibitors of Human Rhinovirus 2 Replication. *Journal of medicinal chemistry*, 50(17), pp.4205-4213.
45. Varnek, A., Fourches, D., Horvath, D., Klimchuk, O., Gaudin, C., Vayer, P., Solov'ev, V., Hoonakker, F., Tetko, I.V. and Marcou, G., 2008. ISIDA-Platform for virtual screening based on fragment and pharmacophoric descriptors. *Current Computer-Aided Drug Design*, 4(3), p.191.
46. Alves, V.M., Muratov, E.N., Zakharov, A., Muratov, N.N., Andrade, C.H. and Tropsha, A., 2018. Chemical toxicity prediction for major classes of industrial chemicals: Is it possible to develop universal models covering cosmetics, drugs, and pesticides?. *Food and Chemical Toxicology*, 112, pp.526-534.

47. Alves, V.M., Capuzzi, S.J., Muratov, E.N., Braga, R.C., Thornton, T.E., Fourches, D., Strickland, J., Kleinstreuer, N., Andrade, C.H. and Tropsha, A., 2016. QSAR models of human data can enrich or replace LLNA testing for human skin sensitization. *Green Chemistry*, 18(24), pp.6501-6515.
48. Alves, V.M., Muratov, E., Fourches, D., Strickland, J., Kleinstreuer, N., Andrade, C.H. and Tropsha, A., 2015. Predicting chemically-induced skin reactions. Part I: QSAR models of skin sensitization and their application to identify potentially hazardous compounds. *Toxicology and applied pharmacology*, 284(2), pp.262-272.
49. Downs, G.M. and Barnard, J.M., 2002. Clustering methods and their uses in computational chemistry. *Reviews in computational chemistry*, 18, pp.1-40.
50. Tropsha, A., 2010. Best practices for QSAR model development, validation, and exploitation. *Molecular informatics*, 29(6-7), pp.476-488.
51. Breiman, L., 2001. Random forests. *Machine learning*, 45(1), pp.5-32.
52. Breiman, L., Friedman, J.H., Olshen, R.A. and Stone, C.J., 1984. Classification and regression trees. Wadsworth & Brooks. *Cole Statistics/Probability Series*.
53. Zakharov, A.V., Varlamova, E.V., Lagunin, A.A., Dmitriev, A.V., Muratov, E.N., Fourches, D., Kuz'min, V.E., Poroikov, V.V., Tropsha, A. and Nicklaus, M.C., 2016. QSAR modeling and prediction of drug–drug interactions. *Molecular pharmaceutics*, 13(2), pp.545-556.
54. Golbraikh, A., Shen, M., Xiao, Z., Xiao, Y.D., Lee, K.H. and Tropsha, A., 2003. Rational selection of training and test sets for the development of validated QSAR models. *Journal of computer-aided molecular design*, 17(2-4), pp.241-253.
55. Schulz, A., Han, Y., He, Z., Bronich, T.K., Kabanov, A.V., Luxenhofer, R. and Jordan, R., 2012. Poly (2-oxazoline) s: An all-around drug delivery system. *Polym. Prepr*, 53, p.354.
56. Han, Y., He, Z., Schulz, A., Bronich, T.K., Jordan, R., Luxenhofer, R. and Kabanov, A.V., 2012. Synergistic combinations of multiple chemotherapeutic agents in high capacity poly (2-oxazoline) micelles. *Molecular pharmaceutics*, 9(8), pp.2302-2313.

CHAPTER III: POLY(2-OXAZOLINE) MICELLES WITH VISMODEGIB ENHANCES TARGETING OF SHH PATHWAY IN GENETIC MODEL OF MEDULLOBLASTOMA¹

3.1 SUMMARY

The distribution of drugs from the blood into brain tumors is limited by the blood-brain barrier (BBB) and serum protein binding, reducing the efficacy of brain tumor treatment. Here we report a nanoparticle delivery system based on poly(2-oxazoline) micelles (POx) that addresses these obstacles, bringing new efficacy to promising brain tumor therapies under development. The SHH-pathway inhibitor vismodegib, effectively treats SHH-dependent basal cell carcinoma, but has not been as effective in medulloblastoma. We formulated vismodegib in POx micelles (POx-vismo) and show that this nanoparticle formulation improved vismodegib efficacy for medulloblastoma, demonstrated in the treatment of endogenous medulloblastomas that form *in vivo* in transgenic hGFAP-Cre/SmoM2 (G-Smo) mice. Importantly, while extra-neural toxicity often limits the dosing of systemically-administered brain tumor therapies, POx-vismo formulation reduced systemic toxicity. Mechanistic studies show that nanoparticle delivery decreased vismodegib binding to serum proteins and improved brain and tumor drug penetration without penetration of the nanoparticle carrier into the CNS. The POx system is a versatile drug delivery platform, and our results show the broad potential for POx micelle delivery to make existing brain tumor treatments newly effective.

¹ This chapter previously appeared as a manuscript soon to be submitted.

3.2 Introduction

Current therapy for medulloblastoma, with surgery, radiation and chemotherapy, allows most medulloblastoma patients to survive >5 years, but causes long-term neuro-cognitive injury. Personalized medicine using molecularly targeted agents (MTAs) directed against the particular genetic addictions and vulnerabilities of tumor cells may target medulloblastoma cells with greater effectiveness and specificity, potentially improving therapeutic efficacy and toxicity [1]. About one-third of medulloblastomas show SHH pathway hyper-activation, and for these patients, targeted inhibition of SHH signaling may improve therapy [2]. Vismodegib, a small molecule inhibitor of SHH receptor component Smoothed (SMO), is FDA-approved for the treatment of basal cell carcinoma and is under clinical evaluation in other SHH-driven cancers such as metastatic colorectal, advanced stomach and pancreatic cancer [3]. In medulloblastoma vismodegib treatment produces initial responses, but these responses in have been short-lived, consistently ending in treatment failure [4-6].

The physicochemical properties of vismodegib may limit its brain bio-availability and contribute to its limited efficacy for medulloblastoma. Due to the physicochemical properties of vismodegib in combination with its extremely low aqueous solubility (0.1 ug/ml in at pH 7.0), and oral bioavailability of 31.8%, the drug is currently approved as oral dosage form [7]. However, oral administration of vismodegib presents a challenge in pediatric population most at risk for medulloblastoma [8]. Vismodegib has high affinity to serum proteins, including acid-glycoprotein and albumin, aqueous solubility of vismodegib is extremely low (0.1 ug/ml in at pH 7.0) resulting in >99% of the drug circulating in protein bound form [9]. Data from human studies show that the low unbound fraction of vismodegib in blood limits its brain bioavailability. In a Phase I study of vismodegib in pediatric medulloblastoma patients, the ratio of CSF vismodegib to the total drug

in the plasma was 0.0026, however once the ratio was calculated relative to non-protein bound drug it was as high as 0.53 (0.26–0.78) [10]. These data highlight the potential for reduced protein binding to improve vismodegib pharmacokinetics in the CNS.

A variety of nanoparticles, which are 1-100 nm structures, have been employed for drug delivery to the brain. Several classes of nanoparticles have been developed for delivery of hydrophobic molecules, such as PLGA based nanoparticles, liposomes and polymeric micelles. Several nanoparticle-based therapeutic products have been approved for clinical use, and more are currently under development or clinical evaluation [11, 12]. Encapsulation of drugs in nanoparticles has been shown to enhance the solubility of hydrophobic agents, to extend their systemic circulation, to provide sustained release of the drug, to improve drug exposure, to enhance drug accumulation in target tissues and to minimize the off-site effects [13, 14]]. Importantly, these systems may enhance drug delivery without depending on the expression of a receptor that cancer cells might down-regulate to become resistant. Polymeric micelles, formed by the self-assembly of amphiphilic block polymers are a nanoparticle technology that has shown promise in clinical implementation [15]. For example, Genexol-PM, paclitaxel-loaded nanoparticle system comprising a block copolymer of poly(ethylene glycol) (PEG) and poly(DL-lactide) (PLA) by Samyang Biopharmaceuticals is clinically approved in South Korea [16]. Similarly, NC-6004, a cisplatin-loaded polymeric micelle system based on PEG and modified poly(L-glutamic acid) developed by Nanocarrier showed enhanced platinum exposure both in plasma and tumor in preclinical studies and is currently evaluated in Phase III clinical studies. [17]. However, these systems have been limited by rather low drug loading and/or chemical structure of the loaded drugs.

POx polymer micelles represent core-shell structures, in which the core and shell can be easily fine-tuned to optimize drug incorporation and release and to modify drug pharmacokinetics and biodistribution [18]. These optimizations are enabled by the flexibility and richness of the POx polymer chemistry, which has a polar backbone and side groups of diverse structure and polarity [19, 20]. We have previously shown that nanoparticle-sized micelles formed from poly(2-oxazoline) amphiphilic block copolymers (POx polymer) can be used to deliver poorly soluble drugs and drug combinations across broad spectrum of chemical space [21, 22]. POx-formulated drugs form stable micelles of narrow size range (10-100nm), which can be lyophilized and re-dispersed without loss of the particle size, drug loading, or drug activity [23, 24]. The POx polymer micelle system is unique in its ability to incorporate unprecedentedly large amounts of insoluble drugs [23, 24]. We hypothesized that loading vismodegib into POx micelles, would improve drug delivery to the brain and tumor and make previously failed brain tumor therapies newly effective.

In this report, we developed and evaluated POx-vismo, a POx polymer micelle formulation of vismodegib, for the treatment of medulloblastoma. To test this formulation, we generated mice with primary medulloblastomas by breeding transgenic SmoM2 mice that harbor a Cre-dependent, oncogenic, constitutively active allele of Smo [25], with GFAP-Cre mice that express Cre recombinase in stem cells of the developing brain [26]. The resulting G-Smo mice develop medulloblastoma with 100% frequency by P10 (Figure 3.1) and if left untreated die from tumor progression by P20 [27]. We treated G-Smo mice with either POx-vismo or control formulations of vismodegib in oral suspension or dissolved in NMP/PEG mixture as control parenteral formulation (c-vismo) and then compared efficacy and pharmacokinetics. This preclinical study showcases the translational potential of POx micelles to improve the therapeutic efficacy of

vismodegib in SHH-driven and highlights the broad potential of the POx platform for optimizing drug delivery for brain tumor therapy.

3.3 Materials and Methods

Materials

All materials for the synthesis of poly(2-oxazoline) block copolymer (Methyl trifluoromethanesulfonate, 2-methyl-2-oxazoline, 2-n-butyl-2-oxazoline), N-Methyl-2-pyrrolidone (NMP), poly (ethylene glycol) with 300 average molecular weight (PEG300), FSA powder and Acetone were purchased from Sigma Aldrich (St. Louis, MO). Vismodegib free base was purchased from LC Laboratories (Woburn, MA). For the c-vismo formulation, vismodegib was dissolved in n-methyl pyrrolidone (NMP) and then diluted in polyethylene glycol 300 (PEG300) to a final vismodegib concentration of 21 mg/mL. No vismodegib precipitation was observed.

Water and acetonitrile (HPLC grade) were purchased from Fisher Scientific Inc. (Fairlawn, NJ). PCNA antibody for immunohistochemistry was purchased from Abcam (Cat# ab92552; Cambridge, MA). Alexa-647-conjugated antibodies to pRB were purchased from Cell Signaling Technology (cat# 8974; Danvers, MA). To prepare tumors for flow cytometry, papain was purchased from Worthington Biochemical Corporation (Lakewood, NJ) and Fix&Perm[®] cell fixation and permeabilization kit was purchased from Thermo Fisher Scientific.

Preparation of POx-vismo micelles

The amphiphilic triblock copolymer (P(MeOx39-b-PBuOx25-b-PMeOx39)), $M_n = 8.2$ kg/mol, PDI = 1.11) was synthesized and characterized as previously described (21). Vismodegib-loaded polymeric micelle formulation (POx-vismo) was prepared by the thin film hydration method (23). Briefly, stock solutions of the polymer and vismodegib (10 mg/ml in acetone) were mixed together at the pre-determined ratios (2:10-8:10 drug to polymer w/w ratios). The organic solvent was evaporated at 60 °C under a stream of nitrogen gas to form a thin-film of drug-polymer

homogenous mixture. To obtain well-dried thin film, the films were dried in the vacuum chamber (approx. 0.2 mbar) overnight. Next, the thin films were rehydrated with saline and then incubated at 60 °C for 10 min to self-assembly into drug-loaded polymeric micelles solution. The formed POx-vismo micelles were centrifuged at 10,000 rpm for 3 minutes (Sorvall Legend Micro 21R Centrifuge, Thermo Scientific) to remove non-loaded vismodegib.

Characterization of POx-vismo micelles

The Z_{ave} and the polydispersity index (PDI) of POx-vismo were determined using a Nano-ZS (Malvern Instruments Inc., UK) dynamic light scattering (DLS) equipment. Briefly, each sample was diluted with saline to yield 1 mg/mL final polymer concentration before the measurement. Z_{ave} and the polydispersity index (PDI) of POx-vismo were determined by cumulate analysis. Results are the average of three independent micelle samples measurements.

The morphology of POx-vismo micelles was determined using a LEO EM910 TEM operating at 80 kV (Carl Zeiss SMT Inc., Peabody, MA). Digital images were obtained using a Gatan Orius SC1000 CCD Digital Camera in combination with Digital Micrograph 3.11.0 software (Gatan Inc., Pleasanton, CA). One drop of each diluted Vismodegib nanoparticle solution (dilute 500 or 1000 times using saline) was deposited on a copper grid/carbon film for 5 min and excess solution was wiped off using fine filter paper. Then one drop of negative staining solution (1% uranyl acetate) was added and allow to dry for 10 s prior to the TEM imaging.

The final concentration of vismodegib in POx-vismo micelles was determined by HPLC (Agilent Technologies 1200 series) using Agilent eclipse plus C18 3.5 μ m column (4.6mm \times 150mm) with a mixture of acetonitrile/water (30%/70% v/v, 0.01% trifluoroacetic acid mobile phase. The samples were diluted with mobile phase to final concentration of 100 μ g/mL of vismodegib (and injected (10 μ L) into the HPLC system. The flow rate was 1.0 mL/min, and

column temperature was 40 °C. Detection wavelength was 245 nm. Vismodegib concentration was quantified against free vismodegib analytical standards.

Loading efficiency (LE) and loading capacity (LC) calculations. The following equations were used to calculate LE and LC of vismodegib in POx-vismo micelles:

$$LE (\%) = M_{\text{drug}} / (M_{\text{drug added}}) \times 100\%, \quad (1)$$

$$LC (\%) = M_{\text{drug}} / (M_{\text{drug}} + M_{\text{excipient}}) \times 100\%, \quad (2)$$

Where M_{drug} and $M_{\text{excipient}}$ are the mass of the solubilized drug and polymer excipient in the solution, while $M_{\text{drug added}}$ is the weight amount of the drug added to the dispersion during the preparation of the micelle formulation.

Stability of POx-vismo micelles was evaluated by measuring both the loading of vismodegib in the POx-vismo micelles as well as the Zave and PDI of the micelles overtime. The POx-vismo micelles solutions (10 mg/mL of polymer concentration) were incubated in saline at 4 °C for 1 month. At pre-determined time points the aliquots were removed and the vismo concentration was measured by HPLC and the Zave and PDI of the POx-vismo were measured by DLS as previously described.

Nanoparticle stability after lyophilization

Freshly prepared POx-vismo micelles solution (100 μ L, 1 mg/mL of vismodegib in saline) was immediately frozen in liquid nitrogen for 5 min and lyophilized to obtain white powder of POx-vismo. Powder formulation of POx-vismo was resuspended in DI water to form POx-vismo micelles solution. Zave and PDI of resuspended POx-vismo were measured by DLS. The actual drug loading in POx-vismo was confirmed by HPLC analysis as described above. For HPLC

analysis, resuspended POx-vismo solution was centrifuged (10,000 rpm and 3 minutes) to remove any drug or polymer precipitate formed during the resuspension of the lyophilized powder.

Release of vismodegib from POx-vismo micelles

Release of vismodegib from POx-vismo micelles was investigated using membrane dialysis method against 10% solution of BSA in phosphate buffered saline (pH 7.4) at 37 C. Briefly, POx-vismo was diluted in saline to final concentration of 0.6 mg/mL of vismodegib. Subsequently, 100 μ L of the diluted POx-vismo solutions were loaded into floatable Slide-A-Lyzer MINI dialysis devices (500 μ L capacity, 3.5 kDa MWCO; Thermo Fisher Scientific). The dialysis devices (n=3) were floated in 20 mL of 10% BSA in PBS solution in compliance with the perfect sink conditions requirements. At each time point the samples were withdrawn from dialysis devices and the amount of vismodegib was quantified by HPLC. Drug release profiles were constructed by plotting the percentage of vismodegib released from POx-vismo micelles over time.

Mouse breeding

Medulloblastoma-prone G-Smo mice were generated from the cross between hGFAP-Cre (generously shared by Dr. Eva Anton, UNC) and SmoM2loxP/loxP (Jackson labs, Stock #005130) mouse lines. All mice were of species *Mus musculus* and crossed into the C57BL/6 background through at least five generations. All animal studies were carried out with the approval of the University of North Carolina Institutional Animal Care and Use Committee under protocol 16-099.

Measurement of pharmacodynamic response by pRB quantification

Groups of 4 replicate mice G-Smo mice were injected IP on postnatal days 12 with the indicated dose and formulation of vismodegib. After the indicated interval, tumors from these mice were dissected free and dissociated as previously described [46]. Briefly, we incubated tumors in papain (20 units/ml; Worthington Biochemical Corporation) at 37°C for 15 min. Tumors were then triturated and cells were separated from the debris by centrifugation in a discontinuous density gradient of ovomucoid inhibitor. Dissociated cells were then treated with the Fix & Perm[®] Cell Fixation and Permeabilization Kit per manufacturer instructions (Thermo Fisher Scientific). Fixed cells were incubated in 1:50 dilution of anti-phospho-Rb/Alexa Flour[®] 647 conjugated (Cell Signaling Technology) and 1:100 dilution of FX Cycle[™] Violet Stain for 2 hours in the dark on ice. Flow cytometry was then performed on an LSR Fortessa (BD Biosciences). Technical controls included no stain, single-stained and fluorescence-minus-one samples.

Tumor pathology studies

Groups of 4 replicate mice G-Smo mice were injected IP on P10-12 with the indicated dose and formulation of vismodegib. After 24 hours, mouse brains including tumors were harvested, fixed, embedded in paraffin and processed for IHC as previously described [47] using antibodies to PCNA (Cell Signaling Technology, Danvers, MA, USA). Similarly, mouse brains including tumors were harvested from mice in the survival study as they reached the humane end point or P35 and processed for IHC. Stained slides were digitally acquired using an Aperio ScanScope XT (Aperio, Vista, CA, USA).

In vivo toxicity studies

Toxicity of Pox-vismo and c-vismo was evaluated in healthy Wt C57BL/6 mice. We administered vismodegib in the indicated doses and formulations to groups of 3 replicate mice on days P10-P12 and then every over day until P21. Mice were weighed daily and examined for health defects. As mice at P12-21 are expected to gain weight steadily, we used the weights of age matched littermate controls to define the expected weight at each time point. Mice consistently weighing less than 90% of the controls were considered to be growth impaired.

In vivo efficacy studies

G-Smo mice were randomized into the indicated treatment groups with a minimum of 8 replicate mice per group. The indicated treatments were administered IP daily on P10-P12 and then every over day until P35, unless mice first developed symptoms of tumor progression. Symptoms of tumor progression included hunched posture, paucity of movement, ataxia and weight loss. All mice with symptomatic tumors were euthanized. The EFS was defined as the survival time until the development of symptoms. Survival times for each group were compared by Log Rank analysis.

IR-MALDESI Imaging of the spatial distribution of vismodegib

For MALDESI imaging, 2 replicate G-Smo mice were injected with each formulation. Mouse brains were dissected free and placed on a foil barrier over dry ice for rapid freezing. 10 μm frozen sections of brains in the sagittal plane were prepared in a cryotome, briefly thaw-mounted on glass microscope slides that had been uniformly coated with prednisolone as an internal standard using a pneumatic sprayer (TM-Sprayer, HTX Technologies, Carrboro, NC, USA), and then maintained at -10 °C on the sample stage of the IR-MALDESI source chamber

prior to analysis. The stage translated the sample step-wise across the focused beam of an IR laser ($\lambda = 2.94 \mu\text{m}$, IR-Opolette 2371; Oportek, Carlsbad, CA, USA), which desorbed sample material from adjacent $100\mu\text{m}$ diameter sampling locations. An electrospray (50/50 mixture of methanol/water (v/v) with 0.2% formic acid) ionized the desorbed neutral molecules, and resulting ions were sampled into a high resolving power Thermo Fisher Scientific Q Exactive Plus (Bremen, Germany) mass spectrometer for synchronized analysis. The mass spectrometer was operated in positive ion mode from m/z 200 to 800, with resolving power of 140,000FWHM at m/z 200. With high mass measurement accuracy (MMA) within 5 ppm maintained using protonated and sodiated adducts of diisooctyl phthalate as two internal lock masses at m/z 391.28428 and 413.26623, vismodegib and prednisolone were identified as protonated molecular ions $[M+H]^+$ at m/z 421.01695 and m/z 361.20095, respectively. To generate images from mass spectrometry data, raw data from each voxel was converted to the mzXML format using MSConvert software [48]. These mzXML files were interrogated using MSiReader, a free software developed for processing MSI data [49].

Pharmacokinetic analysis

3 replicate G-Smo mice were used for each dose and formulation. The mice were injected IP on P12 with 100 mg/kg POx-vismo or 100 mg/kg c-vismo. At indicated sampling times, 4 replicate mice were euthanized. From these mice, blood samples were collected by cardiac puncture. The brains, including forebrain and tumor tissue, were also removed, washed in ice-cold saline, weighted, homogenized in a glass tissue homogenizer (Tearor™, BioSpec Products, Inc.) and spiked with internal standard (reserpine) solution and calibration standard solution. Subsequently, samples were treated with 1% formic acid in acetonitrile and then centrifuged to

obtain the supernatant. The supernatants were transferred to 96-well plate, acetonitrile was evaporated and the reconstitution solution (acetonitrile/water/0.1% formic acid) was added to each sample. The plate was centrifuged again and the supernatant that transferred to analysis plate (tomec). After sealing the analysis plate with Easy Pierce foil, tissue samples were analyzed by LC-MS. Chromatographic separation was carried out on a HALO PFP column (2.1×50 mm, 5 μm; Advanced Materials Technology, Wilimington, DE, USA) using a Shimadzu UFLC system equipped with a binary pump, a vacuum degasser and an autosampler (PAL system, Lake Elmo, MN, USA). The column oven was maintained at 40 °C. The mobile phase consisting of water and acetonitrile (containing 0.1% of formic acid) (90:10, v/v) was performed at a flow rate of 0.5 mL/min. The samples were kept at 4 °C in the autosampler. The mass spectrometry was performed on Thermo TSQ Quantum Ultra (Thermo Fisher Scientific, Waltham, MA, USA). Ionization was operated using an atmospheric pressure chemical ionization (APCI) source in positive ion mode. The APCI source was operated with an ionspray voltage of 5000 V. The capillary temperature was 300 °C. The MS recordings were carried out in selected reaction monitoring (SRM) mode with specific ion transitions of precursor ion to product ion at m/z 647.4→191.2 with collision energy (CE) of 38 eV, declustering potential (DP) of 85 V and entrance potential (EP) of 15 V for TY501, and at m/z 473.3→143.3 with CE of 23 eV, DP of 55 V and EP of 10 V for IS. The total analytical time was 5 min. PK analysis was performed using Phoenix Winnonlin. Initial estimates, AUC, and C_{max} was determined using naïve pooling NCA. A one compartment model was fit to the data and PK parameters K_a , V_d , and CL were obtained from the models. Simulations were executed using the obtained parameters. All statistical significance was at the 95% confidence level.

NMR analysis

G-Smo mice were injected IP on P12 with 50-100 mg/kg POx-vismo or 50-100 mg/kg c-vismo. 4h post injection, 3 replicate mice were euthanized. From these mice, blood samples were collected by cardiac puncture. The brains, including forebrain and tumor tissue, were also removed, washed in ice- cold saline and frozen. 600 μ l of 100% acetonitrile was added to the frozen tissue (70-200 mg), then tissue was homogenized with pestle, frozen and thawed. Next, 400 μ l of water was added, followed by the thorough vortexing. The sample was frozen and thawed again. Supernatant was separated by centrifugation and lyophilized. The powder was resuspended in 600 μ l deuterated methanol. The ^1H NMR spectra were acquired at 25 $^\circ\text{C}$ using a 19.97 T Bruker spectrometer equipped with a 5 mm HCN NMR probe with a one-pulse sequence using a 90° flip angle, with a 1.5 s presaturation pulse on residual water, a 2.5 s acquisition time and 1.5 s relaxation time resulting in a 4 s repetition time. The sweep width was 6,000 Hz and acquired with 15,000 complex points, and 128 transients.

All NMR spectra were processed using ACD/1D NMR Manager software (version 12.0; Advanced Chemistry Development). Imported FIDs were zero-filled to 32,000 points, and an exponential line broadening of 0.3 Hz was applied before Fourier transformation. Phase and baseline correction were conducted for the spectra. Peaks were integrated and values were exported to Excel for data processing.

BSA binding analysis

Vismodegib binding to bovine serum albumin (BSA) was evaluated by measuring decrease in fluorescence emission spectra of tryptophan residues of BSA. Increasing concentrations of POx vismo or c-vismo were incubated in fetal bovine serum diluted with PBS to final BSA

concentration of approx. 40mg/ml for 15 min at 25 °C. Emission spectra were recorded from 300 to 440 nm after excitation at 295 nm using SpectraMax M5 spectrometer. Both excitation emission slits were set at 1 nm. Presented data represents average of triplicate samples. To evaluate the release of vismodegib and binding to BSA over time, POx-vismo or c-vismo samples were added to 250 µl of FBS and incubated at 37 °C for predetermined time points. After the incubation, the samples were transferred to a prewarmed 10 kDa MWCO Vivacon filter tube and spun at 12,000xg for 10 min at 37 °C. Filtrates were mixed with acetonitrile and analyzed on HPLC. Presented data represents average of triplicate sample.

Statistical analysis

Statistical analyses for pharmacokinetic profile of vismodegib were performed using the two-tailed student's t-test (Graphpad Prism, version 5.1.). For the survival analyses, the Log Rank test was used.

3.4 Results

Vismodegib can be effectively formulated in poly(2-oxazoline) micelles.

We prepared POx-vismo polymeric micelles using POx polymer P(MeOx39-b-BuOx25-b-MeOx39) ($M_n = 8.2$ kg/mol, \bar{D} (M_w/M_n) = 1.11). We generated micelles with vismodegib:POx polymer ratios of 2:10, 4:10, 6:10 and 8:10 w/w (drug to polymer) using the thin film method [21]. Briefly, we dissolved vismodegib free base and POx polymer in acetone, mixed the components at the desired ratio, and then allowed the solvent to evaporate, leaving a film. We then added saline, and after gentle agitation and heating, drug-loaded micelles formed spontaneously. At all tested ratios, the loading efficiency (LE, %) of vismodegib was nearly 90% and the loading capacity was 13.5-42.4% w/w depending on the drug:polymer ratio (Table 3.1). POx-vismo micelles had an intensity-mean z-averaged particle size (Z_{ave}) of 25-40 nm, narrow size distribution ($PDI < 0.1$) as determined by DLS (Figure 3.2A). The POx-vismo micelles had a neutral surface charge of 8 mV (Figure 3.2B). The particle size and spherical morphology of POx-vismo micelles was further confirmed by transmission electron microscopy (TEM) (Figure 3.2C). At 8:10 vismo:POx ratio, the aqueous concentration of vismodegib in POx-vismo solution was 7.36 mg/mL, which is 73,600-fold higher than the aqueous solubility of free vismodegib (0.1 μ g/mL at pH 7.0) [9]. The POx-vismo micelles were stable during storage at 4 °C. No drug precipitation was observed by visual inspection of the POx-vismo solution. The stability of drug loading and particle size distribution were confirmed by HPLC and DLS respectively (Figure 3.2D). The POx-vismo micelles were also stable after lyophilization; lyophilized POx-vismo micelles could be re-dispersed in water, keeping their drug loading and particles size unchanged (Figure 3.2E). Vismodegib release from the micelles was studied under the perfect sink conditions.

Vismodegib was continuously released from the micelles with approximately the 25% of the drug released in 2h and 90% released in 12h (Figure 3.2F).

Suppression of mitogenic SHH signaling vismodegib in G-smo mice.

Our prior studies of vismodegib administered in the c-vismo formulation at a dose of 100 mg/kg to transgenic medulloblastoma-bearing mice showed initial tumor suppression, followed by rapid recurrence and no increase in event-free survival (EFS) [28]. The initial SHH pathway suppression confirmed that the model was vismodegib-responsive despite the initiating Smo mutation, and that the dose was adequate to produce a pharmacodynamic effect. The absence of a clinically relevant benefit highlighted the need for improved implementation for the therapy to be effective.

To determine if nanoparticle formulation improved the efficacy of vismodegib, we compared G-Smo mice treated with either c-vismo or POx-vismo (Figure 3.1). To analyze the initial suppression of SHH signaling, we harvested tumors 24 hours after a single 100 mg/kg dose of either formulation. Tumors were dissociated, fixed and stained with antibodies to phosphorylated RB (pRB) to mark proliferating cells, which were quantified by flow cytometry. We found that both formulations dosed at 100 mg/kg were equally effective in suppressing pRB ($p=0.9987$) (Figure 3.3A), confirming the pharmacodynamic effect of the dose. We then compared tumor pathology after 3 daily doses of either c-vismo or POx-vismo. We again found similar suppression of proliferation, with reduced tumor size and expression of pRB; analysis of Proliferating Cell Nuclear Antigen (PCNA) produced similar results (Figure 3.3B). These data show that POx-vismo showed similar pharmacodynamics and was at least as effective as c-vismo in the initial suppression of SHH signaling in the tumor.

POx-vismo reduces systemic toxicity of vismodegib

To determine whether nanoparticle delivery altered the systemic toxicity of vismodegib, we placed healthy P10 mouse pups on escalating regimens of POx-vismo or c-vismo and then compared their growth to that of untreated age-matched littermate controls (Figure 3.4). Mice were injected IP with either c-vismo or POx-vismo on postnatal days 10-12 and then every other day until P35, and all mice including littermate controls were weighed daily. Another group was dosed orally with c-vismo. Weight gain for mice on 100 mg/kg POx-vismo IP was similar to untreated controls. In contrast mice on oral vismodegib or IP c-vismo at 100 mg/kg showed significantly decreased weight gain, and this reduced growth was matched by POx-vismo at the 50% higher dose of 150 mg/kg. These studies show that systemic toxicity, detected by reduced weight gain, was markedly less in POx-vismo-treated mice and compared to oral or c-vismo IP.

POx-vismo micelles prolong survival in GEMM model of SHH medulloblastoma

To determine whether nanoparticle delivery affected the therapeutic efficacy of vismodegib when administered as an on-going treatment, we compared the survival of G-Smo mice on a regimen of either POx-vismo or c-vismo. Because vismodegib is typically administered as an oral agent in patients, we also evaluated the efficacy of oral vismodegib in G-Smo mice as an additional control. We randomized G-Smo mice to 4 groups: c-vismo 100 mg/kg oral, c-vismo 100 mg/kg i.p , POx-vismo at 100 mg/kg i.p and or saline-injected controls. Mice were dosed on days 10, 11 and 12 and then every other day until day 35, or until the humane endpoint of progressive tumor symptoms. The survival time to the humane endpoint was considered the EFS. The EFS for G-Smo mice in the saline-injected control group was less than 20 days, consistent with our prior data [29, 30]. Treatment with c-vismo i.p or oral vismodegib at 100 mg/kg both

failed to extend the EFS significantly. However, treatment with 100 mg/kg POx-vismo significantly improved the EFS ($p < 0.001$ Log-rank test) with median EFS increasing from 15 to 22 days and 30% of mice surviving to 35 days (Figure 3.5A). To determine if the failure to extend the survival following the treatment with c-vismo was due to systemic toxicity, we dosed another group of mice with c-vismo at 50 mg/kg. Although a significant pharmacodynamic response was detected (Figure 3.3A), 50 mg/kg c-vismo did not extend survival.

We evaluated the tumor pathology in POx-vismo-treated mice that survived beyond the 20 day survival time of all of groups. In each of these mice, we found regions of highly proliferative cells within the cerebellum, interspersed with regions of differentiated, non-proliferative cells (Figure 3.5B). The regions of non-proliferative cells indicate that vismodegib effectively interrupted SHH-driven proliferation and restricted tumor growth, accounting for increased survival. However, the consistent presence of proliferating cells in adjacent regions shows this response was still partial, and POx-vismo, while more effective, was not curative as a single agent.

POx micelles improve the delivery and retention of vismodegib in tumor and forebrain

To analyze the effect of POx nanoparticle delivery on drug distribution in the CNS, we compared vismodegib concentrations in the forebrain and tumor at different intervals after administration, using infrared matrix assisted laser desorption electrospray ionization (IR-MALDESI). IR-MALDESI uses infrared laser scanning across frozen tissue sections to excite the overlying matrix of ice, causing desorption of endogenous and exogenous ions that can be detected mass spectrometry. This technique quantifies the concentrations of species at all detected molecular weights with spatial resolution, generating ion-specific heatmaps. We validated this technique by imaging endogenous cholesterol, which we found to be at relatively high

concentration in normal brain. Cholesterol concentrations were significantly different in normal forebrain compared to tumor ($p=7.44 \times 10^{-104}$; Figure 3.6A). We used IR-MALDESI to map vismodegib concentrations in sections containing forebrains and tumors from G-Smo mice that were injected IP on P10 with a single 100 mg/kg dose vismodegib, formulated as either c-vismo or POx-vismo. MALDESI detected vismodegib in both tumor and forebrain when harvested 4 hours after injection of either c-vismo or POx-vismo; in contrast to cholesterol, vismodegib concentrations were not significantly different in tumors compared to adjacent forebrain ($p=0.630$; Figure 3.6B). However, POx-vismo treated mice showed higher vismodegib signal at 4h post injection and persistent vismodegib signal 24 hours after administration, while vismodegib was not detectable after 24 hours in c-vismo treated mice. MALDESI thus demonstrated homogenous drug distribution across tumor and forebrain 4 hours after administration of either POx-vismo and c-vismo, and longer lasting vismodegib exposure in both tumor and forebrain after POx-vismo administration.

To compare the pharmacokinetics of vismodegib administered as c-vismo or POx-vismo, we harvested serum, forebrain and medulloblastoma samples from P10 G-Smo mice at varied intervals after a single 100 mg/kg IP dose of either formulation. We then subjected all samples to extraction vismodegib quantification by LC-MS. This analysis showed that POx-vismo produced faster and more long-lasting vismodegib accumulation in tumors, with a higher overall tissue drug exposure. The concentration of vismodegib in tumors reached maximal levels 2h after POx-vismo administration, compared to 4h after c-vismo administration. Moreover, the peak vismodegib concentrations in serum, forebrain and tumors were significantly higher following POx-vismo than c-vismo ($p=0.0063$; Figure 3.7A-C). While vismodegib was not differentially detected at 24 hours in the MS analysis, in contrast to the IR-MALDESI analysis, this difference may be due to the

extraction required for MS, which may lower the sensitivity of the assay relative to MALDESI, which analyzes unextracted tissue.

The tumor:serum (Figure 3.8A) and forebrain:serum (Figure 3.8B) ratios for vismodegib were higher for POx-vismo formulation, indicating improved overall distribution across the BBB when free and protein bound fractions in serum are considered together. Consistent with higher peaks and more sustained concentrations, the total tumor vismodegib exposure, measured as area under the curve (AUC) was significantly higher in tumor and forebrain following administration of POx-vismo compared to c-vismo (Figure 3.8C). POx-vismo also significantly decreased the calculated volume of distribution (Vd) (Figure 3.8D) and clearance (CL) (Figure 3.8E) of vismodegib, indicating that nanoparticle formulation reduced the distribution to non-target organs and improved the retention of the drug in the target tissues. Analysis of vismodegib distribution in non-tumor mice, showed similar results (Figure 3.7), indicating that the improved CNS penetration of vismodegib administered as POx-vismo was not due to tumor-specific changes in the BBB.

Increased CNS drug delivery occurs without brain exposure to the nanoparticle carrier

We developed NMR methods to quantify separately the vismodegib and POx concentrations in samples of serum, forebrain and tumor. We generated samples for NMR studies by administering POx-vismo at concentrations of 50, 100, and 150 mg/kg to tumor bearing mice. We then harvested tumor, forebrain and blood samples 4 hours later and subjected samples to extraction and NMR analysis. We identified signature peaks for vismodegib and POx that could be measured in serum and brain samples following in vivo POx-vismo administration (Figure 3.9A). In serum samples, vismodegib and POx peaks increased in proportion to dose (Figure 3.9A insets). However, only serum samples showed POx polymer concentrations that increased with

dose, and POx polymer was undetectable in forebrain and tumor at all tested doses (Figure 3.9B). In contrast, vismodegib concentrations in tumor, serum and forebrain all increased linearly with dose of POx-vismo and similarly increased with dose of c-vismo (Figure 3.9C). The dissociated serum:brain distributions of vismodegib and POx indicate that the mechanism of improved brain and tumor distribution with PO-x vismo does not involve the POx nanoparticles crossing the BBB.

Nanoparticle carrier reduces vismodegib binding to serum albumin and improves bioavailability.

The exclusion of the nanoparticle carrier from the CNS suggested that the mechanism of nanoparticle effect may occur in the blood. As the penetration of vismodegib into the brain is known to be affected by its binding to serum protein, we determined if POx formulation changes the serum protein binding of vismodegib. We compared albumin binding of vismodegib in POx-vismo and c-vismo formulations by measuring the quenching of the fluorescence of albumin tryptophan [31]. We mixed escalating doses of either POx-vismo or c-vismo with FBS solution (final BSA concentration of approx., 40mg/ml, similar to its concentration in plasma) and then measured tryptophan fluorescence after incubating the samples for 15 min at 25 °C. The fluorescence quenching was lower for samples incubated with POx-vismo versus c-vismo, indicating that POx formulation reduced albumin binding (Figure 3.10A, B). Conversely, the intensity ratio at 340 nm was consistently higher for POx-vismo at each step in the increase of drug (Figure 3.10C). Next, we evaluated protein binding over time at 37 °C to mimic in vivo temperature. After 30 minutes, over 30% of total vismodegib remained unbound, decreasing to 10% over 4 hours. In contrast, the unbound fraction of c-vismo was marginal at 30 minutes. This is consistent with the improved tumor:serum and forebrain:serum ratio measured at early time points (up to 4h) following administration of either POx-vismo or c-vismo (Figure 3.10A,B).

These data show that POx nanoparticle encapsulation reduces vismodegib protein binding, which may be the mechanism for improved CNS penetration of vismodegib in POx-vismo.

3.5 Discussion

Vismodegib has shown clinical efficacy for treatment of SHH-driven cancers but has not been effective for SHH subtype medulloblastoma [5, 32]. Similarly, we previously found that vismodegib solubilized and administered IP, failed to prolong survival in medulloblastoma-bearing mice despite initial SHH pathway suppression [28]. We now show that optimizing vismodegib delivery using nanoparticles markedly improves efficacy and reduces systemic toxicity, providing strong support for the use of the POx nanoparticle platform. We have previously found that the poly(2-oxazoline) micelles are a versatile system for encapsulating small molecule agents in nanoparticles [23, 24], for example solubilizing and delivering the investigational ATR inhibitor VE-821 into the CNS in vivo [33].

The structural properties of amphiphilic polymer (poly(2-oxazoline)s) are the driving factors in the formation of POx-vismo; a hydrophobic block, poly(2-n-butyl-2-oxazoline), provides a hydrophobic core for the encapsulation of poorly soluble drug while hydrophilic block, poly(2-methyl-2-oxazoline), endows POx-vismo with stealth properties that may effectively prevent serum protein binding. Using the poly(2-oxazoline) system, we generated POx-vismo micelles that showed highly uniform nanometer-scale particles with Z_{ave} of 38 nm and a loading capacity of 42% w/w. The high loading capacity POx-vismo enhanced drug solubility in aqueous solution, relative to the native compound. Moreover, POx-vismo was stable in aqueous media for a month without any changes in drug encapsulation and size distribution and lyophilized POx-vismo provides an identical nanoformulation when reconstituted with water, which may facilitate clinical implementation.

Our analyses show that POx formulation increased drug exposure in the CNS, in both medulloblastoma and forebrain and reduced systemic exposure, providing an explanation for both

improved anti-tumor effect and reduced toxicity. POx-vismo produced higher peak vismodegib concentrations in tumor and forebrain, and vismodegib concentrations persisted for longer after POx-vismo administration producing a higher AUC. Although even low doses of vismodegib can induce a pharmacodynamic response, exposure to sub-optimal concentrations of cytotoxic drugs is associated with development of resistance and failure to respond to treatment [34, 35]. Resistance to vismodegib develops rapidly and was identified as main reason for treatment failure [36, 37]. Achieving high and sustained drug concentration in the target tumor tissues may reduce resistance and produce effects sufficiently sustained to prolong survival. Although increased penetration and accumulation of nanoparticle delivered drugs into brain tumors could be associated with tumor-specific changes in BBB, our PK data show that improved CNS penetration did not depend on the presence of tumor, but rather was also seen in WT mice. The decreased global volume of distribution of vismodegib in POx-vismo-treated mice supports lowered exposure in extra-neural organ systems as the mechanism of reduced systemic toxicity.

Our NMR studies provide important insight into the mechanism through which POx nanoparticle encapsulation improves pharmacokinetics. NMR allowed us to simultaneously detect the polymer carrier and the drug, without the need to chemically modify their structures, which was shown to affect polymers biodistribution [38]. We found that the vismodegib component of POx-vismo enters the brain and brain tumor, while the POx component does not. This finding indicates that the nanoparticle carrier releases its payload outside the BBB and underscores the importance of the effect of the nanoparticle carrier on drug dynamics in the blood compartment. Free vismodegib is known to pass through the BBB and within this context, our finding that nanoparticle encapsulation reduces vismodegib serum protein binding, are highly significant. Taken together, our data demonstrate a mechanism in which POx nanoparticle delivery improves

drug penetration into normal brain and brain tumors by increasing the free drug available for passage across the BBB. Importantly, since the nanoparticle does not enter into the CNS, there is reduced potential that it will cause untoward effects on the normal brain.

Our work advances the development of nanoparticle drug delivery for brain tumors by working entirely in a primary, genetic model. Diverse nanoparticles have shown efficacy against medulloblastoma cell lines either in vitro or in xenografts. Nanoparticles consisting of high-density lipoprotein, for example have shown in vitro efficacy [39]. Similarly, glutathione-triggered nanoparticles generated by crosslinking albumin with *N,N'*-Bis(acryloyl)cystamine have been shown to deliver chemotherapeutics in vitro [40]. Poly(lactic-co-glycolic acid) conjugated to polyethylene glycol (PLGA-PEG)-based nanoparticles delivering the SHH pathway inhibitor HPI-1 have been shown effective in flank xenografts in mice [41]. An important next step for these promising technologies is to test nanoparticles against brain tumors that form in genetically engineered mice in which tumors grow in the intracranial space, with an endogenous BBB and surveilled by an intact immune system.

Similar to our studies of PO-x vismo, iron oxide nanoparticle-based therapy (NP-CP-PEI), which uses particles coated with polyethyleneimine-PEG copolymer, has been tested in a primary mouse glioma model. NP-CP-PEI effectively delivered siRNAs that knocked down the activity of the target gene product and produced a therapeutically relevant effect [42, 43]. These studies using a different nanoparticle that may work through different mechanisms, significantly advanced the field by providing in vivo evidence of the potential of nanoparticle-based therapy in a primary tumor model. POx-vismo represents a new advance in demonstrating that this highly versatile delivery system, with known capacity to load a variety of therapeutic agents, can facilitate drug delivery tumors within the CNS through a newly defined mechanism.

Our data clearly show that in mice POx-vismo is less a toxic and more effective alternative to conventional vismodegib. While the ability of POx-micelles to deliver vismodegib to brain tumors in humans remains to be tested, the barriers to implementation in humans are not different than for other investigational agents. Indeed, the parenteral administration of POx-vismo presents advantages in the pediatric population, where orally administered therapies are problematic [8]. The simplicity of polymeric micelles, which do not depend on binding to a specific receptor, may also be an important feature.

Phase 1 trials in humans will be needed to define safe POx-vismo regimens that can be tested for efficacy. Phase 1 trials to test the safety of POx-micelles loaded with other agents are currently on-going and early results of one phase 1 trial showed that poly(2-oxazoline) nanoparticles similar to POx micelles in this study were well tolerated [44]. The improved efficacy of POx-vismo and the need for more effective treatments for SHH-driven cancers support the testing of POx-vismo in humans.

The persistence of proliferating medulloblastoma cells in mice treated until P35 with POx-vismo highlights the need for combinations of pharmacologic agents to forestall resistance. Vismodegib-resistant cells may have different, specific sensitivities that may be defined in future studies of up-regulated signaling pathways in recurrent tumors [45]. Such studies may identify drugs that can combine with vismodegib to achieve cures through targeted therapies.

The versatility of the POx system as a potential carrier for diverse agents allows for delivery of vismodegib combined with other specific inhibitors or chemotherapeutic agents. Our data show that optimization through nanoparticle formulation can improve the therapeutic index and efficacy of systemically administered pharmaceutical agents for brain tumor therapy, with the potential to improve survival and quality-of-life for brain tumor patients. The POx system is a

versatile drug delivery platform, and our results show the broad potential for POx micelle delivery to make existing brain tumor treatments newly effective.

Ratio of drug:polymer by weight	Theoretical drug concentration (mg/ml)	Actual drug concentration (mg/ml)	LE (%)	LC (%)	z-ave diameter (nm)	PDI
2:10	2.00	1.57 ± 0.01	78.6 ± 0.5	13.6 ± 0.08	26.6 ± 2.4	0.07 ± 0.01
4:10	4.00	3.26 ± 0.06	81.6 ± 1.5	24.6 ± 0.5	34.5 ± 5.3	0.03 ± 0.01
6:10	6.00	4.88 ± 0.1	81.3 ± 1.7	32.6 ± 0.7	41.5 ± 5.9	0.03 ± 0.01
8:10	8.00	7.36 ± 0.15	92.0 ± 1.9	42.4 ± 0.9	38.3 ± 0.3	0.08 ± 0.01

Table 3.1 Actual vismodegib concentration, LE (%), LC (%), nanoparticles size and size distribution of POx-vismo micelles prepared at indicated drug:polymer ratios. (n = 3 ± SD)

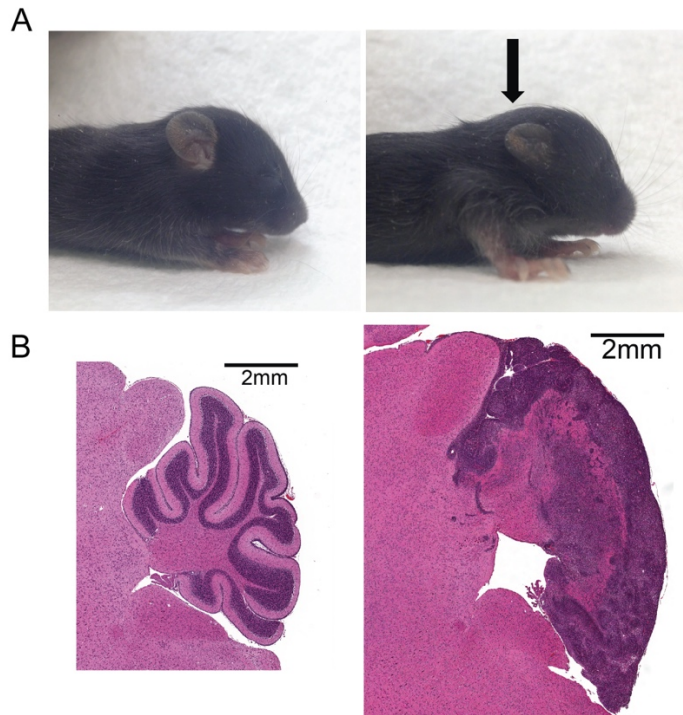


Figure 3.1 Comparison of normal and G-Smo mice at P15. (A) Head shape and (B) H&E stained sagittal sections of the cerebellar region of normal (left) and G-Smo (right) mice.

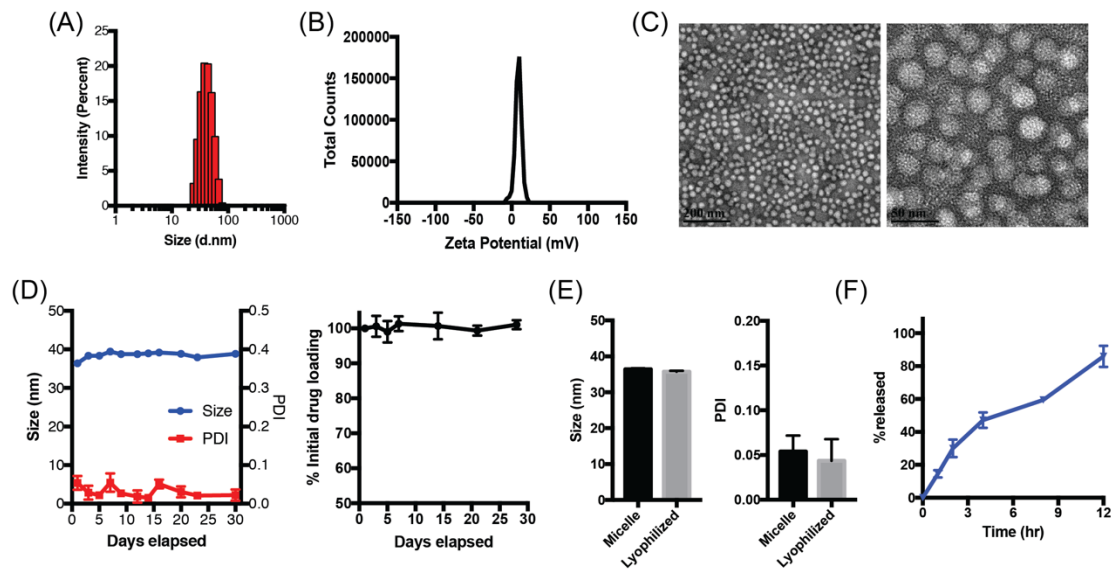


Figure 3.2 POx-vismo micelles form stable, nanometer-scale spheres. (A) Particle size distribution measured by DLS (z-average, D_z) (B) Zeta potential (50) and (C) morphology, shown by TEM. Scale bar = 200 nm (left), 50 nm (right). (D) Stability of the POx-vismo micelles at 4 °C as determined by actual drug measurements (left) and size distribution (right) over time. (E) Size of particles after reconstitution of lyophilized POx-vismo. (F) Vismodegib release from POx-vismo incubated in fetal bovine serum solution (10% in PBS) at 37 °C over time.

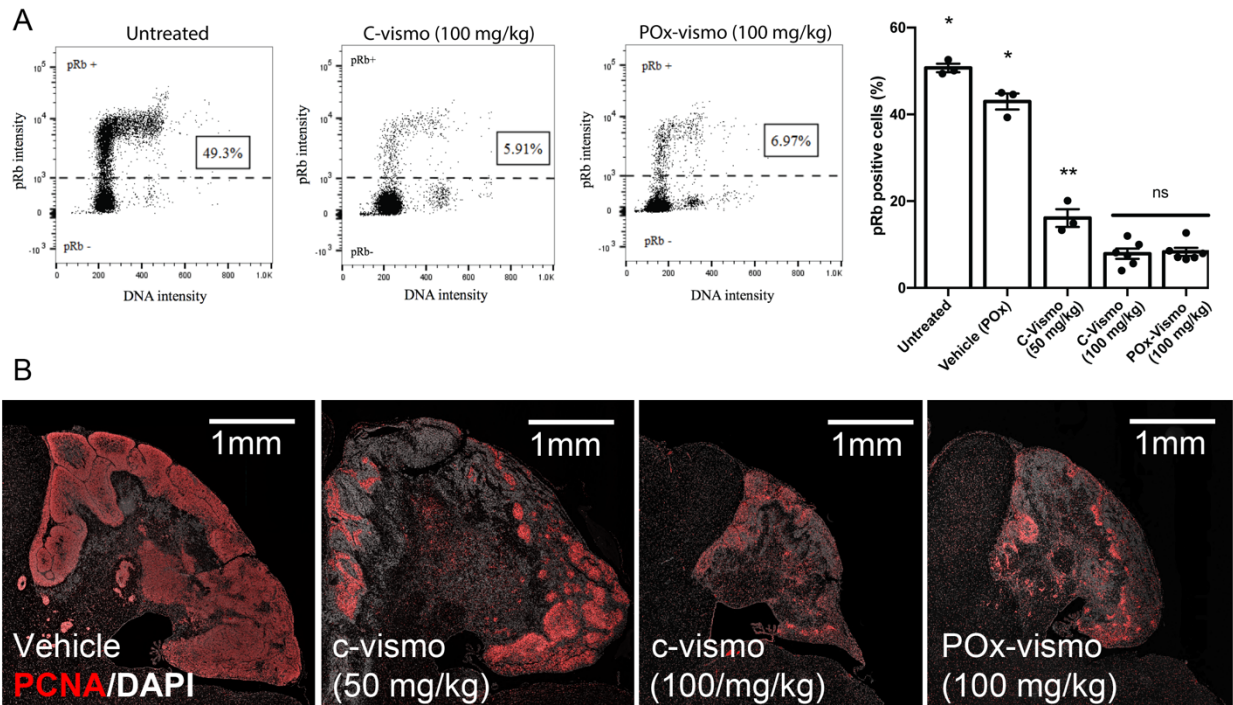


Figure 3.3 Pharmacodynamic response to POx-vismo and c-vismo. (A) Flow cytometry quantification of pRB+ cells in untreated tumors and in tumors 24h after a single administration of POx-vismo and c-vismo at the indicated doses, compared to POx vehicle-injected controls. In the 2D plots, cells representative replicates treated as indicated are plotted according to pRB intensity versus DNA content. The dotted line indicates the threshold of detection for pRB. The pRB+ fractions for all replicates in each treatment group are graphed to the right, with columns indicating the means and error bars indicating the SEM. (B) PCNA immunofluorescent staining of sagittal medulloblastoma sections from representative P13 G-Smo mice, 24h after three daily IP injections of the indicated formulation. Nuclei are counterstained with DAPI.

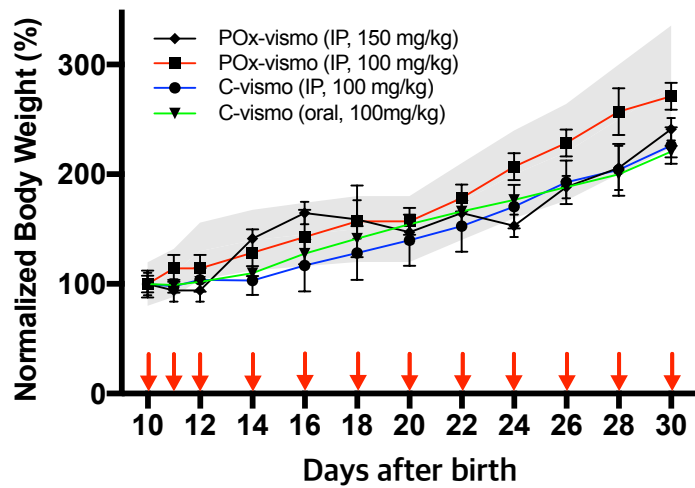


Figure 3.4 Comparison of weight gain shows that mice tolerate POx-vismo better than c-vismo.

The weights of mice treated with the indicated formulations are graphed over time. The gray range indicates the mean weights \pm SEM of littermate controls.

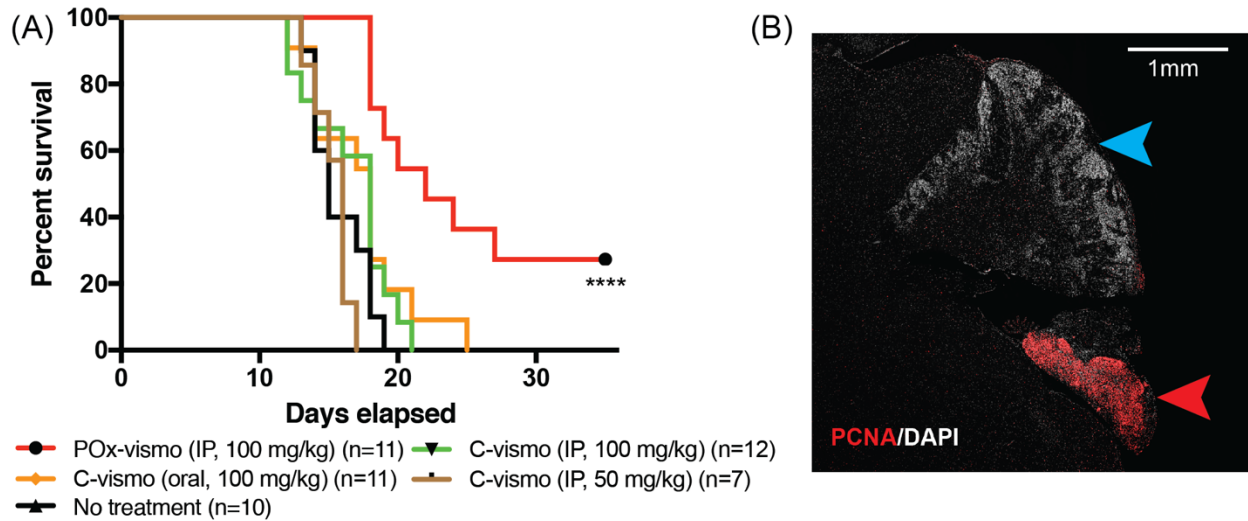


Figure 3.5 Increased efficacy of POx-vismo compared to c-vismo. (A) Kaplan-Meier survival curve for G-Smo mice treated POx-vismo or c-vismo at the indicated doses, compared to no treatment; **** indicates $p < 0.001$ (vs. No treatment). All other curves showed no statistically significant difference compared to No treatment. (B) PCNA immunofluorescent staining (red), in a sagittal medulloblastoma section from a representative P35 G-Smo mouse, treated with 100 mg/kg of POx-vismo (P35). Nuclei are counterstained with DAPI. Red arrowhead indicates a region of proliferative tumor. Blue arrowhead indicates a differentiated, non-proliferative region.

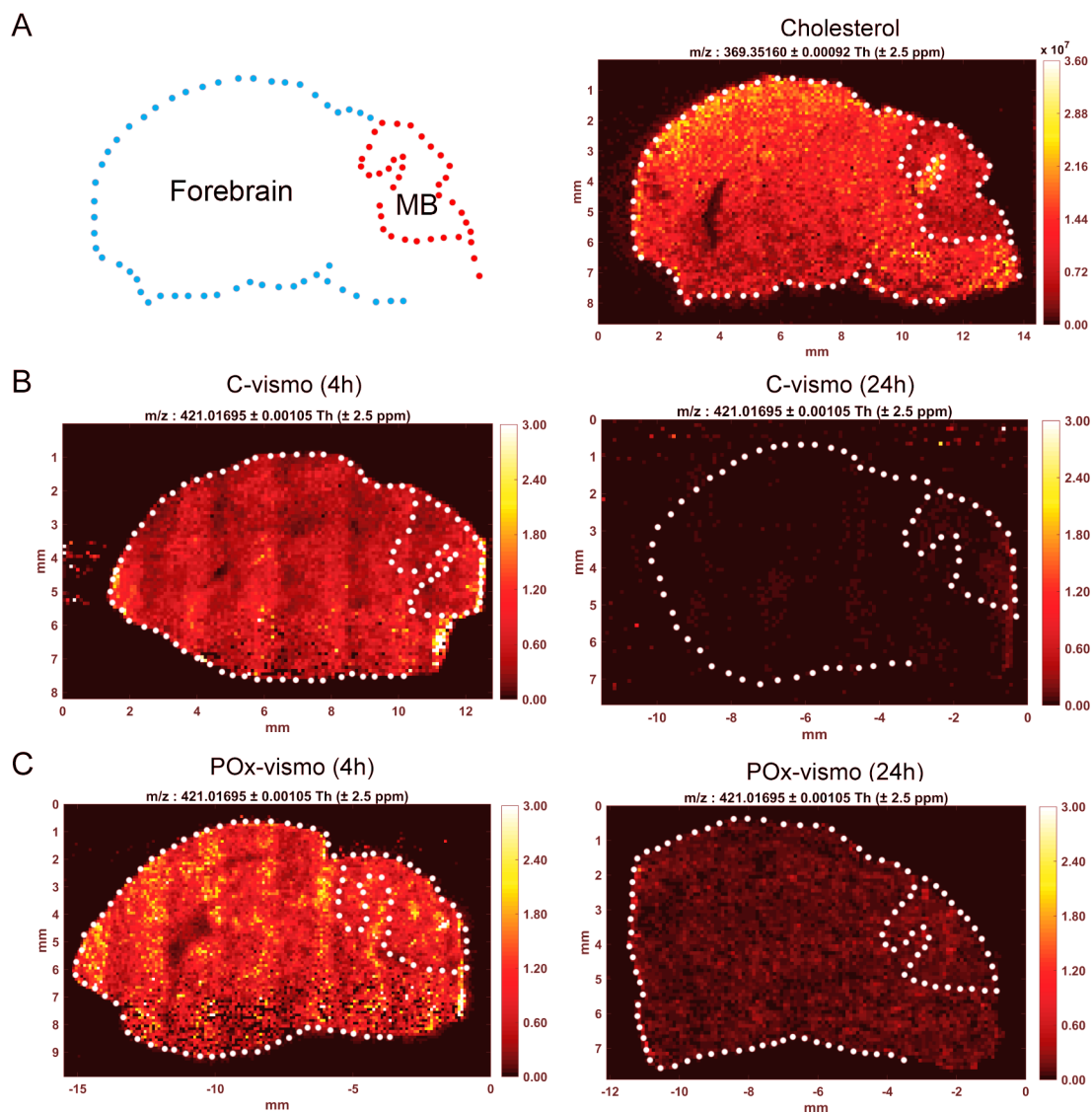
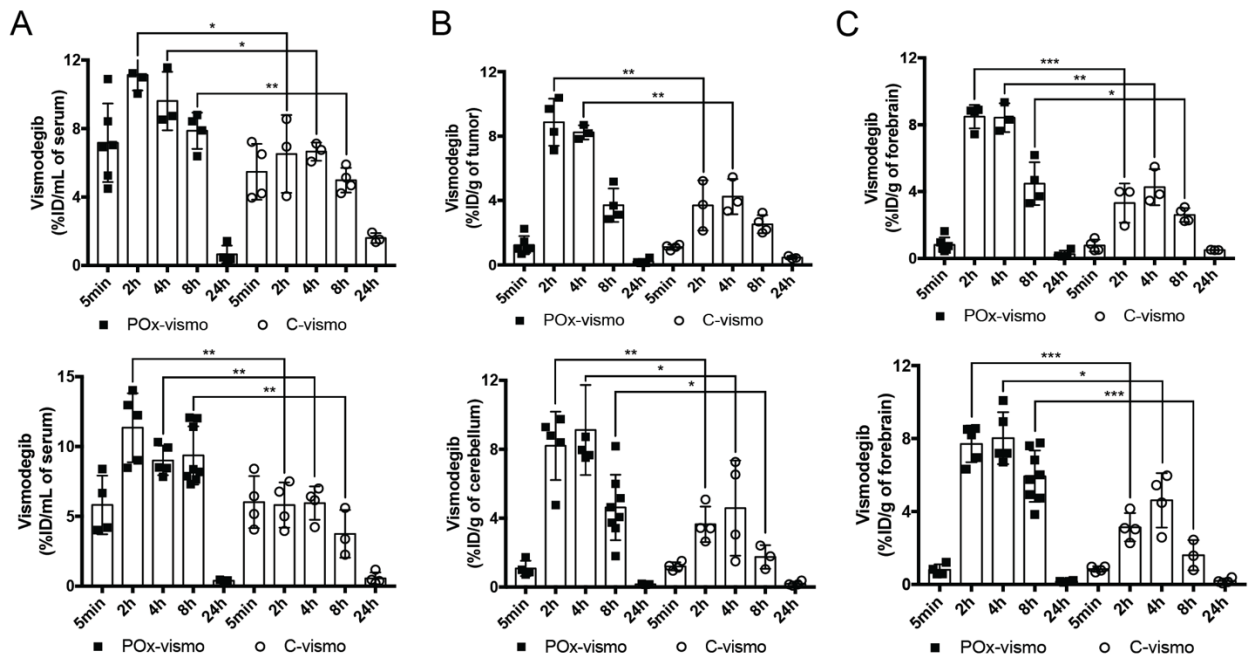


Figure 3.6 Widespread vismodegib distribution in the brain, with increased retention after POx-vismo administration, demonstrated by IR-MALDESI. (A) Left panel, contour of brain sample showing forebrain and medulloblastoma (MB) and right panel, IR-MALDESI analysis of cholesterol in a control brain (m/z :369). (B) IR-MALDESI analysis of vismodegib (m/z: 421) in representative sagittal brain sections from G-Smo mice following a single dose of c-vismo at 4h (left) and 24h (right) (C) IR-MALDESI MSI analysis of vismodegib (m/z: 421) as in (B) following a single dose of POx-vismo at 4h (left) and 24h (right).



D PK parameters

Tumor-bearing mice						
Parameters	POx-vismo			C-vismo		
	Serum	Tumor	Forebrain	Serum	Tumor	Forebrain
AUC (0-∞) (ng*hr/mL)	992869.75	574591.17	626488.79	706435.87	350346.09	351019
Vd (mL)	4.73	-	-	11.41	-	-
CL (mL/hr)	0.683	-	-	0.809	-	-
Wild-type mice						
Parameters	POx-vismo			C-vismo		
	Serum	Cerebellum	Forebrain	Serum	Cerebellum	Forebrain
AUC (0-∞) (ng*hr/mL)	1062953.1	644605.5	704583.85	540380.3	288539.5	269031.6

Vd (mL)	3.77	-	-	10.29	-	-
CL (mL/hr)	0.649	-	-	1.22	-	-

AUC(0–∞), area under the curve from time 0–infinite; Vd, volume of distribution; CL, total body clearance.

Figure 3.7 Pharmacokinetic profile of POx-vismo and C-vismo in tumor mice. Vismodegib concentrations in (A) serum (upper: POx-vismo, lower: C-vismo), (B) Tumor (cerebellum) (upper: POx-vismo, lower: C-vismo) and (C) forebrain (upper: POx-vismo, lower: C-vismo), 24 h after following single IP injections of POx-vismo or C-vismo at 100 mg/kg, *p < 0.05, **p < 0.005, ***p < 0.0005. (D) PK parameters at given formulations from tumor-bearing mice and wild-type mice. For A-C, dots indicate data from individual replicates and error bars are the SEM.

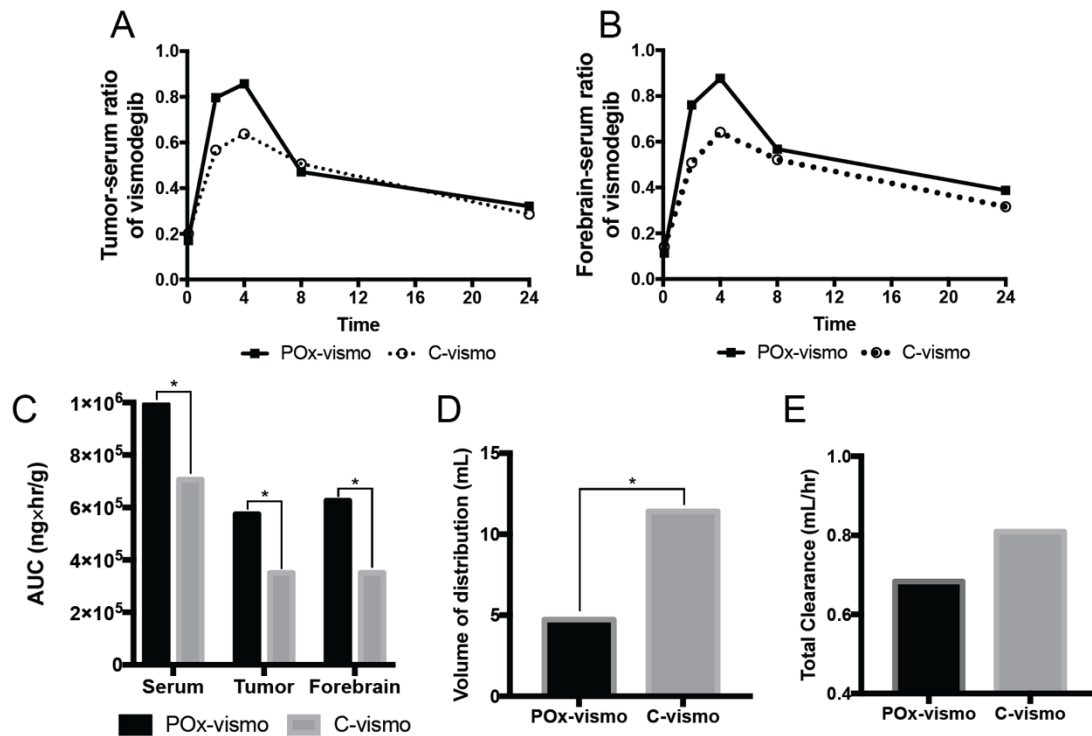


Figure 3.8 POx-vismo show enhanced drug delivery. (A) Tumor:serum and (B) forebrain:serum ratio of vismodegib, (C) AUC, (D) volume of distribution and (E) total clearance of vismodegib following administration of 100 mg/kg of POx-vismo or C-vismo in tumor bearing mice. * $p < 0.05$, ** $p < 0.005$, *** $p < 0.0005$.

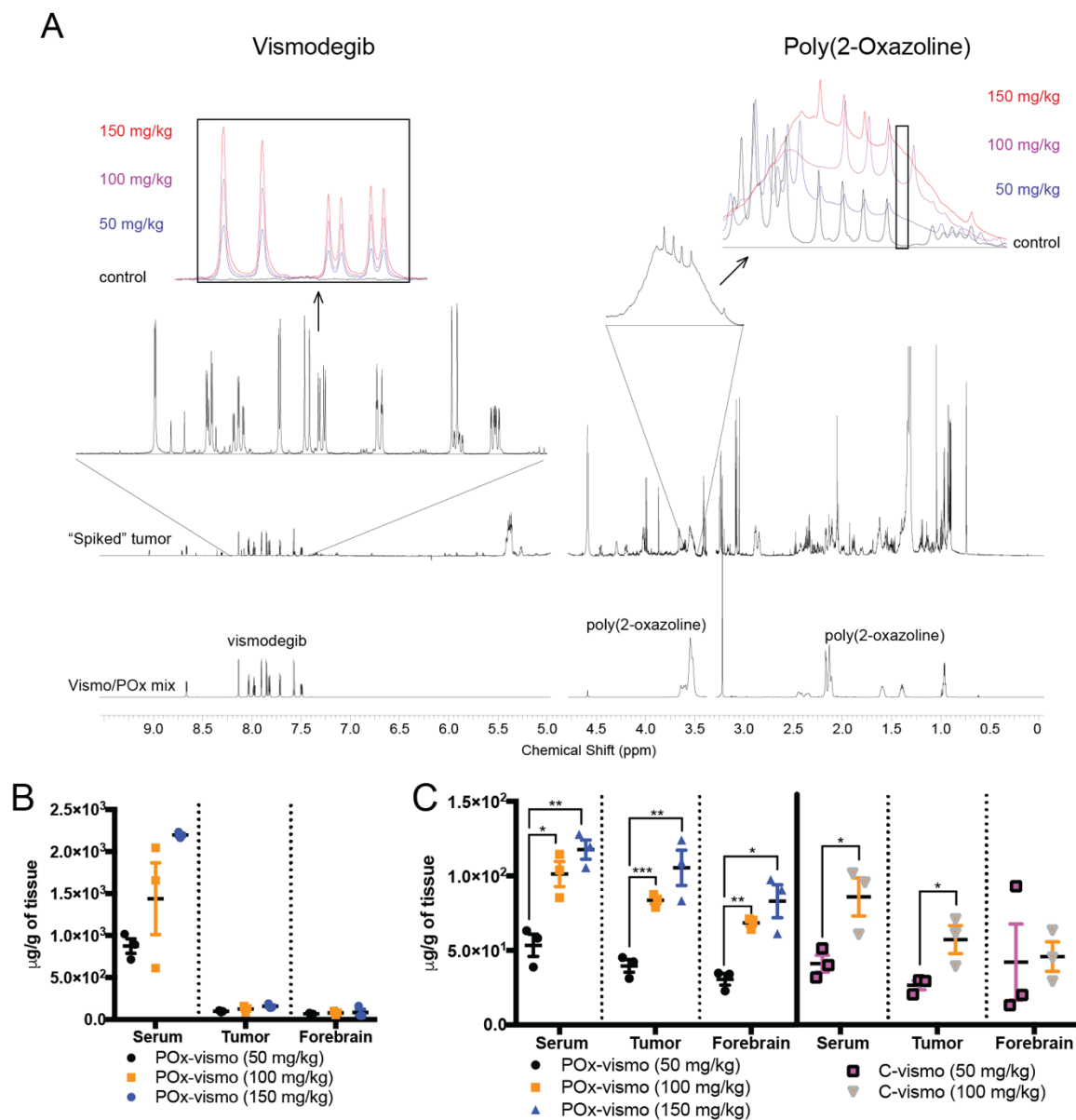


Figure 3.9. Differential distribution of vismodegib and POx components of POx-vismo in the vascular and CNS compartments. (A) NMR spectra with the signature peaks for vismodegib and POx highlighted, Insets show dose-dependent changes in regions of representative spectra from serum samples that correspond to vismodegib or POx. Note that POx peak is a broad peak that spans several, more narrow peaks for unrelated molecules. To maximize specificity, we integrated an area within the broad POx peak that falls between unrelated peaks. The area under

this portion of the curve was proportional to POx concentration over the range of tested standards. (B) POx concentration in serum, tumor and forebrain following IP injection of POx-vismo (C) vismodegib level from POx-vismo and c-vismo injection. *p < 0.05, **p < 0.005, ***p < 0.0005. For B-C, dots indicate data from individual replicates and error bars are the SEM.

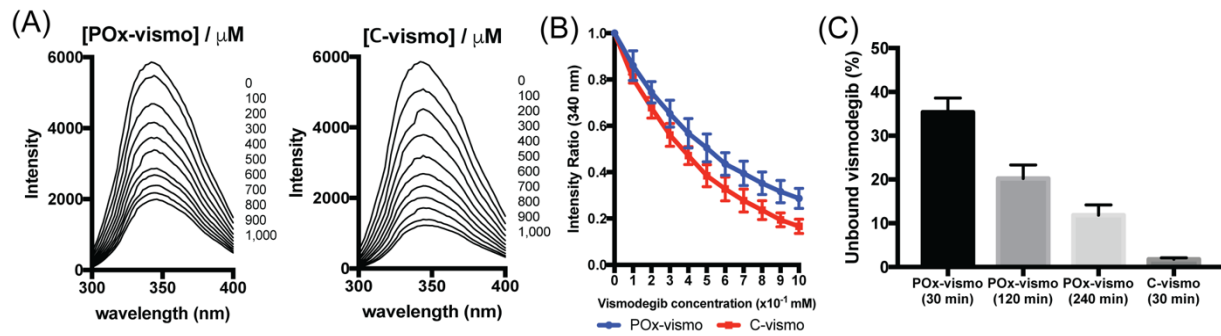


Figure 3.10 Protein binding study of vismodegib (A) Tryptophan fluorescence quenching assay by addition of either POx-vismo or C-vismo at given concentration of vismodegib (right), (B) the fraction of unbound vismodegib by addition of either Pox-vismo or C-vismo in diluted FBS solution. (C) unbound vismodegib after the incubation in FBS. Each point is mean \pm SEM.

REFERENCES

1. Sharma, S.V. and Settleman, J., 2007. Oncogene addiction: setting the stage for molecularly targeted cancer therapy. *Genes & development*, 21(24), pp.3214-3231.
2. Rimkus, T.K., Carpenter, R.L., Qasem, S., Chan, M. and Lo, H.W., 2016. Targeting the sonic hedgehog signaling pathway: review of smoothed and GLI inhibitors. *Cancers*, 8(2), p.22.
3. Vismodegib granted FDA approval for treatment of basal cell carcinoma. 2012. *Oncology (Williston Park)* 26, 174, 213.
4. Yauch, R.L., Dijkgraaf, G.J., Alicke, B., Januario, T., Ahn, C.P., Holcomb, T., Pujara, K., Stinson, J., Callahan, C.A., Tang, T. and Bazan, J.F., 2009. Smoothed mutation confers resistance to a Hedgehog pathway inhibitor in medulloblastoma. *Science*, 326(5952), pp.572-574.
5. Robinson, G.W., Orr, B.A., Wu, G., Gururangan, S., Lin, T., Qaddoumi, I., Packer, R.J., Goldman, S., Prados, M.D., Desjardins, A. and Chintagumpala, M., 2015. Vismodegib exerts targeted efficacy against recurrent sonic hedgehog–subgroup medulloblastoma: results from phase II pediatric brain tumor consortium studies PBTC-025B and PBTC-032. *Journal of Clinical Oncology*, 33(24), p.2646.
6. DOXIL approved by FDA. 1995. *AIDS Patient Care* 9, 306.
7. Aditya, S. and Rattan, A., 2013. Vismodegib: A smoothed inhibitor for the treatment of advanced basal cell carcinoma. *Indian dermatology online journal*, 4(4), p.365.
8. Batchelor, H.K. and Marriott, J.F., 2015. Formulations for children: problems and solutions. *British journal of clinical pharmacology*, 79(3), pp.405-418.
9. Graham, R.A., Hop, C.E., Borin, M.T., Lum, B.L., Colburn, D., Chang, I., Shin, Y.G., Malhi, V., Low, J.A. and Dresser, M.J., 2012. Single and multiple dose intravenous and oral pharmacokinetics of the hedgehog pathway inhibitor vismodegib in healthy female subjects. *British journal of clinical pharmacology*, 74(5), pp.788-796.
10. Gajjar, A., Stewart, C.F., Ellison, D.W., Kaste, S., Kun, L.E., Packer, R.J., Goldman, S., Chintagumpala, M., Wallace, D., Takebe, N. and Boyett, J.M., 2013. Phase I study of vismodegib in children with recurrent or refractory medulloblastoma: a pediatric brain tumor consortium study. *Clinical Cancer Research*, 19(22), pp.6305-6312.
11. Barenholz, Y.C., 2012. Doxil[®]—the first FDA-approved nano-drug: lessons learned. *Journal of controlled release*, 160(2), pp.117-134.
12. Yamamoto, Y., Kawano, I. and Iwase, H., 2011. Nab-paclitaxel for the treatment of breast cancer: efficacy, safety, and approval. *OncoTargets and therapy*, 4, p.123.

13. Misra, R., Acharya, S. and Sahoo, S.K., 2010. Cancer nanotechnology: application of nanotechnology in cancer therapy. *Drug discovery today*, 15(19-20), pp.842-850.
14. Ferrari, M., 2005. Cancer nanotechnology: opportunities and challenges. *Nature reviews cancer*, 5(3), pp.161-171.
15. Kataoka, K., Harada, A. and Nagasaki, Y., 2012. Block copolymer micelles for drug delivery: design, characterization and biological significance. *Advanced drug delivery reviews*, 64, pp.37-48.
16. Lee, K.S., Chung, H.C., Im, S.A., Park, Y.H., Kim, C.S., Kim, S.B., Rha, S.Y., Lee, M.Y. and Ro, J., 2008. Multicenter phase II trial of Genexol-PM, a Cremophor-free, polymeric micelle formulation of paclitaxel, in patients with metastatic breast cancer. *Breast cancer research and treatment*, 108(2), pp.241-250.
17. Mochida, Y., Cabral, H. and Kataoka, K., 2017. Polymeric micelles for targeted tumor therapy of platinum anticancer drugs. *Expert opinion on drug delivery*, 14(12), pp.1423-1438.
18. He, Z., Wan, X., Schulz, A., Bludau, H., Dobrovolskaia, M.A., Stern, S.T., Montgomery, S.A., Yuan, H., Li, Z., Alakhova, D. and Sokolsky, M., 2016. A high capacity polymeric micelle of paclitaxel: Implication of high dose drug therapy to safety and in vivo anti-cancer activity. *Biomaterials*, 101, pp.296-309.
19. Lorson, T., Lübtow, M.M., Wegener, E., Haider, M.S., Borova, S., Nahm, D., Jordan, R., Sokolski-Papkov, M., Kabanov, A.V. and Luxenhofer, R., 2018. Poly (2-oxazoline) s based biomaterials: A comprehensive and critical update. *Biomaterials*, 178, pp.204-280.
20. Seo, Y., Schulz, A., Han, Y., He, Z., Bludau, H., Wan, X., Tong, J., Bronich, T.K., Sokolsky, M., Luxenhofer, R. and Jordan, R., 2015. Poly (2-oxazoline) block copolymer based formulations of taxanes: effect of copolymer and drug structure, concentration, and environmental factors. *Polymers for Advanced Technologies*, 26(7), pp.837-850.
21. Luxenhofer, R., Schulz, A., Roques, C., Li, S., Bronich, T.K., Batrakova, E.V., Jordan, R. and Kabanov, A.V., 2010. Doubly amphiphilic poly (2-oxazoline) s as high-capacity delivery systems for hydrophobic drugs. *Biomaterials*, 31(18), pp.4972-4979.
22. Han, Y., He, Z., Schulz, A., Bronich, T.K., Jordan, R., Luxenhofer, R. and Kabanov, A.V., 2012. Synergistic combinations of multiple chemotherapeutic agents in high capacity poly (2-oxazoline) micelles. *Molecular pharmaceutics*, 9(8), pp.2302-2313.
23. Wan, X., Beaudoin, J.J., Vinod, N., Min, Y., Makita, N., Bludau, H., Jordan, R., Wang, A., Sokolsky, M. and Kabanov, A.V., 2019. Co-delivery of paclitaxel and cisplatin in poly (2-oxazoline) polymeric micelles: Implications for drug loading, release, pharmacokinetics and outcome of ovarian and breast cancer treatments. *Biomaterials*, 192, pp.1-14.

24. Wan, X., Min, Y., Bludau, H., Keith, A., Sheiko, S.S., Jordan, R., Wang, A.Z., Sokolsky-Papkov, M. and Kabanov, A.V., 2018. Drug Combination synergy in worm-like polymeric micelles improves treatment outcome for small cell and non-small cell lung cancer. *ACS nano*, 12(3), pp.2426-2439.
25. Mao, J., Ligon, K.L., Rakhlin, E.Y., Thayer, S.P., Bronson, R.T., Rowitch, D. and McMahon, A.P., 2006. A novel somatic mouse model to survey tumorigenic potential applied to the Hedgehog pathway. *Cancer research*, 66(20), pp.10171-10178.
26. Zhuo, L., Theis, M., Alvarez-Maya, I., Brenner, M., Willecke, K. and Messing, A., 2001. hGFAP-cre transgenic mice for manipulation of glial and neuronal function in vivo. *genesis*, 31(2), pp.85-94.
27. Schüller, U., Heine, V.M., Mao, J., Kho, A.T., Dillon, A.K., Han, Y.G., Huillard, E., Sun, T., Ligon, A.H., Qian, Y. and Ma, Q., 2008. Acquisition of granule neuron precursor identity is a critical determinant of progenitor cell competence to form Shh-induced medulloblastoma. *Cancer cell*, 14(2), pp.123-134.
28. Ocasio, J., Babcock, B., Colaneri, A., Taylor, M., Wilhelmsen, K. and Gershon, T., 2018. MBRS-51. SINGLE CELL TRANSCRIPTOMIC ANALYSIS DEFINES DISCRETE SUBPOPULATIONS IN SHH-DRIVEN MEDULLOBLASTOMAS THAT ARE DIFFERENTIALLY AFFECTED BY VISMODEGIB. *Neuro-Oncology*, 20(Suppl 2), p.i139.
29. Williams, S.E., Garcia, I., Crowther, A.J., Li, S., Stewart, A., Liu, H., Lough, K.J., O'Neill, S., Veleta, K., Oyarzabal, E.A. and Merrill, J.R., 2015. Aspm sustains postnatal cerebellar neurogenesis and medulloblastoma growth in mice. *Development*, 142(22), pp.3921-3932.
30. Gershon, T.R., Crowther, A.J., Tikunov, A., Garcia, I., Annis, R., Yuan, H., Miller, C.R., Macdonald, J., Olson, J. and Deshmukh, M., 2013. Hexokinase-2-mediated aerobic glycolysis is integral to cerebellar neurogenesis and pathogenesis of medulloblastoma. *Cancer & metabolism*, 1(1), p.2.
31. Sułkowska, A., 2002. Interaction of drugs with bovine and human serum albumin. *Journal of molecular structure*, 614(1-3), pp.227-232.
32. Tang, J.C., Hanke, C.W. and Caro, I., 2018. Vismodegib and the Hedgehog Pathway Inhibitors: A Historical Perspective to Current Clinical Application. *Journal of drugs in dermatology: JDD*, 17(5), pp.506-508.
33. Lang, P.Y., Nanjangud, G.J., Sokolsky-Papkov, M., Shaw, C., Hwang, D., Parker, J.S., Kabanov, A.V. and Gershon, T.R., 2016. ATR maintains chromosomal integrity during postnatal cerebellar neurogenesis and is required for medulloblastoma formation. *Development*, 143(21), pp.4038-4052.

34. Liu, W.M., Oakley, P.R. and Joel, S.P., 2002. Exposure to low concentrations of etoposide reduces the apoptotic capability of leukaemic cell lines. *Leukemia*, *16*(9), pp.1705-1712.
35. Wang, E.C., Sinnott, R., Werner, M.E., Sethi, M., Whitehurst, A.W. and Wang, A.Z., 2014. Differential cell responses to nanoparticle docetaxel and small molecule docetaxel at a sub-therapeutic dose range. *Nanomedicine: Nanotechnology, Biology and Medicine*, *10*(2), pp.321-328.
36. Rudin, C.M., Hann, C.L., Laterra, J., Yauch, R.L., Callahan, C.A., Fu, L., Holcomb, T., Stinson, J., Gould, S.E., Coleman, B. and LoRusso, P.M., 2009. Treatment of medulloblastoma with hedgehog pathway inhibitor GDC-0449. *New England Journal of Medicine*, *361*(12), pp.1173-1178.
37. Metcalfe, C. and de Sauvage, F.J., 2011. Hedgehog fights back: mechanisms of acquired resistance against Smoothed antagonists. *Cancer research*, *71*(15), pp.5057-5061.
38. Fonge, H., Huang, H., Scollard, D., Reilly, R.M. and Allen, C., 2012. Influence of formulation variables on the biodistribution of multifunctional block copolymer micelles. *Journal of controlled release*, *157*(3), pp.366-374.
39. Bell, J.B., Rink, J.S., Eckerdt, F., Clymer, J., Goldman, S., Thaxton, C.S. and Platanius, L.C., 2018. HDL nanoparticles targeting sonic hedgehog subtype medulloblastoma. *Scientific reports*, *8*(1), pp.1-10.
40. Catanzaro, G., Curcio, M., Cirillo, G., Spizzirri, U.G., Besharat, Z.M., Abballe, L., Vacca, A., Iemma, F., Picci, N. and Ferretti, E., 2017. Albumin nanoparticles for glutathione-responsive release of cisplatin: New opportunities for medulloblastoma. *International journal of pharmaceutics*, *517*(1-2), pp.168-174.
41. Chenna, V., Hu, C., Pramanik, D., Aftab, B.T., Karikari, C., Campbell, N.R., Hong, S.M., Zhao, M., Rudek, M.A., Khan, S.R. and Rudin, C.M., 2012. A polymeric nanoparticle encapsulated small-molecule inhibitor of Hedgehog signaling (NanoHHI) bypasses secondary mutational resistance to Smoothed antagonists. *Molecular cancer therapeutics*, *11*(1), pp.165-173.
42. Kievit, F.M., Wang, K., Ozawa, T., Tarudji, A.W., Silber, J.R., Holland, E.C., Ellenbogen, R.G. and Zhang, M., 2017. Nanoparticle-mediated knockdown of DNA repair sensitizes cells to radiotherapy and extends survival in a genetic mouse model of glioblastoma. *Nanomedicine: Nanotechnology, Biology and Medicine*, *13*(7), pp.2131-2139.
43. Kievit, F.M., Wang, K., Ozawa, T., Tarudji, A.W., Silber, J.R., Holland, E.C., Ellenbogen, R.G. and Zhang, M., 2017. Nanoparticle-mediated knockdown of DNA repair sensitizes cells to radiotherapy and extends survival in a genetic mouse model of glioblastoma. *Nanomedicine: Nanotechnology, Biology and Medicine*, *13*(7), pp.2131-2139.

44. Moreadith, R.W., Viegas, T.X., Bentley, M.D., Harris, J.M., Fang, Z., Yoon, K., Dizman, B., Weimer, R., Rae, B.P., Li, X. and Rader, C., 2017. Clinical development of a poly (2-oxazoline)(POZ) polymer therapeutic for the treatment of Parkinson's disease—Proof of concept of POZ as a versatile polymer platform for drug development in multiple therapeutic indications. *European Polymer Journal*, 88, pp.524-552.
45. Bertrand, K.C., Faria, C.C., Skowron, P., Luck, A., Garzia, L., Wu, X., Agnihotri, S., Smith, C.A., Taylor, M.D., Mack, S.C. and Rutka, J.T., 2018. A functional genomics approach to identify pathways of drug resistance in medulloblastoma. *Acta neuropathologica communications*, 6(1), pp.1-6.
46. Lee, H.Y., Greene, L.A., Mason, C.A. and Manzini, M.C., 2009. Isolation and culture of post-natal mouse cerebellar granule neuron progenitor cells and neurons. *JoVE (Journal of Visualized Experiments)*, (23), p.e990.
47. Garcia, I., Crowther, A.J., Gama, V., Miller, C.R., Deshmukh, M. and Gershon, T.R., 2013. Bax deficiency prolongs cerebellar neurogenesis, accelerates medulloblastoma formation and paradoxically increases both malignancy and differentiation. *Oncogene*, 32(18), pp.2304-2314.
48. Kessner, D., Chambers, M., Burke, R., Agus, D. and Mallick, P., 2008. ProteoWizard: open source software for rapid proteomics tools development. *Bioinformatics*, 24(21), pp.2534-2536.
49. Robichaud, G., Garrard, K.P., Barry, J.A. and Muddiman, D.C., 2013. MSiReader: an open-source interface to view and analyze high resolving power MS imaging files on Matlab platform. *Journal of the American Society for Mass Spectrometry*, 24(5), pp.718-721.
50. Zarogoulidis, P., Karamanos, N.K., Porpodis, K., Domvri, K., Huang, H., Hohenforst-Schmidt, W., Goldberg, E.P. and Zarogoulidis, K., 2012. Vectors for inhaled gene therapy in lung cancer. Application for nano oncology and safety of bio nanotechnology. *International journal of molecular sciences*, 13(9), pp.10828-10862.

CHAPTER IV: NOVEL POLY(2-OXAZOLINE) BLOCK COPOLYMER WITH AROMATIC HETEROCYCLIC SIDE CHAINS AS A DRUG DELIVERY PLATFORM¹

4.1 SUMMARY

Here we report a novel poly(2-oxazoline)-based block copolymer with the aromatic heterocyclic side chains in one block and demonstrate its potential application as a drug delivery platform. The copolymer was synthesized via the condensation of *N,N*-dimethylbiguanide with the methyl ester side chain in poly(2-methoxycarboxyethyl-2-oxazoline) block (PMestOx) of the PMeOx-PMestOx diblock copolymer. We confirmed the *N,N*-dimethylbiguanide condensation with PMestOx and the complete conversion of the side chain to the *N,N*-dimethyl-1,3,5-triazine-2,4-diamine-6-ethyl moiety by physicochemical analysis. The PMeOx-PcBOx copolymer self-assemble into polymeric micelles in aqueous solution. Successful encapsulation into these micelles has been demonstrated for 1) several poorly soluble drugs, such as bruceantin and LY2109761, and 2) dichloro(1,2-diaminocyclohexane)platinum(II) (DachPt). The first class of drugs is incorporated possibly via hydrogen bonding and pi-pi interactions with the PcBOx side groups, while the second one is likely forms coordination bonds with the same side groups. The capability of this new copolymer to solubilize a uniquely diverse set of active pharmaceutical ingredients suggest potential application in drug delivery.

¹ This chapter previously appeared as an article in press. The original citation is as follows: Hwang, Duhyeong et al., “Novel poly(2-oxazoline) block copolymer with aromatic heterocyclic side chains as a drug delivery platform”, *Journal of Controlled Release*, 2019, DOI: 10.1016/j.jconrel.2019.06.037

4.2 Introduction

With an increasing number of approved drugs, the design of novel drug molecules has become more complicated. The challenge in drug design is the concurrent demand for achieving higher therapeutic potency with proper physicochemical properties and lowering toxicity. Large pharmaceutical companies employ high throughput screening (HTS) to find lead compounds, but the structure optimization that takes place after HTS often results in therapeutic failure. It is well-known that the increased structural complexity of therapeutic compounds is positively correlated to drug development success rate [1]. Ergo, the use of additional strategies, such as rational drug design, is a necessity to help simplify this complex, failure-prone process [2]. One potential approach to simplify drug development is to take advantage of drug delivery systems. Drug delivery systems can enhance the therapeutic efficacy and expand the viable drugs by compensating for undesirable physicochemical properties of therapeutic agents and modulating their pharmacokinetics, biodistribution, and cellular uptake [3-5].

Among a variety of drug delivery systems, the most successful approach thus far is the encapsulation of physicochemically challenging active pharmaceutical ingredients (APIs) in nanoparticles [6, 7]. Currently, several drug delivery-based products are approved for the clinic, and many clinical and preclinical studies are in progress [8]. For example, the liposomal formulation of Amphotericin B dramatically decreased the risk of systemic side effects of the compound [9]. Abraxane[®], a nanoparticle albumin-bound paclitaxel, has eliminated the use of toxic excipients [10], and lipid nanoparticle formulations can transform siRNA into a useful therapeutic which acts on a previously undruggable target [11].

However, the majority of reported nanoformulations are limited by the API's physicochemical properties. For example, liposomes are suitable carriers for hydrophilic, slightly basic compounds

[12, 13]. On the other hand, previously reported polymeric micelles are most suitable to load hydrophobic drugs, because the driving force for drug encapsulation is overwhelmingly due to hydrophobic interactions [3].

N,N-dimethylbiguanide, known more commonly as metformin, has largely been used as an anti-diabetic medication. It has a strong capacity to form hydrogen bonds due to its nitrogen-rich structure [14]. It was also reported that *N,N*-dimethylbiguanide can condense with alkyl ester compounds to form heteroaromatic (triazine) ring structures which exhibit strong pi-pi interactions [15]. We designed a novel polymer functionalized with the condensed form of *N,N*-dimethylbiguanide based on poly(2-oxazoline)s which takes advantage of hydrogen bonding and pi-pi stacking interactions inherent in this structure. These new interactions may assist in the solubilization of otherwise incompatible small molecules. The novel polymer self-assembles into nanoparticles in aqueous medium and shows the ability to encapsulate a diverse space of therapeutic agents. Taken together, this novel polymer may increase the success rate of drug development.

4.3 Materials and Methods

Chemicals

All chemicals for polymer synthesis and dichloro(1,2-diaminocyclohexane)platinum(II) (DachPt) were purchased from Sigma-Aldrich (St. Louis, MO). Oxaliplatin was purchased from LC Laboratories (Woburn, MA). Metformin hydrochloride (*N,N*-dimethylbiguanide hydrochloride) was purchased from Tokyo Chemical Industry Co., Ltd. (Portland, OR). *N,N*,6-trimethyl-1,3,5-triazine-2,4-diamine (cBG) was purchased from Santa Cruz Biotechnology (Dallas, TX). 2-methoxycarboxyethyl-2-oxazoline (MestOx) was synthesized as previously reported [16]. For synthesis of the polymers, the reagents (methyl trifluoromethanesulfonate (MeOTf), 2-methyl-2-oxazoline (MeOx), MestOx, 2-*n*-butyl-2-oxazoline (BuOx)) and solvent (acetonitrile (ACN)) and others were dried by refluxing over calcium hydride (CaH₂) under inert nitrogen gas and subsequently distilled prior to use [17]. P[MeOx₃₅-*b*-BuOx₂₀-*b*-MeOx₃₅] (P2) was synthesized as described previously [17]. Cell counting kit (CCK-8) was purchased from Dojindo Molecular Technologies (Rockville, MD).

Polymer characterization

NMR spectra were recorded on an INOVA 400 at room temperature (RT). The spectra were calibrated using the solvent signals (CDCl₃ 7.26 ppm, (CD₃)₂SO 2.50 ppm, D₂O 4.80 ppm). Matrix-assisted laser desorption/ionization time-of-flight mass spectroscopy (MALDI-TOF MS) was performed on a Sciex 5800 MALDI-TOF/TOF mass spectrometer and 2-(4'-Hydroxybenzeneazo)benzoic acid (HABA) (20 mg/mL in acetonitrile) was used as the matrix. Gel permeation chromatography (GPC) was performed on a GPCmax VE-2001 system (Viscotek) (RI detector mode, PSS SEC column (GRAM 100Å 8 x 300 mm, SDV 5µm) with *N,N*-

Dimethylformamide (DMF) (25 mM LiBr, 1 mL/min) as eluent and calibrated against Polymethylmethacrylate (PMMA) standards.

Synthesis of Methyl-P[MeOx₆₀-*b*-MestOx₃₀]-piperidine (PMeOx-PMestOx)

Under dry and inert conditions, 32.2 mg (0.2 mmol, 1 eq) of initiator (MeOTf) and 1015 mg (11.93 mmol, 60 eq) of MeOx monomer were dissolved in 4 mL dry acetonitrile at RT. The mixture was stirred at 80 °C for 4 h. After cooling to RT, the monomer for the second block, MestOx (942 mg, 6.01 mmol, 30 eq), was added and the mixture was stirred at 80 °C overnight. The polymer was terminated by addition of 0.1 mL piperidine (1.01 mmol, 5 eq) and the mixture was stirred overnight at RT. An excess of K₂CO₃ was added to the mixture, and then the mixture was allowed to stir for 12 h. After filtration of the mixture, 5 mL of chloroform-methanol mixture (1:1) was added to the filtrate containing the product (PMeOx-PMestOx). After precipitation of the polymer by ice-cold diethyl ether (approximately 50 times the volume of polymer solution of diethyl ether was added), the product was isolated by centrifugation and organic solvent was decanted. The polymer product was dissolved in ~50 mL of DI water and dialyzed against DI water (3.5 kDa membrane) for 3 days, changing the water every day, to remove organic solvent and any remaining monomers. The resulting solution was lyophilized, and the polymer was obtained as a white powder (1428 mg, 73%). GPC (DMF (25 mM LiBr)): Mn = 13.4 kg/mol (PDI 1.038); ¹H NMR (D₂O, 298 K): 2.4–2.7 (4H, CO-CH₂-CH₂-CO-OCH₃); 3.2–3.7 (7H, -N-CH₂-CH₂, -CO-O-CH₃); 1.8–2.0 (3H, -CO-CH₃).

Synthesis of Methyl-P[MeOx₆₀-*b*-(2-*N,N*-dimethyl-1,3,5-triazine-2,4-diamine-6-ethyl-2-oxazoline)₃₀]-piperidine (PMeOx-PcBOx)

N,N-dimethylbiguanide (Metformin) free base was prepared as previously reported [18]. Briefly, metformin hydrochloride (4.51 g, 27.27 mmol) was suspended in isopropyl alcohol (*i*-PrOH) (40 mL) and potassium hydroxide (1.83 g, 32.62 mmol) was added to the suspension at 50 °C. The white slurry was stirred at 50 °C for 2 h, and then the mixture was cooled to RT. The resulting mixture was filtered and the filter-cake was washed with acetone (2 x 10 mL). The combined filtrates were concentrated under reduced pressure yielding a white solid (metformin free base). Yield: 98% (3.45 g); ¹H NMR (400 MHz, D₂O) δ 3.07 (s, -N-(CH₃)₂). Subsequently, *N,N*-dimethylbiguanide free base (1.55 g, 12.02 mmol (20-fold excess amount of MestOx unit in polymer)) was added to a solution of PMeOx-PMestOx (200 mg, 22.2 μmol (0.6 mmol of total MestOx unit)) in dimethylformamide (DMF) (15 mL). The mixture was stirred at 75 °C for 48 h to form PcBOx. The reaction mixture was then diluted with DI water and dialyzed against DI water to completely remove unreacted free *N,N*-dimethylbiguanide and organic solvent. The polymer was obtained as a white powder (162 mg, 81% yield) after lyophilization from water. ¹H NMR (D₂O, 298 K): 2.2–2.7 (4H, CO-CH₂-CH₂-C₃N₃(NH₂)(N(CH₃)₂); 2.6–3.0 (6H, C₃N₃(NH₂)(N(CH₃)₂); 3.1–3.7 (4H, -N-CH₂-CH₂-); 1.8–2.0 (3H, -CO-CH₃).

Analysis of PMeOx-PcBOx structure

UV-Vis spectroscopic analysis was performed to investigate the formation of poly(2-*N,N*-dimethyl-1,3,5-triazine-2,4-diamine-6-ethyl-2-oxazoline) (PcBOx) structure in PMeOx-PcBOx. Samples (PMeOx-PcBOx, PMeOx-PMestOx, and cBG, and *N,N*-dimethylbiguanide) were dissolved (equimolar *N,N*-dimethylbiguanide or cBG units) in DI water and UV absorption spectra were measured over the wavelength range of 200 to 300 nm in 1 nm steps. (SpectraMax M5,

Molecular Devices). In order to investigate the mass shift of PMestOx after conjugation with *N,N*-dimethylbiguanide and confirm the formation of the defined structure using MALDI-TOF/TOF analysis, we synthesized a PcBOx homopolymer from MestOx homopolymer with a degree of polymerization (DP) of 10 as described above. MALDI-TOF/TOF was performed on a Sciex 5800 MALDI-TOF/TOF mass spectrometer and 2-(4'-Hydroxybenzeneazo)benzoic acid (HABA) (20 mg/mL in acetonitrile) was used as the matrix. Polymer samples were dissolved in acetonitrile (2 mg/mL). Analytes were prepared by mixing 10 μ L of matrix and 5 μ L of polymer samples. Samples were applied using the dried droplet method.

Titration analysis

PMeOx-PcBOx (12 mg) was dissolved in 10 mL 0.01N HCl solution and titrated with 0.1N NaOH solution added in increments of 0.020 mL after the pH values were stabilized. Titration assay for control samples (saline, cBG and PMeOx-PMestOx) was performed at the same molar concentration of cBG units with the same volume of titrant. Derivative $\Delta\text{OH}/\Delta\text{pH}$ was plotted from the obtained titration curves to investigate the buffering-capacity of samples.

Self-assembly of PMeOx-PcBOx in aqueous solution and particle formation

Briefly, the sample was diluted with DI water to yield 1 mg/mL final polymer concentration before the measurement. Particle z-average effective diameter and polydispersity index (PDI) were measured by dynamic light scattering (DLS) (Nano-ZS, Malvern Instruments, UK). Results are the mean of three independent sample measurements. The morphology of PMeOx-PcBOx particle in aqueous media was determined using a LEO EM910 TEM operating at 80 kV (Carl Zeiss SMT Inc., Peabody, MA). One drop of PMeOx-PcBOx solution (1 mg/mL final polymer concentration)

was deposited on a copper grid/carbon film for 5 min and excess solution was wiped off using fine filter paper. Then one drop of negative staining solution (1% uranyl acetate) was added and allowed to dry for 10 s prior to the TEM imaging. Digital images were obtained using a Gatan Orius SC1000 CCD Digital Camera in combination with Digital Micrograph 3.11.0 software (Gatan Inc., Pleasanton, CA). Two dimensional nuclear Overhauser effect spectroscopy (2D NOESY) NMR measurement were performed for both PMeOx-PMestOx and PMeOx-PcBOx in D₂O at 1 mg/mL polymer concentration to investigate the molecular interactions of the polymers in aqueous media. Critical micelle concentration (CMC) of PMeOx-PcBOx was determined by DLS [19]. PMeOx-PcBOx solution in DI water (1 mg/mL) was gradually diluted with DI water and derived count rates (kcps) were measured in triplicate after mixing. The CMC was taken as the polymer concentration at which a significant and consistent increase in derived count rate was observed [19].

Drug encapsulation

Encapsulation of water-insoluble drugs and in vitro drug release

Drug-encapsulated polymeric nanoparticle formulations were prepared by the thin film hydration method as previously described [17]. For bruceantin, LY2109761, imiquimod, paclitaxel, SN-38, LY364947, GDC-0941, aclacinomycin A, wortmannin, and GW788388 stock solutions of PMeOx-PcBOx and drugs in chloroform:methanol (9:1) solution were mixed together at the pre-determined ratios (3:10 drug to polymer w/w ratio (LY2109761), 2:10 w/w ratio (bruceantin and imiquimod), 1:10 w/w ratio (paclitaxel, SN-38, wortmannin, LY364947, GDC-0941, aclacinomycin A, GW788388)). Ratios were determined by starting at 1:10 ratios and then proceeding to higher (2:10 and 3:10) if the 1:10 ratios had high encapsulation efficiency. The

organic solvent was evaporated at 58 °C under a stream of inert gas to form a thin-film of drug-polymer homogenous mixture. Next, the thin films were hydrated with saline and then incubated for 5-10 min at 45 °C to form drug-encapsulated polymeric micelle solutions. All samples were prepared with 2 mg of polymer and hydrated with 200 µL of saline. The formed micelle solutions were centrifuged at 10,000 rpm for 3 minutes (Sorvall Legend Micro 21R Centrifuge, Thermo Scientific) to remove any precipitate of unloaded drug or polymer. The final concentration of drugs in PMeOx-PcBOx micelles was analyzed by HPLC (Agilent Technologies 1200 series) using a mixture of acetonitrile/water (70%/30% v/v for bruceantin, imiquimod, wortmannin, GW788388 and paclitaxel; 50%/50% v/v for LY2109761, GDC-0941, aclacinomycin A, LY364947, and SN-38) as the mobile phase. The samples were diluted with mobile phase to final concentration of ~100 µg/mL of drugs and injected (10 µL) into the HPLC system. The flow rate was 1.0 mL/min, and column temperature was 40 °C. Detection wavelength were 227 nm for bruceantin, paclitaxel, LY2109761, GDC-0941, GW788388, aclacinomycin A, LY364947 and SN-38 and 254 nm for imiquimod and wortmannin. Drug concentration was quantified against free drug calibration curves.

The drug release from PMeOx-PcBOx nanoparticle was studied using the membrane dialysis method against phosphate buffered saline (PBS), pH 7.4 at 37 °C. Briefly, the drug loaded PMeOx-PcBOx nanoparticle formulations (paclitaxel and Bruceantin) were diluted with saline to obtain solution of approximately 0.1 mg/mL of polymer. Then the diluted nanoparticle formulations (100 µL) were placed in 100 µL floatble Slide-A-Lyzer MINI dialysis devices with a MWCO of 3.5 kDa (Thermo Scientific) and suspended in 20 mL of PBS to comply with sink conditions. Three devices were used for every time point. At each time point, the samples were withdrawn from the dialysis device and the remaining drug amount of sample were quantified by

HPLC as described above. Stability of both nanoparticle formulations (paclitaxel and Bruceantin) was investigated via monitoring drug loading (HPLC) and size distribution (DLS) for 8 days at 4 °C.

Accounting for molecular characteristics of insoluble drugs

The number of hydrogen bond acceptors and donors in each drug substance were counted by Chem3D. The number of rotatable bonds in each drug substance was counted as previously reported [20]. Briefly, any single bond not in ring structures, except for the bonds connected to the terminal atom and the bonds present in amide bonding, were counted as 1. The Log P values of polymer unit structures and each drug substance were predicted by Chem3D. The definition of electron deficient aromatic ring herein is an aromatic ring, which has more electron withdrawing atoms or groups than electron donating atoms or groups. The score of each drug substance is the number of the parameters which meet our criteria: 1) electron deficient aromatic ring is present, 2,3) the number of hydrogen bonding acceptors and donors are more than 6 and 2, respectively, 4) LogP is less than 3, and 5) the number of rotatable bonds is more than 5.

Encapsulation of platinum-based drug (DachPt)

DachPt powder (5 mg) was suspended in PMeOx-PcBOx (10 mg) aqueous solution (3 mL) and the reaction mixture was refluxed for 48 h. After that the mixture was cooled to RT and centrifuged to precipitate free DachPt. Clear supernatant solution was then dialyzed against DI water for 3 days in 3.5 kDa dialysis membrane and lyophilized to obtain powder form of DachPt-loaded PMeOx-PcBOx (DachPt-PMeOx-PcBOx). Actual Pt loading was measured via Inductively coupled plasma mass spectrometry (ICP-MS) analysis using NexION 300D inductively coupled

plasma mass spectrometer (PerkinElmer, USA) equipped with SC4-DX autosamplers (ESI, USA). Decomposition of the samples matrix was performed by heating at 70 °C for 20 h after the addition of trace metal grade nitric acid (20% aqueous solution) and hydrochloric acid (5% aqueous solution). Digested samples were diluted (1:10) with DI water, a second dilution (1:100) was performed with 2% nitric acid. ICP-MS was operated in standard mode, all operating parameters were optimized to meet requirements as defined by the manufacturer prior to method calibration and analysis. Calibration curves were constructed using a zero point standard and a six point calibration curve in a range 1-100 ppb. Five replicates were analyzed per sample. Quantification was performed with Bi as an internal standard.

Loading efficiency (LE) and loading capacity (LC) calculations

The following equations were used to calculate LE and LC of drug in PMeOx-PcBOx micelles:

$$LE (\%) = M_{\text{drug}} / (M_{\text{drug added}}) \times 100\%, \quad (1)$$

$$LC (\%) = M_{\text{drug}} / (M_{\text{drug}} + M_{\text{excipient}}) \times 100\%, \quad (2)$$

Where M_{drug} and $M_{\text{excipient}}$ are the mass of the solubilized drug and polymer in the solution respectively, while $M_{\text{drug added}}$ is the weight amount of the drug added to the dispersion during the preparation of the micelle formulation.

Cell culture and cytotoxicity

In vitro cytotoxicity of DachPt-PMeOx-PcBOx, oxaliplatin, and PMeOx-PcBOx was evaluated in MDA-MB-231 and 344SQ cancer cell lines by following previously reported method [21] using [2-(2-methoxy-4-nitrophenyl)-3-(4-nitrophenyl)-5-(2,4-disulfophenyl)-2H-

tetrazolium, monosodium salt] (WST-8) (Cell-Counting Kit-8 assay). Briefly, cells were seeded in 96-well plates at a density of 5,000 cells/well 24 h prior to the treatment. Subsequently, cells were treated with DachPt-PMeOx-PcBOx, oxaliplatin, or PMeOx-PcBOx in full medium at the same concentration of platinum. Following 72 h, the incubation medium was removed, and 100 μ L of fresh medium with WST-8 (10 μ L/well) was added and incubated for 4 h at 37 °C.

Subsequently, absorbance was read at 450 nm using a plate reader (SpectraMax M5, Molecular Devices). Cell survival rates were calculated and normalized to the control untreated wells. Data represents average of six replicates in means \pm standard deviation (SD). The mean drug concentration required for 50 % growth inhibition (IC₅₀) was determined using Graphpad Prism 7 software.

4.4 Results

Polymer synthesis and post-polymerization modification.

We first synthesized PMeOx-PMestOx diblock copolymer as the starting material via living cationic ring-opening polymerization [16] and then converted it to *N,N*-dimethylbiguanide derivative by the polymer analogous condensation reaction of the MestOx block with *N,N*-dimethylbiguanide (Figure 4.1). The full conversion of PMestOx was confirmed by ^1H NMR spectra (^1H NMR (CDCl_3 , 298 K)) of the reaction mixture as the methyl ester signal of the polymer (at δ 3.5 ppm) disappeared after the condensation with *N,N*-dimethylbiguanide (Figure 4.2). The block length and the molecular weight of the PMeOx-PMestOx precursor were confirmed via ^1H NMR spectroscopy (^1H NMR (D_2O , 298 K)) (Figure 4.3) (PMeOx = 60, PMestOx = 30, M_n = 9.9 kg/mol) and gel permeation chromatography (M_n = 13.4 kg/mol, PDI = 1.038).

After the purification of PMeOx-PcBOx, ^1H NMR spectrum of precursor (PMeOx-PMestOx), cBG, and PMeOx-PcBOx were analyzed to confirm the conversion of cBOx structure (^1H NMR ($(\text{CD}_3)_2\text{SO}$, 298 K)). The disappearance of the methyl ester signal (marked by arrow in Figure 4.4A and not present in 4.4C) suggests that there was a complete conversion from methyl ester to a new structure. The ^1H NMR spectrum of the newly synthesized side chain was nearly identical to that of the reference molecule (cBG) (Figure 4.4B and 4.4C) indicating that the condensed cBG-like ring structure was formed on the side chain of the polymer, consistent with PcBOx. Also, new peaks attributed to protons g and f appeared at 3.0 ppm and 6.6 ppm, respectively. There were no changes exhibited in the NMR spectrum of the other polymer block (PMeOx) (Figure 4.4A and 4.4C, proton a). This suggests the conversion of PMeOx-PMestOx to PMeOx-PcBOx was successful and proceeded without side reactions. The ^{13}C NMR spectrum of PMeOx-PcBOx was also identical to that of the reference molecule (cBG) (Figure 4.5) indicating

the formation of cBG structure on the side chain of the polymer and the disappearance of the methyl ester signal (51 ppm) suggests a complete conversion from methyl ester to cBG structure. Also, new peaks attributed to four carbons appeared at 36 ppm, 165.4 ppm, 168.8 ppm, and 176.5 ppm. There were no changes exhibited in the NMR spectrum of the other polymer block (PMeOx) (Figure 4.5).

We performed UV-Vis spectroscopic analysis to investigate the formation of the PMeOx-PcBOx structure. As shown in Figure 2A, the UV spectrum of the PMeOx-PcBOx showed specific peak absorbance around 227 nm while uncondensed *N,N*-dimethylbiguanide did not show particular UV absorbance. We found only PMeOx-PcBOx exhibited a clear peak absorbance around 227 nm (PMeOx-PcBOx) confirming the formation of the PcBOx structure. These results suggest the methyl ester group in PMestOx had been condensed with *N,N*-dimethylbiguanide to form PcBOx. The PMeOx-PcBOx and cBG UV measurements were done with equimolar amounts of cBG molecules and PcBOx side chains, meaning we would expect nearly identical absorbance, which we see in Figure 4.6A. This, along with the NMR data, indicate a full conversion of the PMestOx unit to PcBOx.

To show the mass shift of PMestOx unit after conjugation with *N,N*-dimethylbiguanide, MALDI-TOF analysis was performed on PcBOx homopolymer with DP of 10. MALDI-TOF MS of the PMestOx revealed the expected spacing of 157.07 m/z corresponding to the MestOx monomer, while after the condensation reaction the spacing increased to 236.14 m/z. This data provides evidence supporting the condensation of *N,N*-dimethylbiguanide with PMestOx yielding the PcBOx structure (spacing of 236.14 m/z corresponding to repeating unit of PcBOx) (Figure 4.7).

The pH-dependent protonation of PMeOx-PcBOx polymer in saline was evaluated by titration (Figure 4.6B). The titration curve and dOH/dpH curve of cBG clearly showed its proton buffering profile and its pKa was estimated to be around 5. PMeOx-PcBOx copolymer also had similar but broader protonation profile, whereas PMeOx-PMestOx didn't show any proton buffering capacity. This indicates the protonation profile of PMeOx-PcBOx was derived from the cBG moiety.

Self-assembly of PMeOx-PcBOx copolymer

Self-assembly of PMeOx-PcBOx copolymer and formation of particles in aqueous media was investigated by DLS and confirmed by TEM. The particles had a volume measured diameter of 28.0 nm and PDI of 0.28 as determined by DLS (Figure 4.8). The particles were non-spherical, with partially elongated morphology (Figure 2C). The dual spherical and elongated morphologies contribute to the high PDI value in the DLS measurements.

To confirm the molecular interaction among PMeOx-PcBOx in aqueous media, two dimensional Nuclear Overhauser Effect Spectroscopy (2D NOESY) NMR measurements were conducted. In the spectra of 2D NOESY NMR (Figure 4.9), PMeOx-PcBOx particles show strong correlation of PcBOx protons (2.6 ppm to 3.0 ppm, 6H, $C_3N_3(NH_2)(N(CH_3)_2)$) with other PcBOx protons (2.2 ppm to 2.7 ppm, 4H, CO-CH₂-CH₂- $C_3N_3(NH_2)(N(CH_3)_2)$) and protons of the polymer backbone (3.1 ppm to 3.7 ppm, 3.1–3.7 (4H, -N-CH₂-CH₂-). This highlights some of the intramolecular and intermolecular interactions present in the PMeOx-PcBOx polymer. In the case of PMeOx-PMestOx, 2D NOESY NMR did not show any correlation of protons of PMeOx-PMestOx. Taken together, this evidence supports that the molecular interaction of PMeOx-PcBOx

arises from PcBOx structure and contributes to the the polymer self-assembly into particles in aqueous media.

To investigate the effect of polymer concentration on the formation of the particle in aqueous solution, the CMC of PMeOx-PcBOx was determined by DLS. Light scattering intensity and count rate of the particle was monitored over a range of PMeOx-PcBOx concentrations and the point where derived count rate becomes constant corresponds to the CMC. As shown in Figure 4.10, the CMC of PMeOx-PcBOx was approximately 40 mg/L in DI water.

Solubilization of poorly soluble small molecules

We examined several poorly soluble active pharmaceutical ingredients to assess their solubilization in PMeOx-PcBOx polymeric micelles and compared it with the solubilization of these molecules in the micelles of our reference polymer P[MeOx₃₅-*b*-BuOx₂₀-*b*-MeOx₃₅] (P2) [17, 22-24]. The molecules examined belonged to different classes including transforming growth factor β (TGF- β) receptor inhibitors (LY2109761, GW788388 and LY364947), protein synthesis inhibitors (bruceantin), toll-like receptor (TLR) 7 agonist (imiquimod), phosphatidylinositol 3-kinase (PI3K) inhibitors (wortmannin and pictilisib (GDC-0941)), microtubule inhibitor (paclitaxel), and topoisomerase inhibitors (Aclacinomycin A and SN-38). In these experiments, we kept the polymer concentration constant at 10 mg/ml and varied the feed concentration of the drug until its maximal solubility was observed. We screened drugs at various ratios, beginning at 1:10 (drug:polymer), and increased the ratio until maximal solubility was obtained. As shown in Figure 4.11, PMeOx-PcBOx micelle formulation displayed a reasonably good capacity for solubilization of several poorly soluble drug compounds (see also Table 4.1). In particular, we solubilized nearly ~3.28 mg/mL of LY2109761 with 24.7% LC and little if any drug precipitate

(82% LE). Bruceantin also showed reasonably good maximal solubilization in this formulation: 1.87 mg/ml, 11.5% LC, 65 % LE. On the other hand, paclitaxel and other drugs were not as soluble as LY209761 and bruceantin (6.8% LC for aclacinomycin A, 6.3% LC for paclitaxel, 4.3% LC for GDC-0941, 3.8% LC for wortmannin), while LY364947 (0.3% LC) GW788388 (0.2% LC), Imiquimod (undetectable) and SN-38 (undetectable) were practically insoluble. Comparison of the solubilization profile of these molecules for PMeOx-PcBOx and P2 triblock copolymer micelles reveals distinct selectivity of each polymer for some of these APIs (Figure 4.11, see also Table 4.1). With P2, we observed the ultra-high loading of bruceantin with least amount of drug precipitate (as much as 9.98 mg/ml, 50.0 % LC, 99 % LE). Also, as previously reported [17], paclitaxel was solubilized at maximal concentration of 6.89 mg/ml (41% LC and 86 % LE). LY2109761 showed fairly high solubilization in P2 micelles (1.5 mg/ml, 14.0% LC, 78 % LE) although it was distinctively less than that observed in PMeOx-PcBOx micelles. Solubilization of aclacinomycin A was low but generally comparable in both micelle systems. On the other hand, GDC-0941 and wortmannin were practically insoluble in P2 system, while they were distinctively more soluble in PMeOx-PcBOx. The other compounds tested (GDC-0941, LY364947, SN-38, and Imiquimod) were practically insoluble in both micelle solutions.

PMeOx-PcBOx micelle formulations displayed sub-100nm size distribution in DLS measurement; 85 nm for paclitaxel (PDI = 0.298, Dv10 = 23.3 nm, Dv50 = 34.6 nm, Dv90 = 80.9 nm), 60 nm for bruceantin (PDI = 0.48, Dv10 = 17.2 nm, Dv50 = 25.2 nm, Dv90 = 42.9 nm), and 50 nm for LY2109761 (PDI = 0.4, Dv10 = 15.5 nm, Dv50 = 21.5 nm, Dv90 = 34.8 nm). TEM images of both formulations are shown in Figure 4.12A and 4.12B and small-sized particles (approximately 30 nm) were observed in both formulations, corresponding to the DLS

measurement (volume-based). Small portions of particle aggregate were observed in both formulations and this may explain the relatively high value of PDI.

We investigated the release profile of encapsulated drugs (Paclitaxel and Bruceantin) in PMeOx-PcBOx. Both Paclitaxel and Bruceantin were continuously released from PMeOx-PcBOx nanoparticle, with over 80% of drugs being released at 24 hour time point (Figure 4.12C). The release rates were similar for Bruceantin in both of the polymers. Interestingly, the release rate was very different for Paclitaxel in P2 vs. PMeOx-PcBOx (Figure 4.12D). After 24 hours, most of the PTX was released in PcBOx whereas not even 50% was released from P2. This kind of release data is consistent with previously published data at this low (10:1) polymer:drug feeding ratio [22]. Both paclitaxel and Bruceantin formulation in PMeOx-PcBOx were proven stable for 8 days at 4 °C as we monitored the drug loading and size distribution (Figure 4.12E and 4.12F).

Finally, we summarized the relationship between LC and the physicochemical properties of the drug molecules that could be related to the interaction with PMeOx-PcBOx (Figure 4.13). The designated potentially “influential” parameters are the presence of electron deficient aromatic structures (EDA), the numbers of hydrogen bonding acceptors (HBA) and donors (HBD), LogP, and the number of rotatable bonds (RBN).

Water-soluble DachPt encapsulation

We investigated whether the cBG side chain of the PMeOx-PcBOx copolymer can facilitate incorporation of platinum drug (DachPt) in the polymeric micelles via coordination bonding. The loading was accomplished by co-incubation of the DachPt and PMeOx-PcBOx micelles in the aqueous solution followed by separation of the drug loaded micelles from unincorporated drug. The total platinum mass percent in the resulting DachPt-PMeOx-PcBOx

formulation was about 17.7 % as measured by ICP-MS. When converted to the equivalent content of DachPt this value results in ~34.5% LC. The analysis of DachPt-PMeOx-PcBOx formulation by DLS revealed a unimodal size distribution with an effective diameter of ~35 nm and PDI of 0.49 (Figure 4.8B), The increase of the particle size and polydispersity when compared to the free PMeOx-PcBOx micelles (~28 nm, PDI = 0.28), was possibly due to conformational changes in the core-forming block and volume increase induced by DachPt incorporation.

In vitro cytotoxicity DachPt-PMeOx-PcBOx formulation

We evaluated the in vitro cytotoxicity of DachPt-PMeOx-PcBOx in comparison with the free oxaliplatin in 344SQ murine NSCLC cells and MDA-MB-231 human breast cancer cell lines. The cytotoxicity was measured by the CCK-8 assay. Free polymer PMeOx-PcBOx was found to be non-toxic in both cell lines up to 4 mg/mL dose. On the other hand, PMeOx-PcBOx-DachPt displayed platinum concentration-dependent cytotoxicity profile in both cell lines, albeit the corresponding its IC₅₀ exceeded those of oxaliplatin by 10 to 50 times (Figure 4.14).

4.5 Discussion

The motivation for our work was to develop an alternative polymer for drug nanoformulations which is compatible with drugs that cannot be otherwise formulated in existing drug delivery platforms. Previously, we described a poly(2-oxazoline)-based polymeric micelle platform, which is unique in its ability to incorporate large amounts of insoluble compounds, as demonstrated across many drugs and drug candidates, such as taxanes [17, 25]. The hydrophobic PBuOx block in P2 (P[MeOx35-b-BuOx20-b-MeOx35]) has polar and hydrated amide functionality in each repeating unit. These micelles represent a unique dual polar/hydrophobic environment for incorporation of drug molecules, such as Paclitaxel [17, 26]. These interactions are facilitated, perhaps, by the relatively small size and flexibility of the of the butyl side chain in the BuOx. In fact, substitution of the butyl group for a more hydrophobic nonyl group results in a drastic decrease in the solubility of taxanes in these poly(2-oxazoline) based micelles [17, 26].

The resultant injectable aqueous micellar solutions are readily prepared and are stable for days and weeks. These formulations can contain up to 50-100 g/L of poorly soluble drugs [22, 24, 25]. The drug to polymer wt. ratio in these micellar formulations is also up to a hundred times better than the amounts of excipients in the current formulations. For example, for paclitaxel, the amount of P2 polymer per 1 g of drug is ~100– and ~10– times less than the amounts of excipients used in Taxol[®] and Abraxane[®], respectively [22]. This high loading contributes strongly to the widening of the therapeutic window and allows high dose therapy as the excipient-based toxicity is drastically reduced [22].

While BuOx-based polymers, such as P2, have been extremely successful solubilizers for over two dozen drugs and drug candidates, there are many compounds which have failed to display equally good solubilization in this system [26]. This has raised a necessity for the structural

modification of the block copolymers to improve solubility of the otherwise failing to be formulated drugs. Advancement in this area has been achieved recently by Luxenhofer group who modified the hydrophobic block in such polymers by replacing a substituted poly(2-oxazoline) for a substituted poly(2-oxazine), which has an additional methylene group in the backbone of the main chain [27]. The hydrophilic blocks (PMeOx) in the new copolymers remained unmodified. A novel selectivity of the new poly(2-oxazine)-based copolymers differentiating them from poly(2-oxazolines) with respect to the drugs that they can solubilize was observed [26, 27]. In particular, P2 was highly effective in solubilizing paclitaxel, but much less effective with curcumin. In contrast, a copolymer containing a hydrophobic block made of 2-n-propyl-2-oxazine, which is a structural isomer of BuOx, had a clear solubilization preference for curcumin vs. Paclitaxel [26, 27].

In the present study, we sought to develop a novel polymeric micelle platform with differential solubilizing capacity that could bring these therapeutic advantages to a new array of insoluble drug compounds. We employed a very different approach to modification of the polymer hydrophobic block. Rather than adjusting the polymer backbone or adding a longer alkyl side chain, we completely replaced the alkyl side chain of PBuOx for a substituted aromatic heterocyclic ring. To test this approach, we designed and synthesized a novel poly(2-oxazoline) diblock copolymer, PMeOx-PcBOx, with an *N,N*-dimethyl-1,3,5-triazine-2,4-diamine-6-ethyl side chain in the “hydrophobic block.” The copolymer structure has been confirmed by the ¹H NMR, 2D NOESY NMR, MALDI-TOF MS, and UV-Vis spectroscopic analysis. The copolymer demonstrated the ability to self-assemble into micelle-like structures.

Next, we evaluated the drug loading capacity of this newly developed copolymer. We used drugs across the chemical space, including those molecules that have failed to be solubilized in P2

polymer. For the selected drugs that were not well formulated in P2 micelles, such as LY2109761 (and Wortmannin and GDC-0941 to lesser extents), the new block copolymer displayed a good solubilization capacity superior to that of P2. Despite having lower hydrophobicity of the core-forming block than P2 (the estimated LogP value of cBOx is -0.27 while that of BuOx is 1.61), PMeOx-PcBOx can still solubilize a variety of drug compounds. Interestingly, all poorly soluble compounds that show reasonably good solubilization in PMeOx-PcBOx micelles (bruceantin and LY2109761,) are moderately hydrophobic and have LogPs of 1.4 and 2.8 respectively. At the same time the more hydrophobic compounds with LogP around 4 and above (including, paclitaxel) are less soluble or practically insoluble in these micelles.

The capability of *N,N*-dimethyl-1,3,5-triazine-2,4-diamine-6-ethyl side chain to engage in multiple interactions with the drug molecules is likely to be important for drug solubilization. In particular, *N,N*-dimethyl-1,3,5-triazine-2,4-diamine-6-ethyl has a three-heteroatom aromatic ring, which is highly electron deficient. It is known that electron-deficient aromatic rings can form stable pi-pi stacking dimers in part due to strong interactions between pi electrons and sigma electron-deficient orbitals [28]. When considering this feature, *N,N*-dimethyl-1,3,5-triazine-2,4-diamine-6-ethyl groups may enable strong pi-pi stacking interactions both with each other, resulting in the self-assembly of the PcBOx blocks in the micelle core, and with drug molecules, some of which also have electron deficient aromatic rings. Indeed, of all the studied drugs, this new polymer has a clear “preference” for LY2109761, which has highly electron deficient aromatic rings.

Additionally, the *N,N*-dimethyl-1,3,5-triazine-2,4-diamine-6-ethyl side chain can serve as both a hydrogen bond acceptor and a hydrogen bond donor. Since hydrogen bond formation requires strict conformational angle and distance [29], the rigid 1,3,5-triazine ring may act as a molecular “scaffold” enabling efficient hydrogen bonding with selected drugs. At the same time,

flexibility of the drug structure may be important for their ability to adjust the angles and distances necessary for maximal hydrogen bonding with the cBOx units. This may explain a tendency for better solubilization observed for some drugs having higher number of rotatable bonds. Interestingly, PMeOx-PcBOx micelles appeared to have solubilization preference for some of the compounds that have higher hydrogen bonding capacity and greater number of rotatable bonds, which is known to be detrimental for drug absorption into target cells [30]. Thus, the new PMeOx-PcBOx block copolymer, and the overall class of poly(2-oxazolines) with side chains containing substituted aromatic heterocycles, may hold the potential to expand the design space of APIs and spark the development of novel polymeric micelle formulations based on multiple drug-polymer interactions.

It could be useful to quantify and correlate the physicochemical properties of drug molecules and their solubilization in PMeOx-PcBOx micelles. For this purpose, we attempted to develop a simplified scoring system using the presence of electron deficient aromatic structures (EDA) as an indicator for pi-pi stacking interaction, the numbers of hydrogen bonds acceptors (HBA) and donors (HBD) as indicators for hydrogen bonding, LogP as an indicator of hydrophobicity, and rotatable bonds number (RBN) as indicator for the ease with which a drug molecule can exhibit specific interactions with the PcBOx side chains. We could not establish a clear and simple correlation between any one parameter and drug solubilization in the PMeOx-PcBOx polymeric micelles. However, when taking into account multiple parameters, this system showed some ability to rationalize the drug solubilization. For instance, bruceantin does not have an electron deficient aromatic ring whereas GW788388 does. But the solubilization of bruceantin in PMeOx-PcBOx micelles was high, whereas that of GW788388 was low. This difference could be explained by additional interactions bruceantin may have in the core of the micelles that

GW788388 does not have (Bruceantin Score=4, GW788388 Score=2). At the same time, the higher point total in this scoring system does not necessarily mean that a given drug is more soluble than another drug with a lower score. A higher score simply means that there is a higher probability of some solubility being achieved. For example, aclacinomycin A scored the highest among all analyzed compounds (Score=5), but its solubilization was far from best and comparable to that of wortmannin that does not have a high hydrogen bonding capacity and has a relatively low number of rotatable bonds. The modest solubilization of aclacinomycin A may be connected to its relatively large volume (molecular mass 811.86 g/mol). Similarly, paclitaxel has a relatively high score (Score=4) but shows modest solubilization, which in addition to the high molecular mass of this drug (853.90 g/mol) may be also induced by its high LogP value. With a larger data set created the relative contributions of each parameter could perhaps be, elucidated and optimized to account for differences in the drug solubilization. A prediction of the success of compounds applicable for a given polymeric micelle formulation would allow the rational design of the copolymers, or conversely, the selection of APIs, which are preferable for a given polymeric micelle system. We hope that this scoring system can provide some intuition for the design of more complex computational models to accurately predict drug solubility in these unique micelle systems.

While relying on different mechanisms for loading hydrophobic drugs, the micelles were still able to produce a similar release profile for Bruceantin. Additionally, for Paclitaxel, the PcBOx allowed access to a different, more complete, release profile at the given 1:10 drug to polymer ratio. Utilizing different block structures, it is possible to tune the release profile of the polymeric micelles. This could be advantageous for tuning in vivo drug pharmacokinetic properties to reduce toxicity or increase therapeutic efficacy.

Heteroaromatic compounds such as substituted 1,3,5-triazine in cBOx are well known to form chelating complexes with a variety of metal species including Ag, Au, Cu, and Pt [28]. In this regard we evaluated and successfully loaded in the PMeOx-PcBOx micelles DachPt, which is an active form of the platinum chemotherapeutics, oxaliplatin and miriplatin. The resulting DachPt-PMeOx-PcBOx formulation displayed an anticancer activity in two different cancer cell lines, albeit in each cell line it had higher IC50 values than oxaliplatin. This difference in IC50 could be attributed to two factors; 1) the cell uptake mechanism is different between nanoparticle (DachPt-PMeOx-PcBOx) and small molecules (oxaliplatin), and 2) the onset of the cell damage is delayed for DachPt-PMeOx-PcBOx due to slower DachPt release mechanism compared to oxaliplatin that readily forms DachPt in cytosolic reducing conditions [31]. Further investigation is warranted to elucidate the mechanism of DachPt release in physiological conditions and cell uptake of the DachPt-PMeOx-PcBOx formulation.

Platinum drugs are widely used chemotherapies of cancer, but are known to cause peripheral neuropathy, especially sensory ataxia, due to the accumulation in the dorsal root ganglion [32]. To reduce this adverse effect, and maximize the therapeutic index, various delivery systems are explored for this drug class [33, 34]. More generally, metal nanoparticle systems are interesting subjects not just for therapeutics, but also for diagnostics and imaging especially in the field of oncology [35]. For example, manganese (Mn) or gadolinium (Gd) containing nanoparticles can be used as MRI contrast agents [36, 37] and gold nanoparticles are known to be useful as CT contrast agents [38]. Ruthenium (Ru) organometallic complexes were reported as photoluminescence imaging agents that can detect hypoxic tumors [39]. While the new polymer class described in this work may not have applications in all these instances, it is truly remarkable

that the same polymer excipient displays ability for incorporating both poorly soluble APIs as well as relatively well solubilized metal complexes used in chemotherapy.

In conclusion, we have designed a novel poly(2-oxazoline)-based block copolymer with a heterocyclic, aromatic side chain that can be used for 1) solubilization of a unique set of poorly soluble compounds that have previously failed in other polymeric systems, as well as 2) loading of platinum drugs through metal complexation. It is promising that the new block copolymer class can expand the application of polymeric micelle technologies to a new set of drugs and impact the drug design space by providing alternatives to hydrophobic interactions as a means of incorporation of poorly soluble APIs in the micelles. Future studies will validate this conclusion for a higher number of compounds and elucidate drug/polymer interaction mechanisms important for predictions of drug solubilization.

Drug	P2											PMeOx-PcBOx									
	10:1		10:2		10:4		10:8		10:10		SD	10:1		10:2		10:3		10:4		SD	
	LE%	LC%	LE%	LC%	LE%	LC%	LE%	LC%	LE%	LC%	LC%	LE%	LC%	LE%	LC%	LE%	LC%	LE%	LC%	LC%	
Imiquimod	6.1	0.6	-	-	-	-	-	-	-	-	0.1	0.0	0.0	-	-	-	-	-	-	0.0	
LY2109761	100.0	9.1	81.7	14.0	-	-	-	-	-	-	0.4	91.5	8.4	92.0	15.5	95.9	22.4	82.1	24.7	0.2	
Bruceantin	100.0	9.1	100.0	16.7	100.0	28.6	100.0	44.4	99.8	49.9	0.3	-	-	65.2	11.5	-	-	-	-	0.7	
SN-38	0.0	0.0	-	-	-	-	-	-	-	-	0.0	0.1	0.0	-	-	-	-	-	-	0.0	
LY364947	12.2	1.2	6.1	1.2	-	-	-	-	-	-	0.4	3.2	0.3	-	-	-	-	-	-	-	
GDC-0941	9.8	1.0	-	-	-	-	-	-	-	-	0.5	44.5	4.3	-	-	-	-	-	-	-	
Aclacinomycin A	40.3	3.9	16.5	3.2	12.0	4.6	-	-	-	-	1.6	36.6	6.8	-	-	-	-	-	-	0.8	
Paclitaxel	100.0	9.1	100.0	16.7	100.0	28.6	86.1	40.8	-	-	1.6	66.9	6.3	-	-	-	-	-	-	1.9	
Wortmannin	16.2	1.6	-	-	-	-	-	-	-	-	0.2	46.6	3.8	-	-	-	-	-	-	1.1	
GW788388	13.1	1.3	-	-	-	-	-	-	-	-	0.1	2.3	0.2	-	-	-	-	-	-	-	

Table 4.1 Loading efficiency (LE%) and capacity (LC%) in P2 or PMeOx-PcBOx for each drug in each feeding ratio. Maximum LE% and LC% were highlighted and SD were calculated only for them.

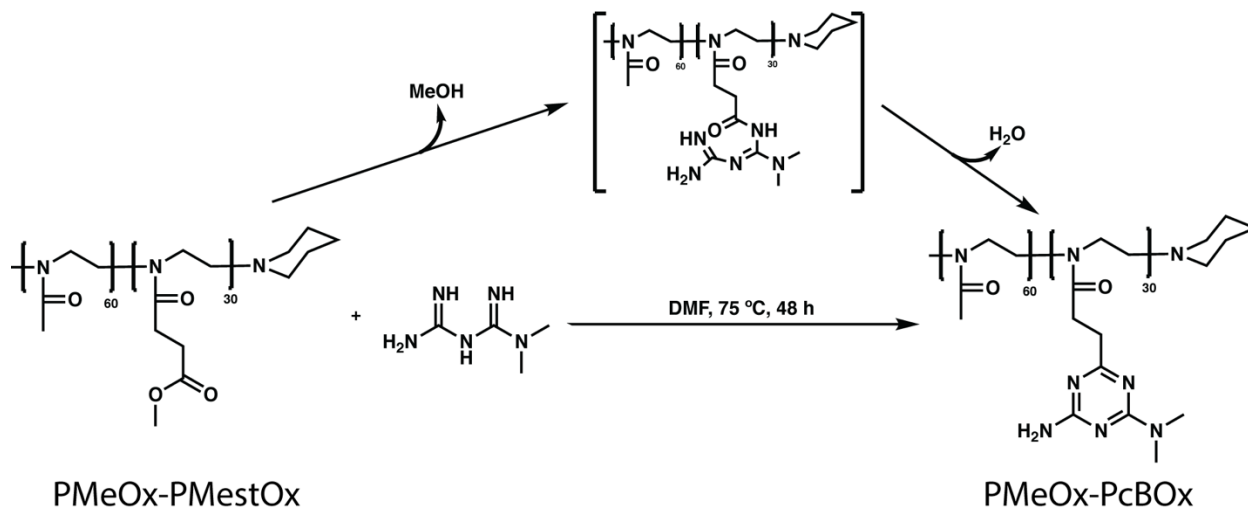


Figure 4.1 Synthesis of PMeOx-PcBOx via *N,N*-dimethylbiguanide condensation.

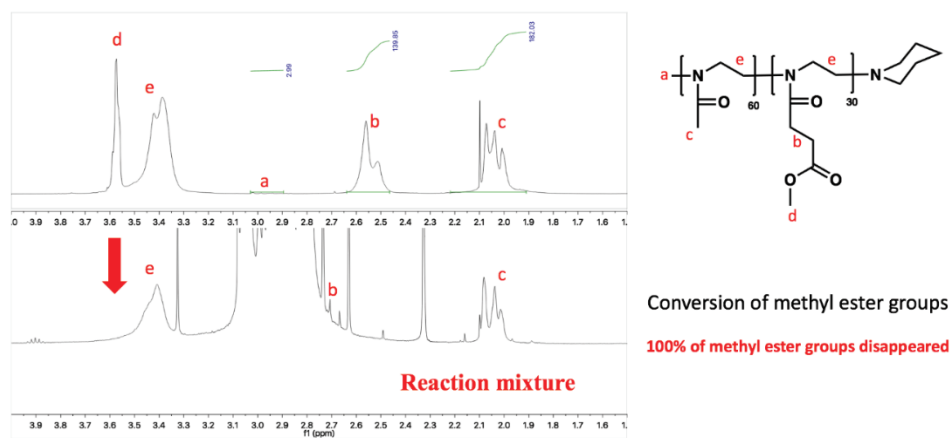


Figure 4.2 ^1H NMR spectra of PMeOx-PMestOx (upper) and reaction mixture (PMeOx-PMestOx and *N,N*-dimethylbiguanide free base in DMF) (lower) (CDCl_3 , 298K).

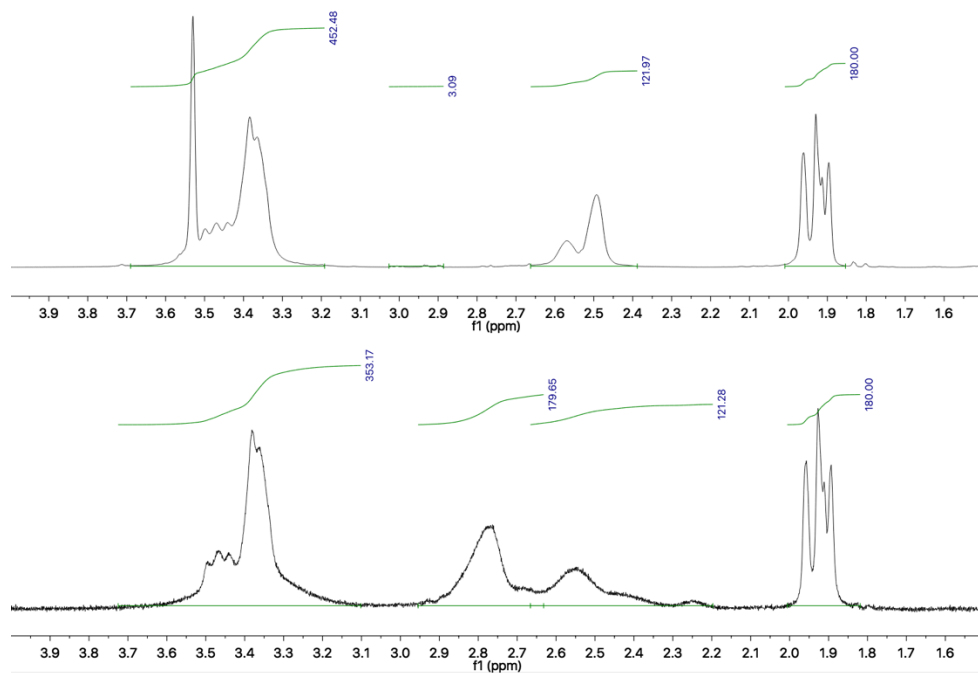


Figure 4.3 ¹H NMR spectra of PMeOx-PMestOx (upper) and PMeOx-PcBOx (lower) (D₂O, 298K).

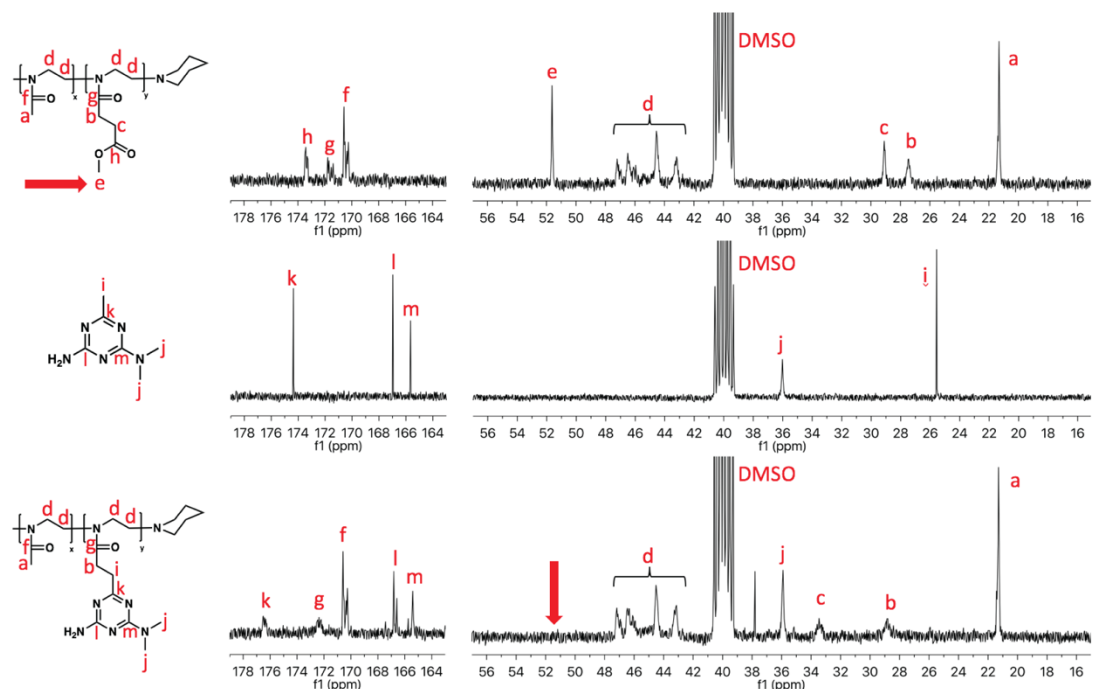


Figure 4.5 Overlay of the ^{13}C NMR spectra of PMeOx-PMestOx, cBG and PMeOx-PcBOx (^{13}C NMR ((CD_3) $_2\text{SO}$, 298 K).

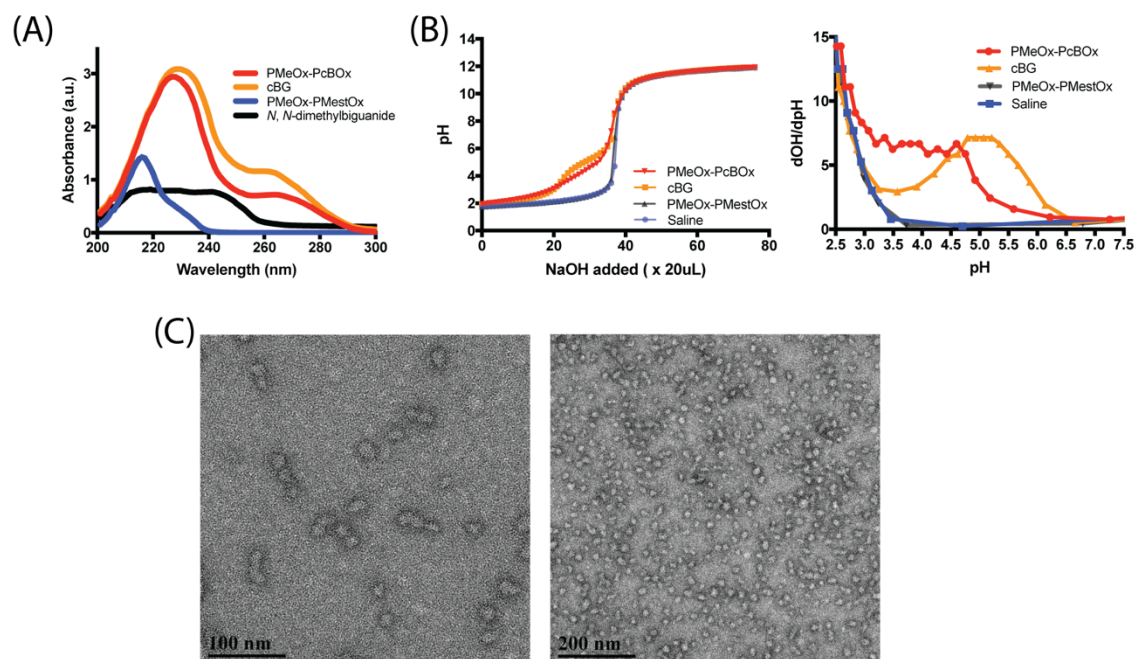


Figure 4.6 (A) UV spectra of PMeOx-PcBOx, cBG, PMeOx-PMestOx and *N,N*-dimethylbiguanide in the range of 200–300nm. (B) Acid-base titration curves (left) and derivative plot dOH/dpH as a function of pH (right) of PMeOx-PcBOx, cBG, PMeOx-PMestOx and saline. (C) TEM image of self-assembled PMeOx-PcBOx. Scale bar = 200 nm (left), 50 nm (right).

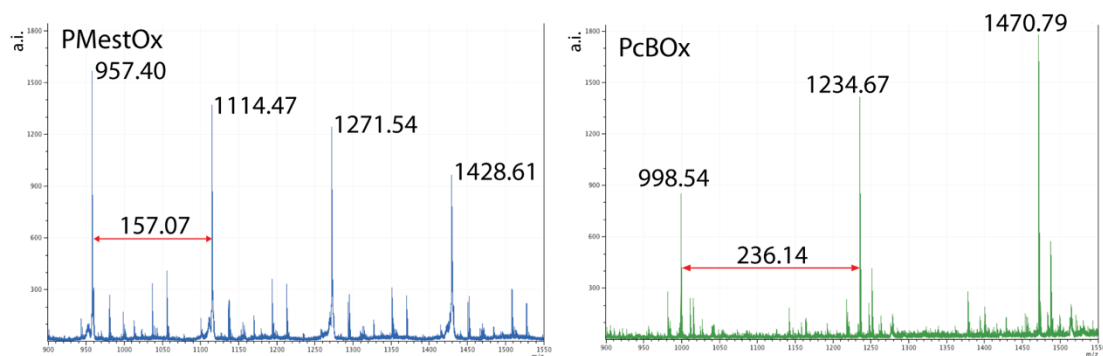
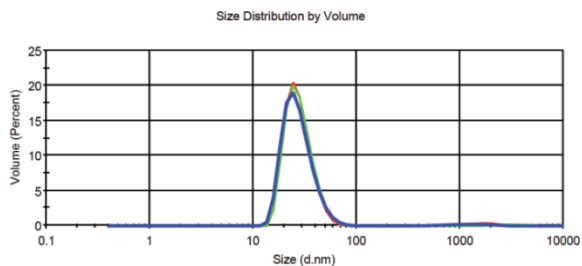


Figure 4.7 MALDI-TOF MS analysis of PMestOx and PcBOx homopolymers.

(A)

	Size (d.nm):	% Volume:	St Dev (d.nm):
Z-Average (d.nm): 36.88	Peak 1: 27.93	97.5	8.404
PdI: 0.277	Peak 2: 1578	2.5	603.8
Intercept: 0.932	Peak 3: 0.000	0.0	0.000

Result quality : Good



(B)

	Size (d.nm):	% Volume:	St Dev (d.nm):
Z-Average (d.nm): 88.99	Peak 1: 411.9	4.7	243.3
PdI: 0.486	Peak 2: 34.77	94.9	20.32
Intercept: 0.925	Peak 3: 4744	0.4	1031

Result quality : Good

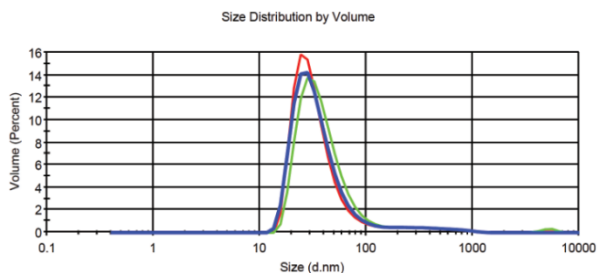


Figure 4.8 Volume based size distribution of (A) PMeOx-PcBOx (upper) and (B) DachPt-PMeOx-PcBOx (lower) measured by DLS with 1 mg/mL polymer solution in DI water.

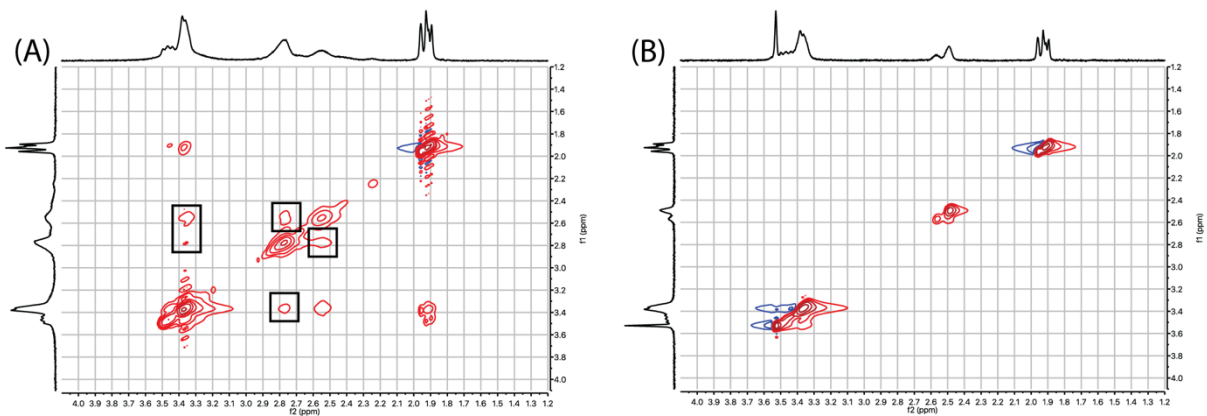


Figure 4.9 2D NOESY NMR spectra of (a) PMeOx-PcBOx (1 mg/mL) and (b) PMeOx-PMestOx (1 mg/mL) in D₂O.

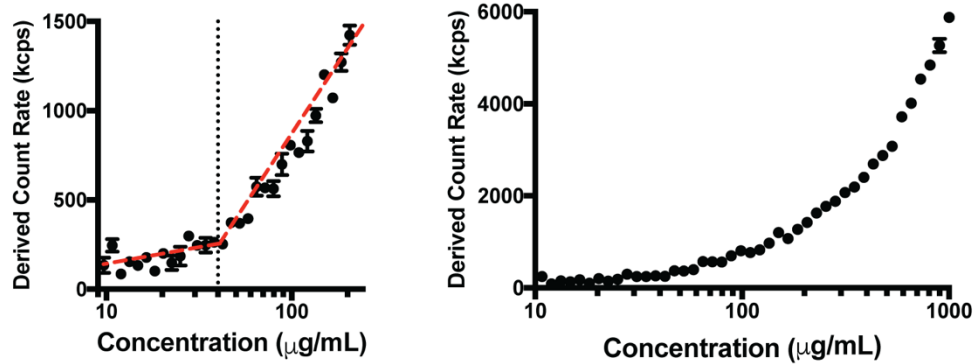


Figure 4.10 Measurement of the CMC of PMeOx-PcBOx in DI water by light scattering measurement.

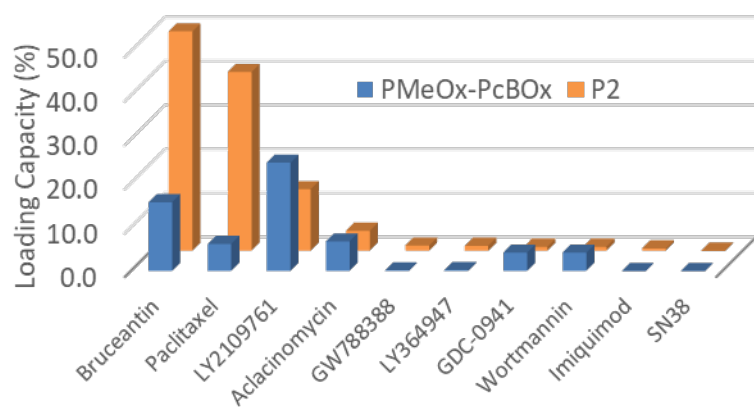


Figure 4.11 Differential solubilization of drugs indicated by their maximum LC in PMeOx-PcBOx (blue bars) and P2 (orange bars). Polymers concentration 10 mg/mL. (n=3 for all drugs and polymers except for GW788388, GDC-0941, and LY364947 in PMeOx-PcBOx groups, which has n=1).

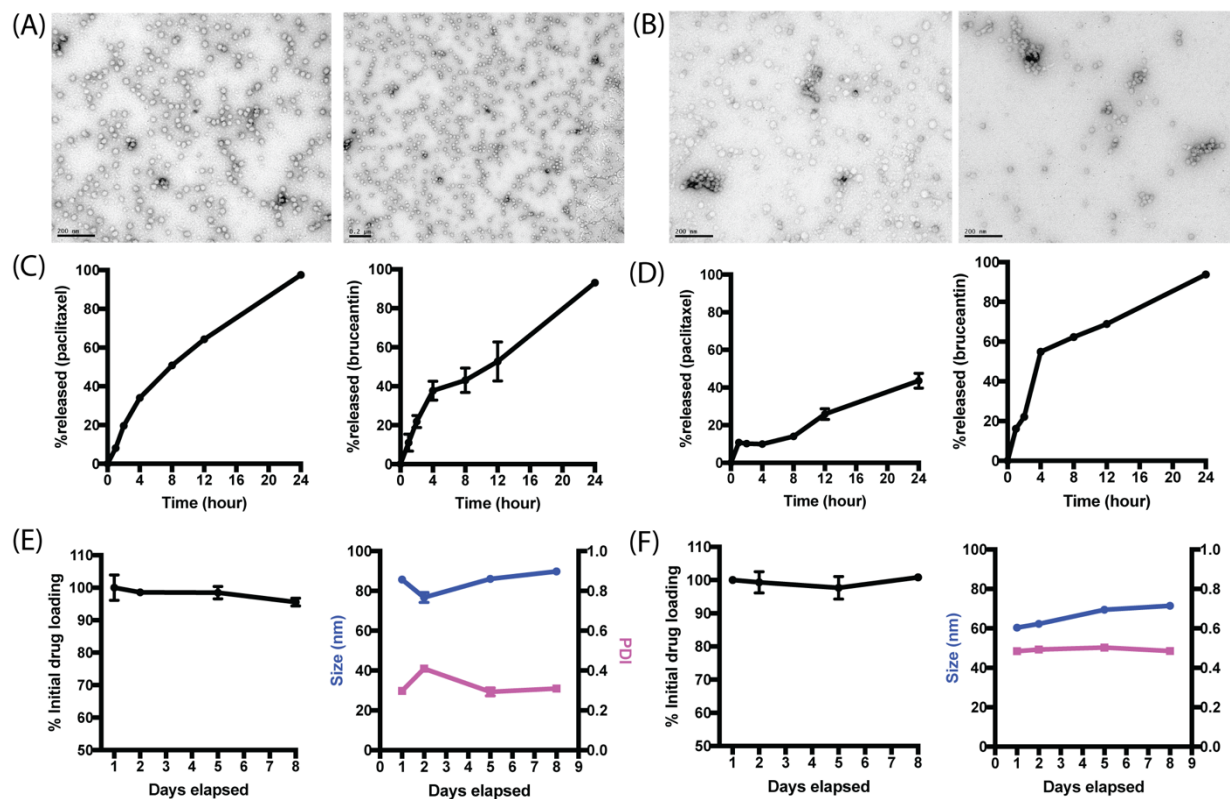
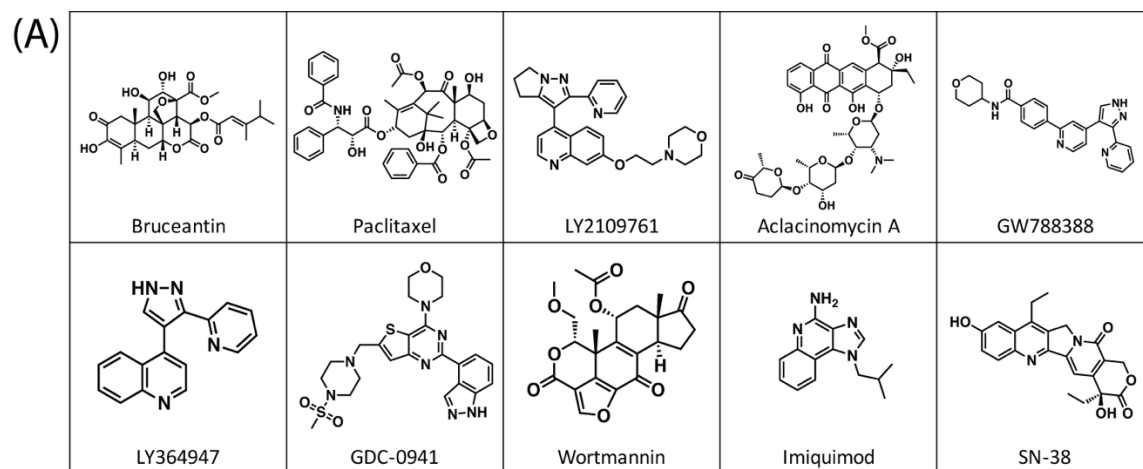


Figure 4.12 TEM image of (A) Paclitaxel-PMeOx-PcBOx formulation and (B) Bruceantin-PMeOx-PcBOx formulation, Release profile of (C) paclitaxel (left) and bruceantin (right) from PMeOx-PcBOx nanoparticle formulation and (D) paclitaxel (left) and bruceantin (right) from P2 polymer and stability profile of (E) Paclitaxel-PMeOx-PcBOx formulation and (F) Bruceantin-PMeOx-PcBOx formulation (n=3)



(B)

Drug	MW (g/mol)	LC % (P2)	LC % (PMeOx-PcBOx)	EDA	HBA	HBD	LogP	RBN	score
Bruceantin	548.59	50.0	15.7	-	8	3	1.4	6	4
Paclitaxel	853.91	40.7	6.2	+	9	3	4	14	4
LY2109761	441.52	14.0	22.3	+	7	0	2.8	6	4
Aclacinomycin A	811.86	4.6	6.8	+	15	4	2.2	10	5
GW788388	425.48	1.3	0.2	+	6	2	3.8	6	2
LY364947	272.30	1.2	0.3	+	3	1	4.6	2	1
GDC-0941	513.64	1.0	4.3	+	9	1	2	4	3
Wortmannin	428.44	1.0	3.8	+	6	0	0	4	2
Imiquimod	240.30	0.6	13.6	-	4	1	2.8	2	1
SN-38	392.40	0.0	0.0	-	5	2	1.9	2	1

Figure 4.13 (A) Evaluated drug structures and **(B)** comparison of the maximal LC of each drug in PMeOx-PcBOx and P2 micelles with the molecular characteristics of these drugs. The scores correspond to the presence of electron deficient aromatic rings (EDA), the numbers of hydrogen bonding acceptors and donors (HBA and HBD, respectively), lipophilicity (LogP) and the number of rotatable bonds (RBN).

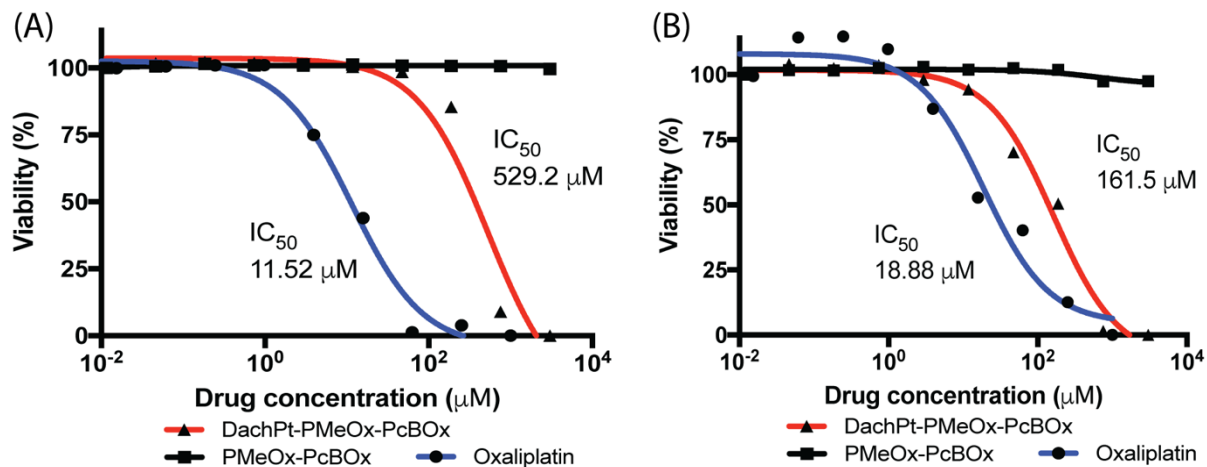


Figure 4.14 Cytotoxicity and IC_{50} values of PMeOx-PcBOx, DachPt-PMeOx-PcBOx and free oxaliplatin in (A) 344SQ murine NSCLC cells and (B) MDA-MB-231 human breast cancer cells. DachPt-PMeOx-PcBOx concentration is presented as the oxaliplatin equivalent concentration. PMeOx-PcBOx concentration is presented as the block copolymer concentration equivalent to that in DachPt-PMeOx-PcBOx formulation.

REFERENCES

1. Méndez-Lucio, O. and Medina-Franco, J.L., 2017. The many roles of molecular complexity in drug discovery. *Drug Discovery Today*, 22(1), pp.120-126.
2. Macalino, S.J.Y., Gosu, V., Hong, S. and Choi, S., 2015. Role of computer-aided drug design in modern drug discovery. *Archives of pharmacal research*, 38(9), pp.1686-1701.
3. Kazunori, K., Masayuki, Y., Teruo, O. and Yasuhisa, S., 1993. Block copolymer micelles as vehicles for drug delivery. *Journal of Controlled Release*, 24(1-3), pp.119-132.
4. Mikhail, A.S. and Allen, C., 2009. Block copolymer micelles for delivery of cancer therapy: transport at the whole body, tissue and cellular levels. *Journal of Controlled Release*, 138(3), pp.214-223.
5. Matsumura, Y. and Kataoka, K., 2009. Preclinical and clinical studies of anticancer agent-incorporating polymer micelles. *Cancer science*, 100(4), pp.572-579.
6. Matsumura, Y. and Kataoka, K., 2009. Preclinical and clinical studies of anticancer agent-incorporating polymer micelles. *Cancer science*, 100(4), pp.572-579.
7. Zhang, L., Gu, F.X., Chan, J.M., Wang, A.Z., Langer, R.S. and Farokhzad, O.C., 2008. Nanoparticles in medicine: therapeutic applications and developments. *Clinical pharmacology & therapeutics*, 83(5), pp.761-769.
8. Bobo, D., Robinson, K.J., Islam, J., Thurecht, K.J. and Corrie, S.R., 2016. Nanoparticle-based medicines: a review of FDA-approved materials and clinical trials to date. *Pharmaceutical research*, 33(10), pp.2373-2387.
9. Walsh, T.J., Finberg, R.W., Arndt, C., Hiemenz, J., Schwartz, C., Bodensteiner, D., Pappas, P., Seibel, N., Greenberg, R.N., Dummer, S. and Schuster, M., 1999. Liposomal amphotericin B for empirical therapy in patients with persistent fever and neutropenia. *New England Journal of Medicine*, 340(10), pp.764-771.
10. Green, M.R., Manikhas, G.M., Orlov, S., Afanasyev, B., Makhson, A.M., Bhar, P. and Hawkins, M.J., 2006. Abraxane[®], a novel Cremophor[®]-free, albumin-bound particle form of paclitaxel for the treatment of advanced non-small-cell lung cancer. *Annals of Oncology*, 17(8), pp.1263-1268.
11. Wu, S.Y., Lopez-Berestein, G., Calin, G.A. and Sood, A.K., 2014. RNAi therapies: drugging the undruggable. *Science translational medicine*, 6(240), pp.240ps7-240ps7.
12. Cern, A., Golbraikh, A., Sedykh, A., Tropsha, A., Barenholz, Y. and Goldblum, A., 2012. Quantitative structure-property relationship modeling of remote liposome loading of drugs. *Journal of controlled release*, 160(2), pp.147-157.

13. Cern, A., Barenholz, Y., Tropsha, A. and Goldblum, A., 2014. Computer-aided design of liposomal drugs: in silico prediction and experimental validation of drug candidates for liposomal remote loading. *Journal of Controlled Release*, 173, pp.125-131.
14. Mondal, S., Samajdar, R.N., Mukherjee, S., Bhattacharyya, A.J. and Bagchi, B., 2018. Unique features of metformin: a combined experimental, theoretical, and simulation study of its structure, dynamics, and interaction energetics with DNA grooves. *The Journal of Physical Chemistry B*, 122(8), pp.2227-2242.
15. Overberger, C.G., Michelotti, F.W. and Carabateas, P.M., 1957. Preparation of Triazines by the Reaction of Biguanide and Esters I. *Journal of the American Chemical Society*, 79(4), pp.941-944.
16. Bouten, P.J., Lava, K., Van Hest, J. and Hoogenboom, R., 2015. Thermal properties of methyl ester-containing poly (2-oxazoline) s. *Polymers*, 7(10), pp.1998-2008.
17. Luxenhofer, R., Schulz, A., Roques, C., Li, S., Bronich, T.K., Batrakova, E.V., Jordan, R. and Kabanov, A.V., 2010. Doubly amphiphilic poly (2-oxazoline) s as high-capacity delivery systems for hydrophobic drugs. *Biomaterials*, 31(18), pp.4972-4979.
18. Koh, M., Lee, J.C., Min, C. and Moon, A., 2013. A novel metformin derivative, HL010183, inhibits proliferation and invasion of triple-negative breast cancer cells. *Bioorganic & medicinal chemistry*, 21(8), pp.2305-2313.
19. Hu, X., Lerch, T.F. and Xu, A., 2018. Efficient and Selective Bioconjugation Using Surfactants. *Bioconjugate chemistry*, 29(11), pp.3667-3676.
20. Veber, D.F., Johnson, S.R., Cheng, H.Y., Smith, B.R., Ward, K.W. and Kopple, K.D., 2002. Molecular properties that influence the oral bioavailability of drug candidates. *Journal of medicinal chemistry*, 45(12), pp.2615-2623.
21. Oberoi, H.S., Nukolova, N.V. and Bronich, T.K., 2011. Dichloro (1, 2-Diaminocyclohexane) Platinum (II)(DACHPt) Loaded Polymer Micelles with Cross-Linked Core: Preparation and Characterization. In *PMSE preprints American Chemical Society. Division of Polymeric Materials: Science and Engineering. Meeting* (Vol. 104, p. 630). NIH Public Access.
22. He, Z., Wan, X., Schulz, A., Bludau, H., Dobrovolskaia, M.A., Stern, S.T., Montgomery, S.A., Yuan, H., Li, Z., Alakhova, D. and Sokolsky, M., 2016. A high capacity polymeric micelle of paclitaxel: Implication of high dose drug therapy to safety and in vivo anti-cancer activity. *Biomaterials*, 101, pp.296-309.
23. Wan, X., Beaudoin, J.J., Vinod, N., Min, Y., Makita, N., Bludau, H., Jordan, R., Wang, A., Sokolsky, M. and Kabanov, A.V., 2019. Co-delivery of paclitaxel and cisplatin in poly (2-oxazoline) polymeric micelles: Implications for drug loading, release, pharmacokinetics and outcome of ovarian and breast cancer treatments. *Biomaterials*, 192, pp.1-14.

24. Wan, X., Min, Y., Bludau, H., Keith, A., Sheiko, S.S., Jordan, R., Wang, A.Z., Sokolsky-Papkov, M. and Kabanov, A.V., 2018. Drug Combination synergy in worm-like polymeric micelles improves treatment outcome for small cell and non-small cell lung cancer. *ACS nano*, 12(3), pp.2426-2439.
25. He, Z., Schulz, A., Wan, X., Seitz, J., Bludau, H., Alakhova, D.Y., Darr, D.B., Perou, C.M., Jordan, R., Ojima, I. and Kabanov, A.V., 2015. Poly (2-oxazoline) based micelles with high capacity for 3rd generation taxoids: Preparation, in vitro and in vivo evaluation. *Journal of controlled release*, 208, pp.67-75.
26. Lübtow, M.M., Keßler, L., Appelt-Menzel, A., Lorson, T., Gangloff, N., Kirsch, M., Dahms, S. and Luxenhofer, R., 2018. More Is Sometimes Less: Curcumin and Paclitaxel Formulations Using Poly (2-oxazoline) and Poly (2-oxazine)-Based Amphiphiles Bearing Linear and Branched C9 Side Chains. *Macromolecular bioscience*, 18(11), p.1800155.
27. Lübtow, M.M., Hahn, L., Haider, M.S. and Luxenhofer, R., 2017. Drug specificity, synergy and antagonism in ultrahigh capacity poly (2-oxazoline)/poly (2-oxazine) based formulations. *Journal of the American Chemical Society*, 139(32), pp.10980-10983.
28. Mooibroek, T.J. and Gamez, P., 2007. The s-triazine ring, a remarkable unit to generate supramolecular interactions. *Inorganica chimica acta*, 360(1), pp.381-404.
29. Taylor, R.O.B.I.N., Kennard, O.L.G.A. and Versichel, W.E.R.N.E.R., 1984. The geometry of the N-H...O=C hydrogen bond. 3. Hydrogen-bond distances and angles. *Acta Crystallographica Section B: Structural Science*, 40(3), pp.280-288.
30. Lipinski, C.A., Lombardo, F., Dominy, B.W. and Feeney, P.J., 1997. Experimental and computational approaches to estimate solubility and permeability in drug discovery and development settings. *Advanced drug delivery reviews*, 23(1-3), pp.3-25.
31. Pendyala, L. and Creaven, P.J., 1993. In vitro cytotoxicity, protein binding, red blood cell partitioning, and biotransformation of oxaliplatin. *Cancer research*, 53(24), pp.5970-5976.
32. Kanat, O., Ertas, H. and Caner, B., 2017. Platinum-induced neurotoxicity: a review of possible mechanisms. *World journal of clinical oncology*, 8(4), p.329.
33. Marupudi, N.I., Han, J.E., Li, K.W., Renard, V.M., Tyler, B.M. and Brem, H., 2007. Paclitaxel: a review of adverse toxicities and novel delivery strategies. *Expert opinion on drug safety*, 6(5), pp.609-621.
34. Lyass, O., Uziely, B., Ben-Yosef, R., Tzemach, D., Heshing, N.I., Lotem, M., Brufman, G. and Gabizon, A., 2000. Correlation of toxicity with pharmacokinetics of pegylated liposomal doxorubicin (Doxil) in metastatic breast carcinoma. *Cancer: Interdisciplinary International Journal of the American Cancer Society*, 89(5), pp.1037-1047.

35. Reichert, D.E., Lewis, J.S. and Anderson, C.J., 1999. Metal complexes as diagnostic tools. *Coordination Chemistry Reviews*, 184(1), pp.3-66.
36. Caravan, P., Ellison, J.J., McMurry, T.J. and Lauffer, R.B., 1999. Gadolinium (III) chelates as MRI contrast agents: structure, dynamics, and applications. *Chemical reviews*, 99(9), pp.2293-2352.
37. Mi, P., Kokuryo, D., Cabral, H., Wu, H., Terada, Y., Saga, T., Aoki, I., Nishiyama, N. and Kataoka, K., 2016. A pH-activatable nanoparticle with signal-amplification capabilities for non-invasive imaging of tumour malignancy. *Nature nanotechnology*, 11(8), p.724.
38. Popovtzer, R., Agrawal, A., Kotov, N.A., Popovtzer, A., Balter, J., Carey, T.E. and Kopelman, R., 2008. Targeted gold nanoparticles enable molecular CT imaging of cancer. *Nano letters*, 8(12), pp.4593-4596.
39. Zhang, P., Huang, H., Chen, Y., Wang, J., Ji, L. and Chao, H., 2015. Ruthenium (II) anthraquinone complexes as two-photon luminescent probes for cycling hypoxia imaging in vivo. *Biomaterials*, 53, pp.522-531.

CHAPTER V: SUMMARY AND FUTURE EXPERIMENTS

In this dissertation, I reviewed PM formulations for the delivery of hydrophobic small molecules. BCP segments required for forming amphiphilic copolymers were described in order to aid proper selection of the component of BCPs for efficient solubilization of target hydrophobic small molecules. To improve our understanding on drug solubilization, multi-disciplinary approaches were described for investigating detailed molecular interaction between hydrophobic segment of BCPs and encapsulated drug. In addition, important issues on physicochemical properties of PMs and clinical outcome of PMs were explored to draw the attention on advanced PK analysis of PMs to investigating subpopulation of PMs in clinical investigation.

In Chapter II, we report a novel computer-aided strategy for rational design of PMs for poorly soluble drugs. We have developed novel descriptors of drug-polymer complexes that were employed to build models to predict both drug loading efficiency (LE) and loading capacity (LC) via QSPR approach. Total 41 hydrophobic drugs were tested in PM formulation by using poly(2-oxazoline)-based block copolymer at different concentration either individually and in combination with another drugs, which produces 408 data points as micelle formulation that provides both loading efficiency (LE) and loading capacity (LC) in PMs. With the statistical analysis by QSPR with given dataset above, QSPR approach could predict the solubility of model hydrophobic drugs in POx polymer in terms of both LE and LC. Three putative true positive as well as three putative negative hits were confirmed (implying 75% prediction accuracy). The success of the computational strategy suggests its broad utility for rational design of drug delivery

systems.

In Chapter III, we report that optimized vismodegib delivery using PMs markedly improves efficacy and reduces systemic toxicity, providing strong support for the use of the POx platform. Vismodegib has shown clinical efficacy for treatment of SHH-driven cancers but has not been effective for SHH subtype medulloblastoma. Using POx system, we generated POx-vismo micelles that showed highly uniform nanometer-scale particles with Z_{ave} of 38 nm and high loading capacity. Our analyses show that POx formulation increased drug exposure in the CNS, in both medulloblastoma and forebrain and reduced systemic exposure, providing an explanation for both improved anti-tumor effect and reduced toxicity. Our NMR studies provide important insight into the mechanism through which POx nanoparticle encapsulation improves pharmacokinetics. The persistence of proliferating medulloblastoma cells in long-term treatment with POx-vismo highlights the need for combinations of pharmacologic agents to forestall resistance. Our results indicate that optimization through nanoparticle formulation can improve the therapeutic index and efficacy of systemically administered pharmaceutical agents for brain tumor therapy, with the potential to improve survival and quality-of-life for brain tumor patients.

In Chapter IV, we report a novel poly(2-oxazoline)-based block copolymer with a heterocyclic, aromatic side chain that can be used for 1) solubilization of a unique set of poorly soluble compounds that have previously failed in other polymeric systems, as well as 2) loading of platinum drugs through metal complexation. It is promising that the new block copolymer class can expand the application of polymeric micelle technologies to a new set of drugs and impact the drug design space for poorly soluble drugs by providing alternatives to hydrophobic interactions as a means of incorporation of poorly soluble APIs in the micelles. Future studies will validate

this conclusion for a higher number of small molecule compounds and elucidate drug/polymer interaction mechanisms important for predictions of drug solubilization.